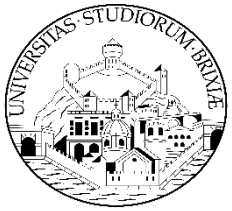

UNIVERSITÀ
DEGLI STUDI
DI BRESCIA

DOTTORATO DI RICERCA IN TECHNOLOGY FOR HEALTH

Settore scientifico disciplinare CHIM/07

CICLO XXXVI

ELEMENTAL ANALYSIS OF AIR PARTICULATE MATTER FILTERS BY X-RAY FLUORESCENCE UNDER GRAZING INCIDENCE

Dottoranda:

PAOLA CIRELLI

Supervisore:

Prof.ssa LAURA BORGESE

TABLE OF CONTENTS

Abstract (*English*)

The consequences of air pollution are extensive, affecting not only people's cardiovascular and respiratory system but also degrading the environment, impacting biodiversity, and causing climate change. Despite a decrease in the emissions of particulate matter (PM) of around 30% from 2000 to 2021 in Europe, air pollution is still a major health concern for Europeans. To further decrease the emissions of atmospheric pollutants, the identification of the sources of particulate matter is of great importance, as well as its chemical composition.

Particulate matter is usually collected on air filtering polytetrafluoroethylene (PTFE) membranes to determine mass and chemical composition. Besides the analytical methods, which require filter solubilization with toxic acids, X-ray Fluorescence analysis (XRF) has emerged as a valid technique for the determination of PM composition, with the advantages of being faster, cheaper, and non-destructive. Air filters can be directly analysed with XRF spectrometers in geometrical configuration 0-90°, generally used for Total Reflection X-ray fluorescence (TXRF) analysis of residues on X-ray reflectors. Though the condition of total reflection is not fully reached, this geometrical configuration enhances the fluorescence signal and the determination of metals (i.e. Pb) in PM goes well below the environmental limits. Filters are measured in XRF under grazing incidence condition, after a preparation procedure called Smart Store®. This consists in sandwiching the sample between two thin adhesive polymeric foils, to avoid material loss and sample contaminations, and to remove the plastic ring stretching the PTFE membrane that impedes the sample illumination when filters are analysed with TXRF spectrometers. Quantitative data can be obtained thanks to the external calibration approach, by means of calibration lines that are built for each element of interest. These lines are built comparing the known elemental concentration of samples and the detected fluorescence intensity. This procedure requires the use of reference samples, consisting in air filters with known mass deposition.

During this doctorate, calibration samples were realized nebulizing a solution of known elemental concentration with a particle generator and collecting the obtained aerosol onto a filter. By changing the nebulization time and the concentration of the solution, it is possible to obtain filters in a wide range of elemental mass loading. The concentration range of the calibration samples was selected considering the limits imposed by the European Commission (EC) for the protection of health in the two Air Quality Directives

(2004/107/EC, 2008/50/EC). The obtained samples were deeply studied and analysed with X-ray spectrometers in different geometrical configurations of the incident beam and the detector (45°/45° and 0°/90°) and with synchrotron radiation, to evaluate the feasibility of the method. The results contribute to the standardization of this method, which was proposed to ISO with the project NP 23971 “Analysis of air PM filters by XRF under grazing incidence”.

The realized calibration samples are suitable for the development of calibration curves for the quantification of PM elemental content by means of all the XRF based spectrometers. The proposed method is faster, cheaper, easier, and more sustainable than conventional methods, representing a green alternative for air quality monitoring.

Abstract (*Italiano*)

Le conseguenze dell'inquinamento atmosferico sono molteplici e colpiscono non solo il sistema cardiovascolare e respiratorio delle persone, ma degradano anche l'ambiente, influiscono sulla biodiversità e causano il cambiamento climatico. Nonostante una diminuzione delle emissioni di particolato (PM) di circa il 30% tra il 2000 e il 2021 in Europa, l'inquinamento atmosferico rappresenta ancora una delle principali preoccupazioni per la salute degli europei. Per diminuire ulteriormente le emissioni di inquinanti atmosferici, è di grande importanza l'identificazione delle fonti del particolato, nonché la sua composizione chimica.

Il particolato viene solitamente raccolto su membrane filtranti in politetrafluoroetilene (PTFE), per determinarne la massa e la composizione chimica. Oltre ai metodi analitici, che richiedono la solubilizzazione del filtro con acidi tossici, l'analisi tramite spettroscopia di fluorescenza ai raggi X (XRF) si stia dimostrando una strategia valida per la determinazione della composizione del PM, con il vantaggio di essere più veloce, più economica e non distruttiva. I filtri dell'aria possono essere analizzati direttamente con spettrometri XRF in configurazione geometrica 0-90°, generalmente utilizzati per l'analisi della fluorescenza a raggi X a riflessione totale (TXRF) di residui sui riflettori per analisi a raggi X. Sebbene la condizione di riflessione totale non sia completamente raggiunta, questa configurazione geometrica potenzia il segnale di fluorescenza e la determinazione dei metalli pesanti (es. Pb) nel PM va ben al di sotto dei limiti ambientali. I filtri vengono misurati in XRF in condizioni di incidenza radente, dopo una procedura di preparazione denominata Smart Store®. Questa consiste nel racchiudere il campione tra due sottili fogli polimerici adesivi, per evitare perdite di materiale e contaminazioni del campione, e nel rimuovere l'anello di plastica che tende la membrana in PTFE che impedisce l'illuminazione del campione quando i filtri vengono analizzati con gli spettrometri TXRF. Informazioni quantitative possono essere ottenute grazie all'approccio della calibrazione esterna, mediante linee di calibrazione costruite per ciascun elemento di interesse. Queste linee vengono costruite confrontando la concentrazione elementare nota dei campioni e l'intensità di fluorescenza rilevata. Questa procedura richiede l'utilizzo di campioni di riferimento, costituiti da filtri dell'aria con deposizione di massa nota.

I campioni di calibrazione sono stati realizzati nel corso di questo dottorato nebulizzando una soluzione di concentrazione elementare nota con un generatore di particelle e raccogliendo l'aerosol ottenuto su un filtro. Modificando il tempo di nebulizzazione e la concentrazione della soluzione è possibile ottenere filtri in un'ampia gamma di concentrazioni elementari. L'intervallo di concentrazione dei campioni di calibrazione è stato selezionato considerando i limiti imposti dalla Commissione Europea (CE) per la tutela della salute nelle due direttive sulla qualità dell'aria (2004/107/CE, 2008/50/CE). I campioni ottenuti sono stati studiati approfonditamente e analizzati con spettrometri a raggi X in diverse configurazioni geometriche del fascio incidente e del detector (45°/45° e 0°/90°) e con radiazione di sincrotrone, per valutare la fattibilità del metodo. I risultati contribuiscono alla standardizzazione di questo metodo, che è stato proposto all'ISO con il progetto NP 23971 "Analisi dei filtri dell'aria di PM mediante XRF a incidenza radente".

I campioni di calibrazione realizzati sono adatti per lo sviluppo di curve di calibrazione per la quantificazione del contenuto elementare del PM mediante spettrometrica di fluorescenza di raggi X, in qualsiasi configurazione. Il metodo proposto è più rapido, economico, semplice e sostenibile rispetto ai metodi convenzionali, rappresentando un'alternativa ecologica per il monitoraggio della qualità dell'aria.

INTRODUCTION

The goal of this thesis is demonstrating that it is possible to analyse directly air filters with X-ray based instrument and obtain quantitative information about the elemental composition of particulate matter by means of calibration curves. For this purpose, calibration samples of air filters were created and characterized with different instruments. Then these samples were analysed with several XRF spectrometers to build calibration curves. With the proposed method air quality monitoring is made more accessible, being faster, greener and more cost-effective than conventional methods for filter analysis. This work supports the development of the ISO standard 23971 "Grazing Incidence XRF Analysis of air filters", aiming at establishing XRF as a reference technique for the analysis of air filters.

The thesis is organised in six chapters.

Chapter 1 presents an introduction about particulate matter, with a focus on its sources and effects. Guidelines imposed by European Commission for facing air pollution are described, with particular reference to the Zero pollution Action Plan and the Air Quality Directives (2004/107/EC, 2008/50/EC). The method to sample air particulate matter is described, together with the standardized methods for the determination of the concentration of metals. Besides conventional methods, also X-ray based techniques can be used to analysed air filters, and this was demonstrated in several studies of the Chem4Tech laboratory of the University of Brescia.

In *chapter 2* all the instruments that were used in this research project are presented, with a distinction between X-ray based instruments and other instruments. All the instrument parameters and the measuring conditions are explained.

Chapter 3 represents the proof of concept of the proposed method for direct filter analysis. Some mono element reference filters are analysed with 3 different commercial total reflection X-ray fluorescence spectrometers (TXRF). Calibration line for lead is built, proving the applicability of the method.

Chapter 4 is dedicated to reference materials (RMs). First, a broad overview of RMs is given, emphasising how they are produced and characterised in accordance with the ISO Guides. Then the discussion focuses on the case of RMs of particulate matter filters, their availability on the market and the production of calibration samples of air filters in the Chem4Tech

laboratory. The assessment of homogeneity and stability and the repeatability of the production of the calibration samples are discussed.

Chapter 5 describes the procedure that was followed in order to align the samples before measurements with a diffractometer, synchrotron radiation and a custom made TXRF. The sample under study, indeed, is non-conventional and the measuring conditions should be carefully selected to obtain optimized results.

In *chapter 6* the calibration lines obtained analysing the prepared calibration samples are presented and discussed, with a distinction between data obtained with EDXRF and TXRF spectrometers.

1. STATE OF THE ART

1.1.Particulate matter: definition, sources, and effects

Air pollution is a pressing global concern that poses significant threats to human health, the environment, and the planet's overall well-being. It is a complex issue arising from a variety of sources, both natural and human-made, that release harmful substances into the atmosphere. These pollutants include particulate matter, sulfur dioxide, nitrogen oxides, carbon monoxide, volatile organic compounds, and various other toxic gases and chemicals. Particulate matter (PM) is one of the major air pollutants and is made of a mixture of solid particles and liquid droplets. Particles differ in terms of size, chemical composition, and other physical and biological characteristics depending on the time and place. The major components of PM include metals, organic compounds including materials of biological origin, inorganic carbonaceous material and sulphate, nitrate, ammonium, and other ions.

Particulate matter is categorized based on their aerodynamic diameter, with distinctions made between coarse, fine and ultrafine particles. Coarse particles, or PM_{10} (less than 10 μm in diameter), are mostly composed of biological material (pollen, endotoxins, fungus, and bacteria), sea salts, and insoluble minerals coming from the crust. Fine and ultrafine particles, $PM_{2.5}$ and $PM_{0.1}$ respectively according to the particle diameter, consist of particles with a carbon core, hydrocarbons, particles formed from oxides of sulfur and nitrogen (Adams et al. 2015). To understand the real dimension of these particles, Figure 1 gives an example of the dimension of PM_{10} and $PM_{2.5}$ compared with a human hair and a beach sand. Sources of PM may be natural, such as volcanic eruptions, dust storms and forest fires, or related to human activity, like combustion of fuel, traffic, industrial activity. It is therefore clear that exposure and sources of PM significantly varies among different regions of the world (Mukherjee and Agrawal 2017). There are significant differences in terms of chemical composition of PM in

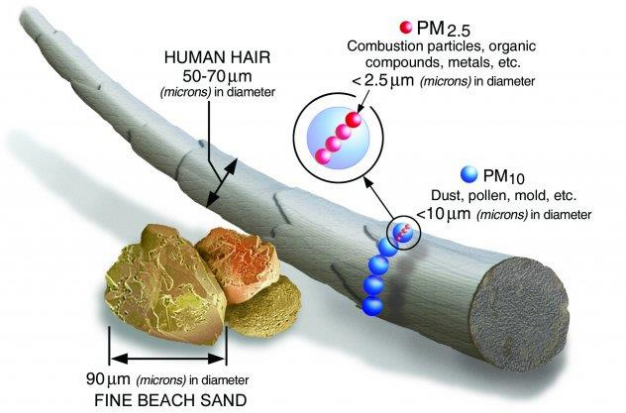

Figure 1 - Size comparisons for PM particles [source: www.epa.gov]

urban, industrial and rural areas, as well as seasonal trends in PM concentration, which is strongly affected by meteorological factors.

Despite the concentration and the composition of PM differ from place to place, it is associated with the most severe air pollution induced health effects. Particles, indeed, are so small that can be inhaled and reach the lungs, penetrating deeper in the alveoli. Long term exposure to PM is associated with problems related to the respiratory system, such as an increased incidence of pneumonia and lung cancer and the development of asthma (Abelsohn and Stieb 2011). Several epidemiological studies have assessed the connection between air pollution and cardiovascular disease. Once PM penetrate in the pulmonary system, it causes inflammation that can affect the systemic circulation. A prolonged exposure to PM can lead to heart failure, stroke, cardiac arrhythmias and other cardiovascular diseases (Krittanawong et al. 2023; Lee et al. 2014). In addition to the respiratory and the cardiovascular systems, PM can hurt also other organic systems, contributing to neurological disorders, such as Alzheimer's disease, Parkinson's disease and dementia. Also genotoxicity, kidney issues, gastrointestinal and reproductive systems were proven to be affected by PM exposure (Garcia et al. 2023). It is estimated that exposure to fine particulate matter caused 238000 premature deaths[1] in 2020 in Europe (European Environment Agency (EEA) 2022).

Beside human health, air pollution leads to environmental degradation and impacts natural ecosystems and biodiversity. According to its composition, PM can contribute to acidification of lakes and streams, changes in the nutrient balance in coastal waters and large river basins, damages to sensitive forests and farm crops and to effects on the diversity of ecosystems. Toxic metals present in PM can lead to harmful impacts on both plants and animals. Despite their low levels in the atmosphere, they can disrupt the biodiversity of soil species and stunt plant growth (EEA 2019).

1.2. The threat of PM in Europe

It is clear the need for controlling and monitoring PM concentration in atmosphere, for the protection of both human health and ecosystems. In this regard, in 2021 the European Commission (EC) adopted the Action Plan: "Towards a Zero Pollution for Air, Water and

[1] Premature deaths are deaths that occur before a person reaches an expected age, which is typically the life expectancy for a country.

Soil", whose main objective is to create a toxic-free environment (European Commission 2022). This can be achieved by reducing air, water, and soil pollution to levels that are no longer deemed hazardous to human health or natural ecosystems while respecting the limits of the planet's capacity. Between 2000 and 2021 in the European Union (EU) emissions dropped by 31% for $PM_{2.5}$ and by 29% for PM_{10}, with a slight increase between 2020 and 2021, of 2% and 1% respectively (EEA 2023). Figure 2 shows the trend in coarse particulate matter emission in the last twenty years (2000-2020). These numbers, however, still need to be improved, as the target goal is a 55% reduction of premature deaths in EU due to PM by 2030. This reduction is projected to be achieved through a reduction in the emissions of $PM_{2.5}$, if all Member States implement the measures foreseen in their Air Pollution Control Programmes.

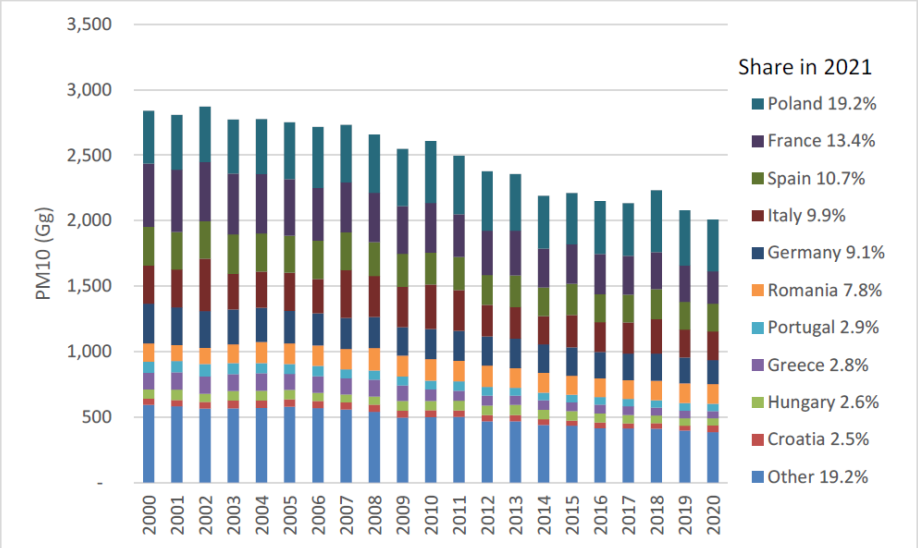

Figure 2 - PM_{10} emission trends in the EU and shares of Member States. Countries are sorted by their contribution to the EU total for 2021. The top 10 countries are displayed. Data for the other 17 reporting countries are summed under 'Other' (EEA 2023)

To face air pollution and to reach its objectives, the EU has a comprehensive clean air policy based on three pillars: reducing air pollution emissions, emissions standards for major sources of pollution, and ambient air quality standards. With a set of directives known as the Air Quality Directives (2004/107/EC, 2008/50/EC) (EU 2004, 2008), the EU aim to protect human health and the environment by establishing specific standards and objectives for

various air pollutants. The directives set limit values for various air pollutants, including PM (PM_{10} and $PM_{2.5}$), sulfur dioxide (SO_2), nitrogen dioxide (NO_2), metals such as lead (Pb), cadmium (Cd), arsenic (As) and nickel (Ni), benzene, carbon monoxide (CO), and ozone. These limit values establish the maximum permissible concentrations of these pollutants in ambient air to protect human health and the environment. The directives also define target values for certain pollutants to be achieved where possible and establish alert thresholds, which, when exceeded, require member states to implement specific measures to reduce pollution levels and protect public health. The directives outline various measures that member states must implement to improve air quality, such as the development of air quality plans, the promotion of cleaner technologies, the reduction of emissions from industrial activities and transport, and the implementation of measures to reduce household emissions.

1.3. PM sampling and metals determination

To monitor PM concentrations in atmosphere it is necessary to sample air PM. The methodology for sampling PM described in the standard EN 12341:2023 "Ambient air - Standard gravimetric measurement method for the determination of the PM_{10} or $PM_{2,5}$ mass concentration of suspended particulate" (UNI 2014) and it is based on the use of air samplers. Thanks to a size-selective inlet, particles with the desired dimensions of aerodynamic diameters are selected and drawn through a filter media at constant flow rate. The difference in filter weight before and after sampling provides the mass of these particulates. The weight gain of the filter is divided by the volume of air sampled to determine the concentration of suspended particulate matter in the specified size range (Pfeiffer 2015). The standard specifies the operational parameters such as sampling period (24 h) and sampler flow rate (2.3 m^3/h), the sampler design and filter characteristics. The main filter media are cellulose fibre, quartz/glass fibre, mixed fibre, and membrane filter type. The choice of the filter is important as substrates are sensitive to environmental factors such as relative humidity. There are several types of filter media and they are usually selected on the basis of the test method used to analysed them. The characteristics that should be taken into account in the choice of the filter medium are various. The filters should be: efficient, by removing more than 99% of the particles from the air drawn; mechanically stable, to minimize leaks and

wear during handling; chemically stable, not to react with the trapped air particles and to retain their porosity and structure (U.S. Environmental Protection Agency 1999).

To determine the concentration of metals in PM, filters should be analysed as described in the standard UNI EN 14902:2005 "Ambient air quality - Standard method for the measurement of Pb, Cd, As and Ni in the PM_{10} fraction of suspended particulate matter" (UNI 2005). According to the standard, after a microwave digestion of the air filter sample, the analysis is performed by graphite furnace atomic absorption spectrometry (GFAAS) or by inductively coupled plasma mass spectrometry (ICP-MS).

The GFAAA method is simple, quick, and applicable to a large number of metals in environmental samples. This technique consists in the absorption by free atoms in the gas phase produced by an atomizer of electromagnetic radiation at specific wavelengths, which are related to the element under investigation. The samples are generally injected into the graphite cuvette as solutions having volumes from 10 to 100 µl. Then the atomization is carried out at temperatures between 2000 and 3000° C. These temperatures produce a collection of gaseous atoms that are exposed to the radiation of hollow cathode. If the ashing step was performed under the proper conditions, little material should be left that might vaporize during atomization and interfere with the analysis. However, background correction devices available for atomic absorption spectrometers overcome these problems. Graphite furnace atomic absorption spectroscopy is not interference-free and can be influenced by the molecular form in which an element is present in the sample (Borges and Holcombe 2017).

On the other hand, ICP-MS is based on the use of a plasma obtained by triggering the formation of ions in a stream of argon through an electrical discharge and accelerating the latter with an oscillating magnetic field. Liquid samples are first nebulised in the sample introduction system, creating a fine aerosol that is subsequently transferred to the argon plasma. The high-temperature plasma atomises and ionises the sample, generating ions which are then extracted through the interface region and into a set of electrostatic lenses called the ion optics. The ion optics focuses and guides the ion beam into the quadrupole mass analyser. The mass analyser separates ions according to their mass-charge ratio, and these ions are measured at the detector. Sample preparation for ICP-MS is relatively simple: biological samples are usually diluted or thermally digested before analysis (Wilschefski and

Baxter 2019). In the case of air filters, the required sample pre-treatment is the microwave digestion.

However, it is well known that microwave digestion is associated with problems with the determination of trace elements in PM (Wang et al., 1996). The variety of matrix constituents, which include organic compounds, silicates and oxides, make PM membrane filters difficult to digest. When it comes to air filters, there are several factors that has a negative impact on the accuracy of ICP-MS analysis, such as sample digestion, air filter impurities, and post-digestion adsorption onto air filter material (Yang et al., 2012). To limit the problems related to the filter digestion, several combinations of different acids and filter substrate were investigated and published in the literature, and some examples are reported in Table 1.

Table 1 - Examples of digestion procedures for aerosol filters

Reference	**Digestion reagents**	**Type of filter**	**Subsequent analysis**
(Elsayed et al., 2021)	8 mL HNO_3 (69%) + 4 mL HF (40%) + 4 mL HCl (37%) + 35.5 mL H_3BO_3 (4%)	Teflon filter, quartz filter	ICP-MS
(Gemeiner et al. 2017)	10 mL aqua regia (22.3%)	Teflon filter, quartz filter	ICP-MS
(U.S. EPA 1999a)	55.5 mL HNO_3 (5.55%) + 167.5 ml HCl (16.75%)	cellulose fiber, quartz/glass fiber, mixed fiber, and membrane filter	ICP-MS, GFAAS
(Celo et al. 2011)	1) 2 mL HNO_3 (40%) 2) 1.5 mL HNO_3 + 3 µL HF 24 µL of 5% H_3BO_3	Teflon filter	ICP-MS, EDXRF
(Wang et al., 1996)	5 ml (1:2) HNO_3 + $HClO_4$- HF, H_3BO_3	Glass fiber filters	ICP-OES
(Smichowski et al., 2005)	100 ml aqua regia	Glass fiber filters	ICP-OES
(Menzel et al., 2002)	1 ml HNO_3, 0.1 ml HF	Cellulose acetate-nitrate filter	ICP-OES

According to the Directive 2008/50/EC, a Member State may employ any alternative method that it can prove produces outcomes that are comparable to those of any of the methods listed in the directive. In this case the results achieved by that method must be corrected to produce results equivalent to those that would have been achieved by using the reference method.

1.4. Alternative methods for metals determination

Since the standardized methods rely on acid digestion, their primary disadvantage is the time consuming, expensive, and environmentally unsustainable preparation procedure. Besides standardized methods, X-ray based techniques have been employed for the analysis of air filters because they are faster and cheaper, they do not need any sample pre-treatment and do not involve destruction or damage of the sample.

The foundation of X-ray fluorescence (XRF) analysis consists in an excitation and relaxation process within the atomic electron shell. When the X-ray beam hits a medium, X-ray photons are absorbed by the atom, which means that their energy is turned into kinetic energy for the orbital electrons of absorber atoms. The atom passes into an excited state by an external energy transfer and then return to the initial state on spontaneous emission of a photon. The energy of the original photon must be larger than the one of the ejected electrons. Because of the excitation state of the atom, an electron of a higher shell moves to the shell where the vacancy was created, emitting an X-ray photon. When this phenomenon occurs, also known as radiative relaxation, the emission of radiation of specific energy is induced, which is specific for the atomic species involved (Figure 3). The characteristic radiation emitted by the material allows to obtain qualitative and quantitative information about the composition of material (Adams 2017).

Even if not every outer electron is allowed to fill an inner vacancy, there are a lot of permitted transactions according to the selection rules of quantum theory. The principal lines or peaks that are generated are the three principal series: K, L and M, which emerge when the inner vacancy being filled is in the K, L or M shell. A series contains several peaks named K, L or M, which mainly differ according to the origin of the outer electron. The most intense peak is called α, the next less intense peaks in descending order are called β, γ, η and l. A further differentiation is made adding a a number as an index, such as α_1 and α_2 for the doublet (Klockenkämper and Von Bohlen 2015).

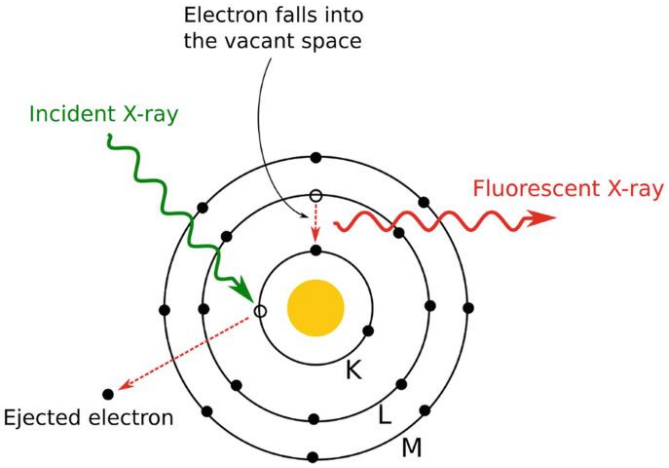

Figure 3 – Principle of X-ray K-shell excitation and fluorescent emission via electron de-excitation. (Vernekohl et al. 2018)

1.4.1. Energy Dispersive X-ray Fluorescence (EDXRF)

Energy Dispersive X-ray Fluorescence (EDXRF) is recognized as a proper technique for the determination of metals and metalloids for atmospheric PM filter samples by the United Stated Environmental Protection Agency (EPA) (U.S. EPA 1999b). Analytical procedures for calculating concentration in ng/m^3 for 44 elements that may be captured on common filter materials used in PM sampling are provided by the XRF method. The method can be applied to elemental analysis of a both fine and coarse particulate because matrix effects significantly vanish when the sample is a thin layer of particles. Also the European Joint Research Centre (JRC) evaluated the potential of EDXRF analysis for the measurements of heavy metals in PM (Yatkin et al. 2011). It was found that this calibration method is filter type and sampling site independent. Literature presents several examples of direct analysis of air filters with EDXRF spectrometers (Elias et al. 2023; Öztürk et al. 2011; Shaltout et al. 2020). The use of this technique for elemental determination in air filters was compared to several others, such as ICP-MS (Niu et al. 2010), particle induced X-ray emission (PIXE) (Calzolai et al. 2008), laser ablation ICP-MS and wet chemical digestion followed by ICP-MS (Brown et al. 2010).

1.4.2. Total reflection X-ray Fluorescence (TXRF)

Recently, also total X-ray fluorescence spectroscopy (TXRF), that represent a variation of the classical EDXRF, has emerged as a good alternative to the ICP-MS and GFAAS techniques for elemental analysis. TXRF is a ″micro-analytical″ technique, because only small amounts of sample, around 0.1 to 10 micrograms, properly deposited on a reflector are analysed (Ruiz 2014). TXRF has been widely applied in the environmental field, and literature presents several examples of application (Allegretta et al. 2019; Dalipi et al. 2017; Marguí et al. 2010). Since TXRF has detection limits that are several orders of magnitude lower than those of standard XRF, it is a valid tool for surface characterization or trace analysis.

The distinction between EDXRF and TXRF is based on the geometry of the experimental configuration of detector and incidence beam. In the conventional setup the detector is positioned at 45° with respect to the sample. The incidence beam hits the surface of the sample with an angle of 45° and the detector is positioned at 90° with respect to the X-ray source. In TXRF spectrometers, the sample is irradiated with a few milliradians grazing angle and the detector is placed at 90° angle on the top of the sample, at a distance of a few millimetres (Adams 2017). Due to this grazing incidence, the primary beam shaped like a strip of paper is totally reflected at the sample support. Figure 4 shows the main geometric difference between EDXRF and TXRF instruments.

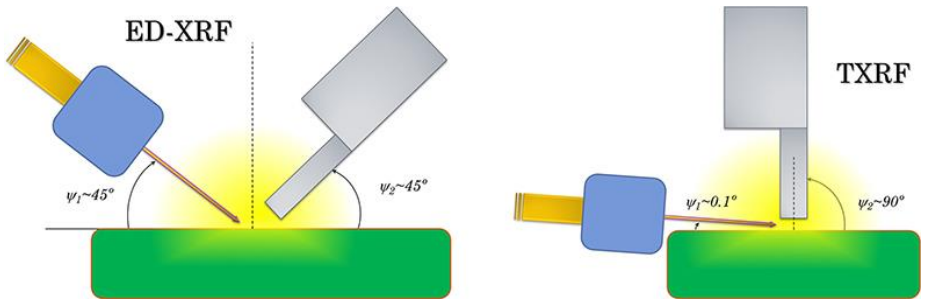

Figure 4 - Comparison between EDXRF and TXRF instrumental setup (Fernández-Ruiz 2019)

The path of an X-ray beam varies from the original when it finds new medium. This means that part of the X-ray beam is reflected toward the first half and the remaining part is

refracted into the second half. The incident angle α_1 and the refracted angle α_2 are both defined by the X-ray beam with respect to the interface according to the Snell's law:

$$n_1 \cos\alpha_1 = n_2 \cos\alpha_2$$

where n_1 and n_2 are the refractive indices of media 1 and 2 respectively (Ruiz 2014)

When the incident X-ray beam is entirely reflected by the sample's surface, with the exception of a small amount that is refracted and penetrates the reflecting medium, the sample is said to have accomplished total reflection. As the penetration increases, the intensity of this evanescent wave decreases exponentially. This condition occurs for angles lower than the critical angle characteristic of the material of the reflector (Wobrauschek 2007). At the critical angle (α_c), the reflectivity of the material increases at its maximum and the penetration depth of the primary beam decreases rapidly to a few nanometres. The penetration depth is low and reflectivity is high below this angle. On the other hand, the reflectivity quickly reduces, and the penetration depth rises if the primary beam strikes the sample at an angle greater than the critical angle (Martina Schmeling 2019). For many materials the angles involved are small, commonly a tenth of a degree and can be easily calculated. For incidence angles lower than α_c, Snell′s law does not give real values for the angle of refraction α_2. In this case, the X-ray beam does not penetrate in the second medium and the interface behaves like a mirror close to the ideal, fully reflecting the incident beam to the first medium. Consequently, for angles below the critical angle, the incident beam interferes constructively with the reflected beam, generating a field of X-ray standing waves (XSW). In this condition, the sample is excited twice: once by the incoming beam and once by the reflected beam, leading to an amplification of the atomic X-ray fluorescence signal. As a result, only a small portion of the sample is analysed; therefore, in order to maximize the fluorescence of the sample it is crucial that the sample is placed precisely inside the standing wave field. The fluorescence intensity is angle dependent as well, since the reflectivity reaches its maximum at the critical angle.

When dealing with TXRF analysis it is convenient to work with thin-film samples for various reasons. When a generic sample is excited to X-ray fluorescence, the intensity of the spectral line of an element is proportional to the concentration of the analyte. This proportionality, however, is not linear because the fluorescence intensity depends also on the mass-absorption coefficient, that measures the effects of matrix composition and represents one of

the main difficulties in calibration (Klockenkämper and Von Bohlen 1989). This coefficient summarizes all possible photon interactions with atoms of that element, and it is a function of the incident photon energy. The self-absorption effects depend on the path length from the sample surface to the location of the atom of interest as well as on the path length from the fluorescing atom through the sample in the direction of the detector (Kregsamer 2009). Another issue that must be taken into account is the presence of secondary fluorescence. A thin-film specimen overcomes both of these challenges. The analysis line intensity for infinitely thin films is directly proportional to the analyte concentration c_j and sample thickness t:

$$N_j \approx c_j K_j t N_0$$

where: N_j net intensity of the spectral line of element j

c_j concentration of the analyte j

K_j proportionality factor for the analyte line

t thickness of the sample

N_0 intensity of the incident monochromatic primary beam

TXRF has been employed for the elemental analysis of PM filters, after microwave digestion of the filter sample (Boman et al., 2010; M. Schmeling 2001), or after cold plasma ashing (Wagner and Mages 2010), or leaching (Samek et al. 2006). By pre-treating the filter sample, however, one of the main advantages of TXRF analysis, which is its non-destructive nature, is lost. Fomba et al. (2020) avoided the digestion step by punching some air filters and placing the cutoff pieces on polished quartz carrier substrates, spiking them with concentrated nitric acid prior TXRF analysis.

1.5. Innovations for sample preparation and elemental analysis

Since EDXRF spectrometers were already employed in the direct analysis of air filters, researchers of the Chemistry for Technologies (Chem4Tech) lab of the University of Brescia came up with the idea of using total reflection X-ray fluorescence (TXRF) spectrometer to directly analyse PM filters. For a case study there was a very large number of PM filters to be analysed (Borgese et al. 2011). The use of conventional analysis techniques would have

required lots of time, destruction of the samples, and above all, a great amount of acid to perform microwave digestion. A greener and faster alternative is represented by TXRF spectrometer, that can be employed to perform a direct analysis of the filters. Teflon filters usually employed to sample air PM are equipped with a plastic ring to stretch the filter and avoid crushing. This ring, however, impedes the passage of X-ray beam when the filter is analysed with TXRF spectrometer. Consequently, the filters were cut in a disc of 30 mm diameter, to remove the ring and match the dimension of the sample carrier used in TXFR analysis. Samples were then plasticized between two thin polymeric foil to avoid material losses and sample contaminations.

This procedure for filter preparation was further investigated the following year (Borgese et al. 2012). Some thin film reference samples were prepared by Atomic Layer Deposition (ALD) depositing titanium dioxide on Teflon filter. These filters were analysed with TXRF spectrometer and used to build a calibration curve, that was used for quantification purposes. Results showed a very good linear correlation between Ti K-alpha peak area and number of ALD cycles, which is linear with mass. This study proved that it is possible to measure air filters with a TXRF spectrometer and perform elemental quantification exploiting the external calibration approach.

Since the filter preparation procedure was satisfactory, it was employed for a source apportionment study (Bilo et al. 2018). This study was conducted in an area close to Brescia, where anthropogenic pollution had contaminated the air and soil, and higher Mn emission were noticed. PM was collected on commercial Teflon filters with 37 mm diameter and then plasticized and cut in a diameter of 30 mm diameter. Both a qualitative and semi-quantitative analysis were performed, using different XRF techniques. More specifically, micro-XRF was used to evaluate the chemical composition of PM deposited on the filters. For semi-quantitative analysis, the samples were analysed with XRF in grazing incidence configuration with synchrotron radiation (SR-XRF) and benchtop TXRF instrumentations.

Finally in 2020 the method for quantitative analysis of air filters with TXRF spectrometer was presented (Borgese et al. 2020). For the assessment of the method some reference materials were needed. Reference samples of PM filters were provided by the Air Quality Research Centre of the University of California Davis, and they consisted in mono-element PTFE filters, characterized by a lead deposition (Yatkin et al. 2016). Samples were analysed

with a custom made TXRF spectrometer equipped with a Rh excitation source. Calibration line was build analysing the detected lead fluorescence intensity and the lead loading onto the filters, and it was built analysing the set of samples for both 5 minutes and 10 minutes. Low detection limit was reached (0.048 μg/cm^2), proving the applicability of this method for environmental monitoring purposes.

It is important to note that a plasticized filter does not represent an ideal sample for TXRF analysis: it is not reflective, not flat, the mass is not negligible and consequently the total reflection condition is not satisfied. For this reason, it is improper to state that TXRF analysis of the samples is performed, because the foundations of total reflection are not respected. Nevertheless, TXRF spectrometers can be employed for the analysis of air filters. The resulting analysis can be defined as an analysis under grazing incidence condition, because the incoming X-ray beam hits the sample at a very small angle.

1.6. Standardization activities

The direct analysis of air filter with X-ray based instruments was proposed to the International Organization for Standardization (ISO) under the name ISO 23971 "Grazing Incidence XRF Analysis of air filters", in the technical committee ISO/TC 201/SC 10 "X-ray Reflectometry (XRR) and X-ray Fluorescence (XRF) Analysis". It was proposed in 2018 and approved as a working item (AWI) in 2022. The standardization of this method would promote air quality monitoring because it allows for easy and fast checks of air pollution. This is of substantial importance also to obtain reliable information for health protection.

The pre-normative activities related to this project were conducted within the scope of a Versailles Project on Advanced Materials and Standards (VAMAS), specifically A34 "Analysis of air PM filters by XRF under grazing incidence", related to the development of reference material (VAMAS 2023). The proposed method for filter analysis, indeed, is based on the use of reference materials to build calibration lines.

The standardization of this method was supported also by the Cost Action (CA) 18130 "*European Network for Chemical Elemental Analysis by Total Reflection X-ray Fluorescence*" (ENFORCE TXRF) (COST 2019) The CA had a duration of 4 years and it

ended in September 2023. It was chaired by Prof. Laura Borgese, and it was made up of 110 members in 24 Countries.

The main aims and objectives of the Action are to coordinate the efforts made at the national and international level to establish TXRF as a reference technique for reliable elemental analysis of solid and liquid matrices. The goal is to employ TXRF technique for both fast screening and accurate quantitative determination of potentially toxic elements, for health and safety reasons. ENFORCE TXRF is organised in four working groups. In particular, working group 2 "*Metrology and Standardisation*" supported the development of the ISO 23971, because its main goal is establishing TXRF as a reference technique for reliable elemental analysis, both for screening and accurate quantitative determination. Pre-normative research activities were contextualized also in the context of working groups 3 "*Sample preparation and Analytical procedures*", which supports the development of specific sample preparation methods and analytical procedures, considering the characteristics of samples, and the development of sample treatment procedures within the framework of green analytical chemistry, such as the plasticization procedure of the filters.

1.7. Objectives of my PhD thesis

This doctoral thesis is aimed at supporting the development of the draft of the ISO 23971 standard. Calibration samples of PM filters were created and analysed with different instruments in several laboratories, in order to test method for direct analysis of filter proposed to ISO community. The results are here presented and discussed.

Collaborative research activities were carried out in the context of COST Action 18130. The Action, indeed, reaches its objectives by creating an infrastructure for scientific communication, exchange, collaboration, fostering new research activities.

2. INSTRUMENTATION

The main goal of this doctorate was to prove that it is possible to analyse directly air filters with X-ray based instrument, to obtain elemental information about the PM composition in a fast way, without destroying the filter sample. The development of an analytical method is founded on three pillars:

1. reference materials (RMs),
2. robust instrumental setup,
3. calibration curves for quantification.

Part of the activities of this doctorate were devoted to the development of calibration samples of PM filters, to test the method of direct analysis of air filters with X-ray based instruments with different spectrometers. Then the measuring conditions were deeply studied and optimized in order to analyse these samples. Finally, part of the activities consisted in the analyses of the developed calibration samples with several XRF spectrometers, to build calibration curves.

Calibration samples were analysed with various instruments to perform a complete characterization and to build calibration curves to support the development of the ISO standard 23971.

2.1. XRF instruments

Samples were analysed with several X-ray fluorescence-based instruments in the laboratory and at synchrotron, following described.

- Bruker EDXRF S2 Ranger, equipped with a Pd X-ray tube, with a maximum power of 50 W. A XFLASH™ Silicon Drift Detector (SDD) with a resolution of 129 eV at Mn-Kα was used. The instrument is also equipped with nine primary filters that can be selected to improve measuring conditions for elements of interest. In this case, measurements were performed at 40 kV and 0.61 mA in helium, with a 500 µm Al filter. The measuring time is set at 200 s and the measured area has a diameter of 28 mm.

- Jeol EDXRF JSX-1000S, equipped with a Rh X-ray tube, operating at 50 kV, 0.03 mA. JEOL's own SDD and newly developed optical system, in combination with filters designed to handle the entire energy range, make it possible to achieve high-sensitivity analysis. It is equipped with 3 collimator types: 0.9, 2, 9 mm. to analyse the samples the measuring time is set at 300 s and a 9 mm collimator was used.

- Shimadzu EDXRF EDX-7200, equipped with a Rh X-ray tube and a high-resolution SDD detector to achieve a higher count rate and detection efficiency. It has an automatic collimator switching in four stages: 1-, 3-, 5-, and 10-mm diameter. The measuring time is set at 300 s, and a 10 mm collimator was used.

- Rigaku EDXRF NEX CG II, equipped with a Pd X-ray tube, operating at 50 kV and 1 mA. A 20 mm collimator is used, and the measuring time is set at 100 s. A Mo secondary target was used to detect Ni, As, Pb, Zn, Cu and a Cu secondary target to detect Ti, V, Mn and Fe.

- Bruker TXRF S2 Picofox is equipped with a Mo X-ray tube and operates at 50 kV and 0.75 mA and multilayer monochromator and silicon drift detector of 30 mm^2 area. The beam is not focused, and the measuring time was set at 600 s to measure the samples under study. Each sample was measured 3 times, after a rotation of approximately 120°. The spectral fitting and deconvolution were performed by the SPECTRA instrument software.

- Bruker TXRF S4 T-STAR® is equipped with three different excitation sources: Mo-K (17.5 keV), W-Brems (35 keV), W-L (8.4 keV); with all excitations the instrument operates at 50 kV, 1 mA. The measurement time is set at 600 s for Mo-K measurements and 1000 s for W-Brems measurements. All measurements are performed in air.

- Rigaku TXRF Nanohunter II is equipped with a Mo X-ray tube, operating at 50 kV and 12 mA, and a SDD detector with an area of 50 mm^2. It allows for angular scans, in the range from 0° to 0.5° and permits the selection of the desired glancing angle and converging angle. Measurements time is set equal to 600 s.

- GNR TXRF Horizon is equipped with a Mo X-ray tube, operating at 40 kV and 15 mA, and a SDD detector with an area of 20 mm^2. All measurements are performed for a time interval of 300 s.

- Atominstitut custom made TXRF Wobicompact is equipped with a Rh X-ray tube operating at 50 kV and 1 mA. It has a 150 mm^2 area SDD (Ketek) and a CCD camera for beam alignment purposes and angle control. It allows manual angular scan by screw rotation with height step width of ±10 μm. The measuring time is set at 600 s.

- GNR Diffractometer Explorer, equipped with a Mo X-ray tube and a Silicon Drift Energy Dispersive detector of 20 mm^2 area to collect fluorescence spectra in total reflection mode. The instrument is then equipped with an X-ray reflectivity (XRR) detector The direct drive torque motors motion in θ-θ geometry, the 240 mm goniometer radius and the motorized (z, χ, ϕ) axes sample stage (Figure 5) provided high accuracy and flexibility in sample positioning and fluorescence signal enhancement. The incidence angle can be scanned with a step of ± 0.0001° thanks to optical encoders, while the sample height minimum adjustment was less than 1 μm. Figure 6 shows the instrumental setup of the diffractometer.

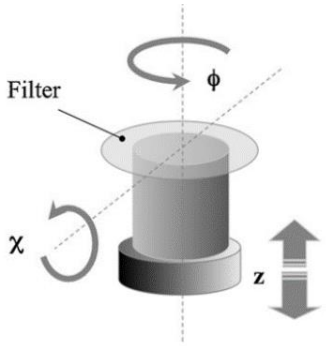

Figure 5 – Motorized axes available on the sample stage of the Explorer diffractometer.

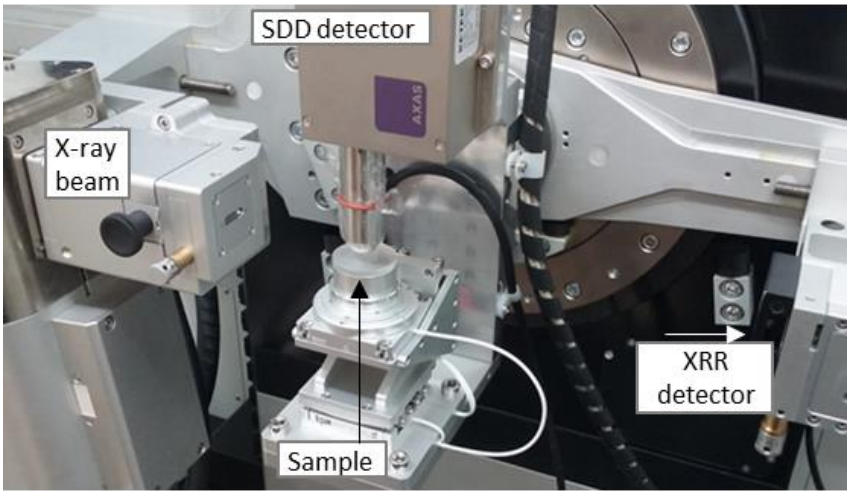

Figure 6 - Setup of the diffractometer Explorer, GNR

- Fischerscope micro-XRF X-ray XDV-SD, equipped with a small spot X-ray beam. It is equipped with a low-power W X-ray tube operating at a maximum power of 50 W (operating at fixed voltage of 10, 30 and 50 kV and within a range of 0.1 to 1 mA), and a Si-PIN semiconductor detector (Peltier cooling at -50 º C) with an energy resolution of 180 eV at 5.89 keV (Mn Kα line). A set of primary filters can be selected to improve measuring conditions for elements of interest. Measurements are performed at 50 kV and 1 mA, with a 1000 µm Al filter. The use of an XYZ programmable motorized stage enables fully automatic measurements. The instrument is controlled by the WinFTM® - V.6.20 software, which is also used for both spectral acquisition and spectral data treatment. Measurement time was set at 300 s for the line scans and 30 s for the 2D maps.

- Horiba Micro-XRF XGT-500, used to obtain the fluorescent X-ray image (or map) of a sample. It is equipped with a Rh X-ray tube and a X-Y stage to scan the sample. This instrument is equipped with capillary lenses with diameters of 10 and 100 µm. Tube voltage and current were run at 50 kV and 1 mA, respectively.

- Bruker micro-XRF M4 TORNADO, optimized for high-speed analyses of points, lines and 2D area scans (element mapping) of any kind of sample. it is very useful to get information about composition and element distribution, even from below the surface. The primary X-ray excitation uses a poly-capillary lens offering small spot

sizes (25 µm) and high X-ray intensity, with a stage speed up to 100 mm/s. It is equipped with a Rh X-ray tube operating at 50 kV and 0.6 mA.

- Additional measurements were performed at the XMaS/BM28 beamline at the European Synchrotron Radiation Facility (ESRF) in Grenoble, where the beam was monochromatized to an excitation energy of 17.452 keV (Mo). The Vortex® SDD detector, of 50 mm^2 area, is protected with a 25 µm thick Be window. During measurements, the sample was placed on a Si wafer to avoid scatter signals. As it can be seen from the Figure 7, on the top of the sample there is the fluorescence detector, while the XRR detector is positioned opposite to the direct beam.

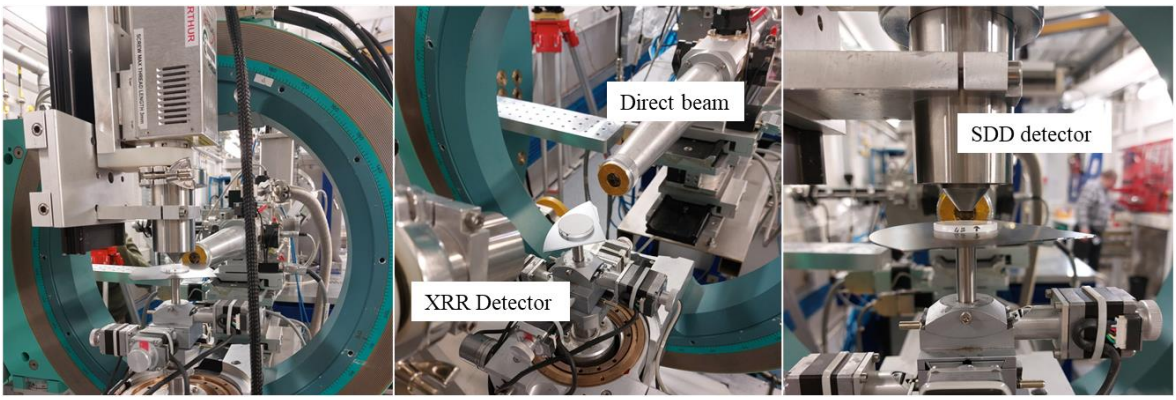

Figure 7 - Instrumental setup at ESRF in Grenoble

Table 2 at the end of this chapter summarized the main features of these spectrometers.

2.2. Other instruments

Inductively coupled plasma-mass spectrometry analysis was performed to evaluate the elemental concentration of the samples. This is indeed the reference method for filter analysis provided by the directive. The study of (Celo et al. 2011) was taken into account in the selection of the digestion procedure of the filters.

The plastic ring stretching the PTFE membrane was removed prior the digestion, the filter was cut in small pieces and placed in a PTFE vessel in the microwave digestor (Berghof Speedwave XPERT). The digestion of the filters was performed using a mixture of nitric acid, hydrofluoric acid, and hydrogen peroxide (7:2:2). In a first digestion cycle, samples

reached a temperature of 130 °C in 15 minutes and were kept at this temperature for 3 minutes; then the temperature reached 200 °C in 15 minutes, and it stayed constant for 20 minutes. After cooling, 0.25 g of boric acid was added to all the vessels and a second digestion cycle was performed: in a 5-minute ramp the temperature of 180 °C was reached and kept for 10 minutes. The obtained digested sample was diluted up to 15 ml with ultrapure water and 5 ml was extracted for ICP analysis. Eleven materials of reference were prepared to calibrate ICP-MS, adding mono-element standard in a matrix made of nitric acid and boric acid in the same proportion as in the PM filter sample digests.

All these analyses were performed thank to collaborations with laboratories of other universities and research centres. Several instruments were used during a research period abroad of three months at the University of Girona, in the Department of Chemistry. Then, two Short Term Scientific Mission (STSM) were supported by the COST Action 18130: one at Bruker GmbH, in Berlin, of 1 week duration, and a second one in the Department of Chemistry and Bioengineering of the Osaka Metropolitan University, in Japan, lasting for 3 weeks. During this second STSM it was possible to visit and perform some measurements at the headquarter of Rigaku in Osaka. The CA ENFORCE TXRF also funded an experimental session at ESRF in Grenoble. Additional experiments were held at G.N.R. Analytical Instruments Group, located in Novara, which is an Italian producer of advanced analytical instruments.

Table 2 - List of X-ray based instruments used to analyse the calibration samples.

Instrument type	Producer	Model	Excitation source	Voltage [kV]	Current [mA]	Atmospheric conditions	Measuring time [s]	Additional info	Location
EDXRF	Bruker	S2 Ranger	Pd	40	0.61	Helium	200	500 µm Al filter	University of Girona
EDXRF	Jeol	JSX-1000S	Rh	50	0.03	Air	300	9 mm collimator	Osaka Metropolitan University
EDXRF	Shimadzu	EDX-7200	Rh	50	1	Air	300	10 mm collimator	Osaka Metropolitan University
EDXRF	Rigaku	NEX CG II	Pd	50	1	Air	100	3 secondary target: Al, Mo, Cu. 20 mm collimator	Rigaku, Osaka
TXRF	Bruker	S2 PICOFOX	Mo	50	0.75	Air	600		University of Brescia
TXRF	Bruker	S4 T-STAR	Mo, W	50	1	Air	600		Bruker, Berlin
TXRF	Rigaku	Nanohunter II	Mo	50	12	Air	600	Angular scan option	Osaka Metropolitan University
TXRF	GNR	Horizon	Mo	40	15	Air	300		GNR, Novara
TXRF	Atominstitut	Wobicompact	Rh	50	1	Air	600	Angular scan option	University of Brescia
Difrattometer	GNR	Explorer	Mo	50	10	Air			GNR, Novara
Micro-XRF	Fisherscope	XDV-SD	W	50	1	Air	300 for line scan 30 for 2D map	1000 µm Al filter, 3 mm collimator	University of Girona
Micro-XRF	Horiba	XGT-500	Rh	50	0.5	Air	20		Osaka Metropolitan University
Micro-XRF	Bruker	M4 TORNADO	Rh	50	0.6	Air			Bruker, Berlin

3. PROOF OF CONCEPT

The possibility of using TXRF spectrometers for analysing directly air filters was proven in (Borgese et al. 2020) using a custom-made instrument. The first step of this doctoral research consisted in testing the applicability of the method with commercially available TXRF spectrometers. Results were published in (Cirelli et al. 2022).

3.1. Materials and methods

The same set of samples analysed in Borgese et al. (2020) are taken into account. Sample consists in lead-loaded reference filters, provided by the Air Quality Research Centre, University of California, Davis (AQRC-UCD), USA. They are four mono-element Pb loaded samples, one multi-element sample containing Pb, and one blank. The Pb mass loaded on the filter membrane for each sample varies from 0.028 to 10.2 μg/cm^2 (Table 3). The PTFE filters used to collect PM are manufactured by Pall (47 mm diameter, 2 μm pore size, 46 μm thickness, Pall Life Sciences, Ann Arbor, MI, USA). These are equipped with a polypropylene ring as a mechanical support structure (Yatkin et al. 2016, 2018). This plastic ring however impedes the passage of the X-ray beam when the filter is analysed with a TXRF spectrometer (Bacon et al. 2019). Filters were sandwiched between two thin transparent sheets of polypropylene (PP, thickness of about 75 μm), removing the plastic ring stretching the PTFE filter, and avoiding material loss. Then, the samples were cut into a disc of the same dimensions of the standard commercially available quartz support (30 mm diameter) and fixed with a spray glue or a silicone grease onto a quartz carrier reflector, before being inserted in the TXRF spectrometer.

Table 3 - Analysed samples and their corresponding elemental loadings.

Sample	**Pb loading [μg/cm^2]**
Blank	0
Multi-elemental (ME)	0.028
Pb 070	0.59
Pb 007	0.685
Pb 078	4.2
Pb 081	10.2

Three different commercial TXRF spectrometers, all providing a monochromatic Mo Kα radiation by means of a multilayer monochromator, are employed in this work: the S2 Picofox (Bruker Nano GmbH), the Nanohunter II (Rigaku) and the Horizon (GNR srl).

With the Nanohunter II spectrometer the reference samples were measured setting the glancing angle at 0.3°. The type of the analysis performed can be defined as a XRF analysis under grazing incidence, using TXRF spectrometers, as the samples under study do not comply with the TXRF conditions, due to their thickness and morphology. Lead loaded reference samples were measured at a fixed geometrical configuration for each spectrometer to identify the contribution of: (1) repeatability of the acquisition, by measuring the analysis sample four times without removing it from the measurement position; (2) repeatability of the alignment, by measuring the sample four times removing it from the measurement position which is set automatically (i.e. taking the sample in and out), but without removing it from the sample holder; (3) sample orientation, repeating the measurement in condition (2) after rotating the sample by 90◦ around its surface axis (azimuthal angle), according to what is reported in (Borgese et al. 2020). Of notice that (2) and (3) are dependent on systematic instrumental contributions linked to those instruments of fixed mechanical design.

3.2. Results and discussions

The spectra of the Pb 070 reference sample measured with the three spectrometers are compared in Figure 8. The substantial differences, notably in the intensity of the emitted signal, are the results of various contributions: tube voltage, current, use of possible excitation modifiers (as beam filters and optical focusing elements), beam footprint on the sample, X-ray glancing angle, detector active area, or sample-detector distance (Klockenkämper and Von Bohlen 2015). The glancing angle cannot be modified in the S2 Picofox and the Horizon, and it is fixed at about 0.07° and 0.08° respectively, with respect to a plane defined by three pins touching a rigid and flat reflector surface. The real angle of incidence on the filters, that are rough and soft, cannot be known precisely. The Nanohunter II allows to choose a glancing angle between 0 and 0.5°, and has a different alignment system, where the sample is lifted until contact with two stopping bars. Usually, the glancing angle is set to around 0.05 degree for TXRF analysis with quartz reflectors. The angular scan

shows that the Pb L_α fluorescence intensity increases with increasing angle of incidence, (Figure 9). The angle value was set to 0.3° for the measurements as the corresponding Pb L_α fluorescence intensity was high while the angle was still far enough from the highest value of the angular range.

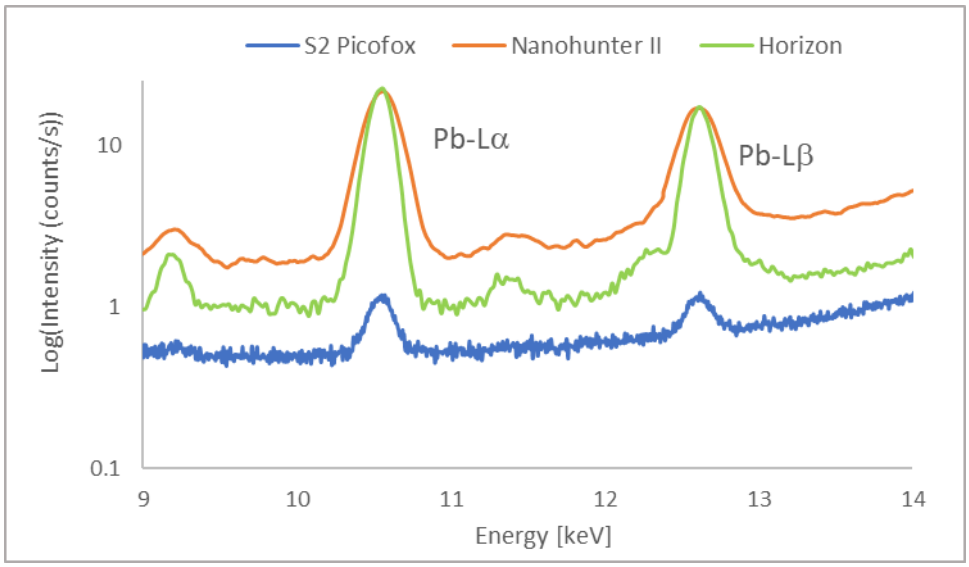

Figure 8 - Spectra in logarithmic scale of the same sample Pb 070 obtained with Horizon, S2 Picofox and Nanohunter II spectrometers.

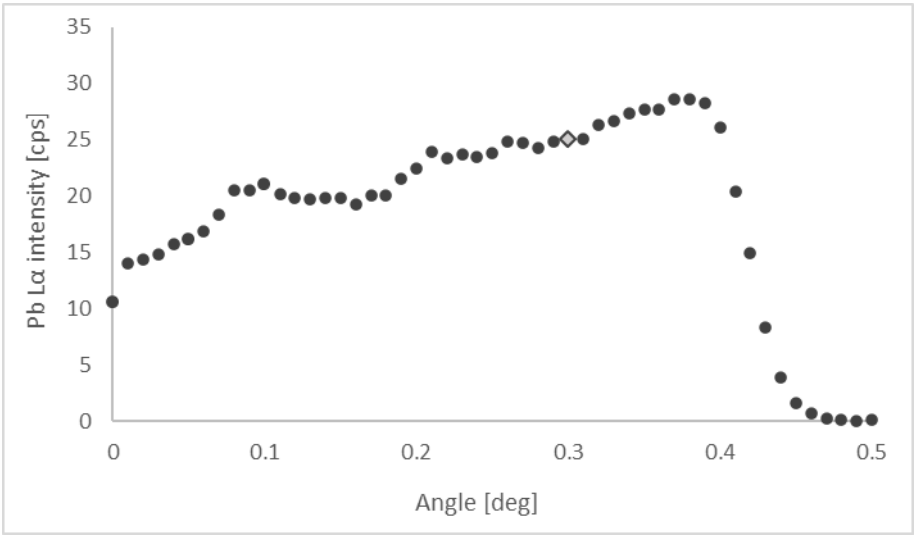

Figure 9 - Angular dependence of the fluorescence emitted intensity, for the sample Pb 070 sample, acquired with the Nanohunter II spectrometer, up to 0.5° corresponding to the limit of the angular scan range.

A direct comparison of the instrument software performances was not possible as the instrumental and experimental parameters were different, with e.g. different dead and acquisition times, X-ray sources and detectors parameters. It is worth noting that such comparison should be implemented on normalized data, based on the contributions of e.g. detector dead time, X-ray flux and acquisition time. In-depth analysis of the related contributions of the X-ray source, detector and other parameters considered by the software during spectra fitting is needed and will be addressed in future works.

The spectra acquired with the three spectrometers were analysed with the same software, the open-source software PyMca (Python multichannel analyser) (Solé et al. 2007), setting the same parameters for evaluating the intensity of Lα and Lβ emission lines of lead. PyMca allows both to extract peak integrated intensities by fitting the theoretical atomic X-ray emission spectra to the experimental one, and peak integrated net intensities by fitting and subtracting the background, as well as to quantify elemental composition through the fundamental parameters' method (Solé et al. 2007).

In the evaluation of the lead fluorescence peaks, the sum of the $L\alpha_1$ and $L\alpha_2$ lines is labelled as the Lα line, while the sum of the $L\beta_1$ and $L\beta_2$ as Lβ. Figure 10 displays the average (over minimum 8 spectra for Nanohunter II, 3 for S2 Picofox and 10 for Horizon) net intensities obtained after spectra fitting, as a function of the Pb mass deposited on the filter. A first evaluation of linear regression based on the coefficient of determination (R^2) is performed. The linear regression of the Horizon data in Figure 10.c shows a coefficient of determination equal to R^2=0.967. Data reported in Figure 10.a, and Figure 10.b for Nanohunter II and S2 Picofox respectively, show that the linear correlation is much worse and standard deviations are higher. On this basis, the accuracy cannot be considered sufficient to proceed with definition of the linear calibration range, LOD (limit of detection) and LOQ (limit of quantification) for the Nanohunter II and the Picofox. Further investigations will be needed to understand the instrumental issues affecting the results. The LOD of a method is defined as the smallest measured concentration of an analyte that is distinguishable from the method blank with a confidence level of 99%. The IUPAC method of the blank analysis was applied considering the uncertainty of ten measurements of the blank sample converted to concentration using the regression equation over the linear calibration range (IUPAC 1997; U.S. EPA 2016). The LOQ was calculated with the same approach, using the multiplication factor of 10 instead of 3 used in the LOD. The obtained LOD is 0.0065 μg/cm^2, and the LOQ

is 0.0131 μg/cm^2. The LOQ is satisfying as it is lower than the concentration of the reference sample with the smallest mass deposition (ME sample = 0.028 μg/cm^2). Moreover, as the threshold of lead concentration in air has been established equal to 0.5 μg/m^3 by both EU and WHO, the presented method can be successfully applied for environmental purposes. Indeed, the threshold Pb concentration corresponds to a Pb mass deposition of 0.415 μg/cm^2 on a 47 mm diameter filter sampled for 24 h at 10 L/min, which is included in the linear calibration range of the method retrieved with the Horizon.

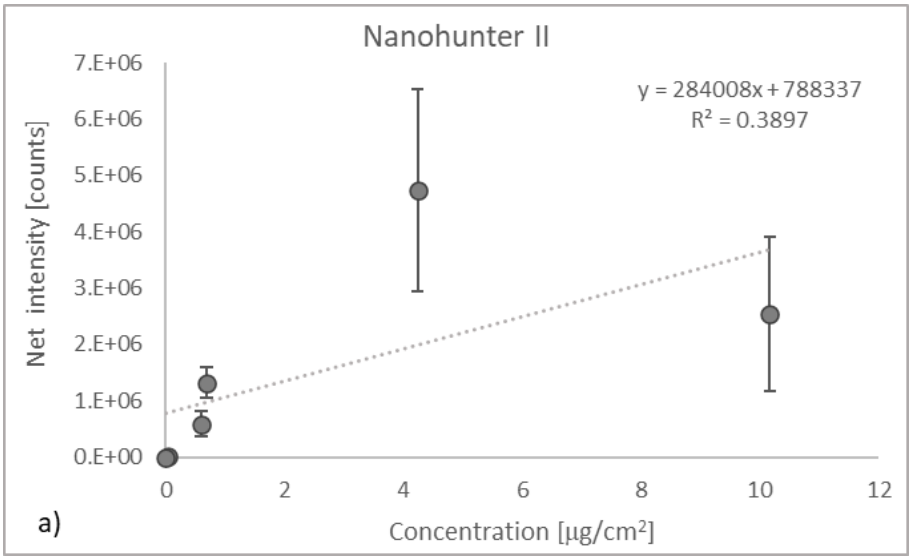

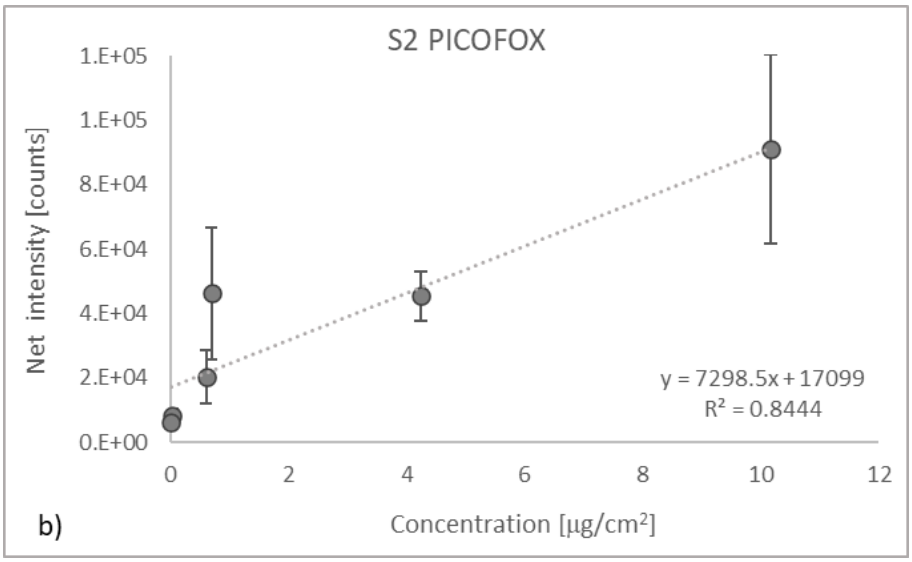

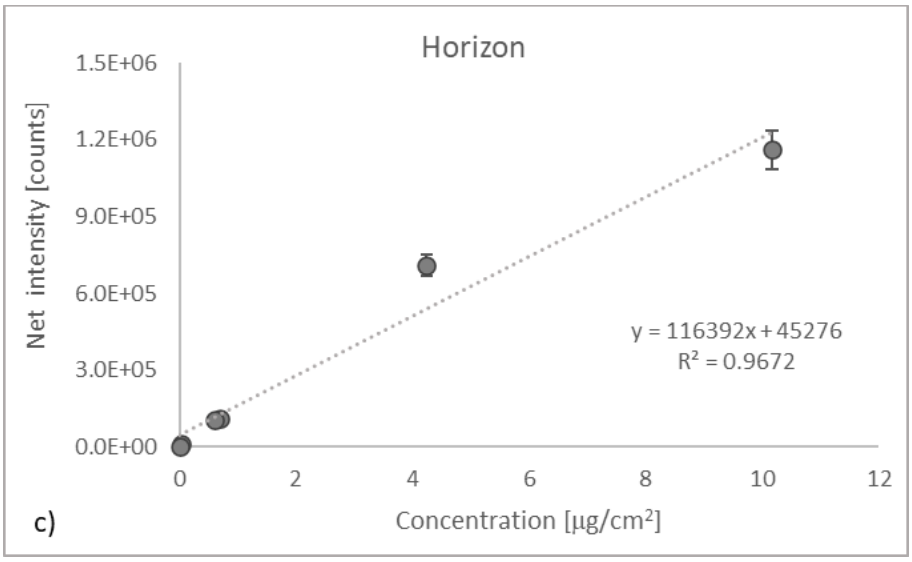

Figure 10 - Average Net Intensity of Pb Lα and Lβ, obtained as a function of mass deposition of the six reference samples, measured with three spectrometers: a) Nanohunter II, 8 replicates per sample; b) S2 Picofox, replicates per sample; c) Horizon, replicates per sample. Error bars represent the standard deviation of the average over the set of measurements.

Relative standard deviations calculated over the whole set of the available measurements in the three conditions stated above are reported in Table 4. As previously mentioned, and reported in (Borgese et al. 2020), three contributions can be assessed: repeatability of the acquisition (1), repeatability of the alignment (2) and sample orientation (3). The first two contributions are related to the instrumental configuration (X-ray flux, detector response, glancing angle, sample to detector distance). While the third parameter is sample dependent, it is dependent from the two previous contributions, and cannot be separated as the sample is extracted from the measuring position to be manually rotated around its centre. To distinguish the different contributions, the average RSD of the net integrated intensity for each set of measurements obtained in the three conditions (1, 2, and 3) is reported in Table 4, excluding the blank sample. Other unknown contributions may affect the results, but it is extremely difficult, even impossible to evaluate them with "blocked" configuration instruments like those considered in this study.

Table 4 - RSD (%) of the net integrated intensity average values of Pb Lα+Lβ of the measurements performed to evaluate (1) repeatability of the acquisition, (2) repeatability of the alignment and (3) sample orientation. Four measurements were considered for each condition. Not all the samples were measured in the aforementioned conditions; therefore, only available data are reported.

	RSD (%)								
	Nanohunter II			S2 Picofox			Horizon		
Conditions	(1)	(2)	(3)	(1)	(2)	(3)	(1)	(2)	(3)
Pb 081	5	14	85	-	-	19	1	1	11
Pb 078	5	4	71	-	-	21	1	1	9
Pb 007	-	13	29	9	18	58	2	1	10
Pb 070	3	8	59	-	-	61	4	4	9
ME	10	16	-	-	-	0	3	1	2
Average	6	11	61	9	18	31	2	2	8

The contribution of the counting statistics is always lower than the positioning inside the sample holder in the Nanohunter II and S2 Picofox, while these are similar for the Horizon spectrometer. This may be due to a higher precision in sample repositioning at the measurement stage (various distances and beam glancing angle), which relies on the mechanical alignment tools used by the instrument (bars or pins). Indeed, for the Horizon, no variation in the data could be appreciated. In the Nanohunter II case, a variation of about 11% in the Pb integrated intensity was observed for conditions (2), which, in addition to a general lack of repeatability in the positioning of the sample, can also be interpreted as an uncertainty in the angular positioning, lateral positioning and sample-to-detector distance. A similar behaviour may be expected for the S2 Picofox spectrometer. The angular dependence of the fluorescence intensity is a well-known phenomenon in XRF analysis (Klockenkämper and Von Bohlen 2015). The third factor highly depends on the sample orientation but cannot be distinguished from all the other instrumental contributions and presents higher RSD (%). For a quantitative analysis undertaken with an internal calibration standard, provided the latter is carefully selected, this dependency is compensated (to a large extent). However, such approach is not applicable in the case of PM filters analysis, for which the elaboration of an external calibration curve, based on the net intensity values, is required. In addition,

the higher variability in the results obtained, together with the contribution of sample orientation, might be attributed to the beam footprint (area of the sample illuminated by the X-ray beam) and the detector active area. In this case, both alignment issues, and particle size and distribution of the sample are particularly relevant. The maximization of the illuminated area by the incoming X-ray beam improves measurement repeatability. This is supported by the comparison with the previous study (Borgese et al. 2020), where better RSDs were obtained with the custom-made instrument, after selecting the best measurements conditions in terms of sample positioning and glancing angle. As the configuration of each instrument has not changed over the measurements, a change of the glancing angle in the mechanical mounting process of the sample, which is not perfectly flat, and rigid may have occurred. This small inclination would influence the fluorescence intensity by changing the analysed volume, resulting in large RSDs.

3.2.1. Absorption effect

A more thorough statistical approach similar to the one implemented in (Borgese et al. 2018) for the validation of TXRF analysis of water was adopted to assess absorption effects on the calibration curve of the Horizon. Indeed, a linear correlation between net integrated intensities and mass loading is expected if negligible or constant matrix effects are present, while a quadratic regression is expected if increasing absorption levels occur with mass loading. In brief, the Mandel Test was performed to assess whether a quadratic model better fits the dependency between the analyte net intensities and their related concentrations than a linear model (Andrade and Gómez-Carracedo 2013). This test, based on the sum of the squared residuals of the two models, revealed that the quadratic model is more suitable for fitting the data, as displayed in Figure 11. The lack of fit (LOF) test was implemented to interpret further the meaning of the linear regression model. This approach is described in (Harvey 2009) for the validation of a standard method. The test was applied on ten replicate measures for each of the six Pb loaded reference samples, that are compared to the values of the linear model. Additionally, the same test was repeated neglecting the sample with the higher mass deposition (sample Pb 081). The LOF results underline that the sample Pb 081 is out from the linear calibration range. Indeed, once Pb 081 is excluded, the representativeness of the linear fit is improved, as demonstrated by an increased coefficient

of determination ($R^2 = 0.9998$). The student t-test at 95% probability proves that the intercept is not significantly different from zero. Therefore, a new regression is performed forcing the intercept equal to zero, (Figure 12).

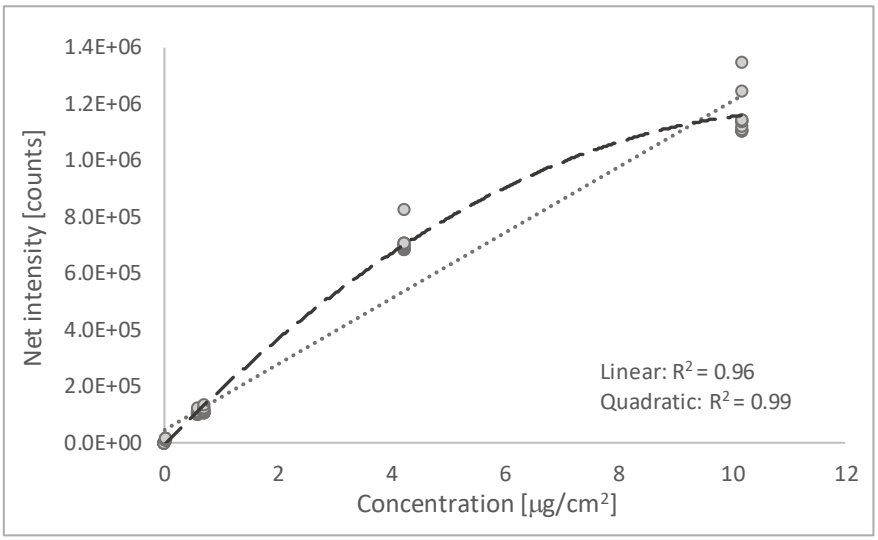

Figure 11 - Dependency of Net Intensity of Pb Lα and Lβ with respect to concentrations, and the linear (dotted) and quadratic (dashed) fit.

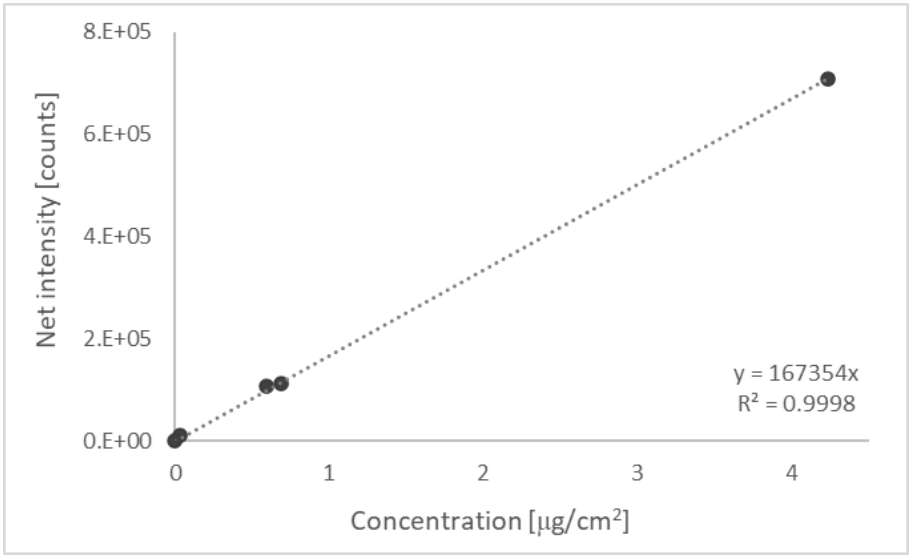

Figure 12 - Linear regression of the net intensity of Pb Lα+Lβ obtained with the Horizon spectrometer, considering only the 5 reference samples (without Pb 081) with the lowest mass depositions.

The exclusion of the Pb081 sample from the linear calibration range defined with the empirical approach can be justified further considering some theoretical principles (Klockenkämper and Von Bohlen 2015). TXRF quantification approach is based on the infinitely thin film samples approximation, which allows establishing a direct linear relationship between the fluorescence net intensities and the concentrations of the analytes in the sample. It means that the mass and the thickness of the test sample placed onto the carrier should be restricted, so that matrix effects are negligible (deposited mass very small), and absorption phenomena are not relevant.

In Borgese et al. (2020), the same lead loaded reference samples were measured but using a custom made TXRF spectrometer, equipped with a Rh X-ray tube and a SDD detector (150 mm^2). The calibration curve was built following the empirical calibration approach and the linear regression goodness was demonstrated with high significance. The choice of measuring the Pb loaded samples also with a Mo X-ray source relies on the wider diffusion of this source in commercially available TXRF spectrometers. The X-ray absorption phenomenon was not observed in Borgese et al. (2020) and the linear regression also included the highest concentration sample (Pb 081), differently to what obtained with Mo equipped spectrometers. Absorption is indeed directly related to the exciting X-ray energy selected. To better understand this point, it may be useful to look closely at the equation of the net intensity I_x. Considering the excitation of a specific element x with a monochromatic radiation of energy E_0, the element fluorescence net intensity I_x can be written as Equation (1):

$$I_x = c_x S_x \frac{1-exp\,[-(\mu/\rho)_M \rho d]}{(\mu/\rho)_M} I_0 = c_x S_x I_0 k_x \quad (1)$$

where:

S_x is the element sensitivity;
c_x is the mass fraction (concentration);
μ/ρ_M is the mass-attenuation coefficient of the layer matrix;
ρ is the density of the layer matrix; d is thickness of the matrix;
I_0 is the intensity of the exciting monochromatic beam.

The fraction part of Equation (1) represents the matrix absorption contribution. This term can be isolated as k_x defined in Equation (2):

$$k_x = \frac{\{1-exp[-(\mu/\rho)_M\, \rho d]\}}{(\mu/\rho)_M} \quad (2)$$

The mass-attenuation coefficient (MAC) reflects the effects of matrix composition as it contains the mass-attenuation coefficient of the primary incoming beam and that of the fluorescence line, considering the beam geometry. It can be evaluated as reported in Equation (3):

$$(\mu/\rho)_M = \sum_{i=1}^{N} c_i \left[(\mu/\rho)_{i,E_0}/sin\alpha + (\mu/\rho)_{i,E_x}/sin\beta\right] \quad (3)$$

where:

c_i is the mass fraction of the different matrix elements i;
α is the glancing angle of the primary X-ray beam;
β is the take-off angle of the fluorescence radiation;
E_0 is the energy of the primary X-ray beam;
E_x is the energy of the analyte emission line.

As in TXRF geometry the incoming X-ray beam has a value of α close to 0 and β close to 90°, the excitation energy attenuation has a far bigger contribution to the MAC than the analyte line itself. The average integrated net intensities measured by the Horizon spectrometer are plotted against the term k_x of Equation (2) (see Figure 13) calculated for each concentration of the reference samples, considering the characteristics of the Horizon spectrometer for the MAC (α=0.08°, β=90°, Mo Kα excitation) and the tabulated values of mass-absorption coefficients (Berger et al. 2010). The coefficient of the linear regression is very high (R^2=0.99), demonstrating that if a linear calibration curve with up to 10 μg/cm^2 of Pb is requested, the term k_x including the exponential term should be considered, accounting for the absorption effect.

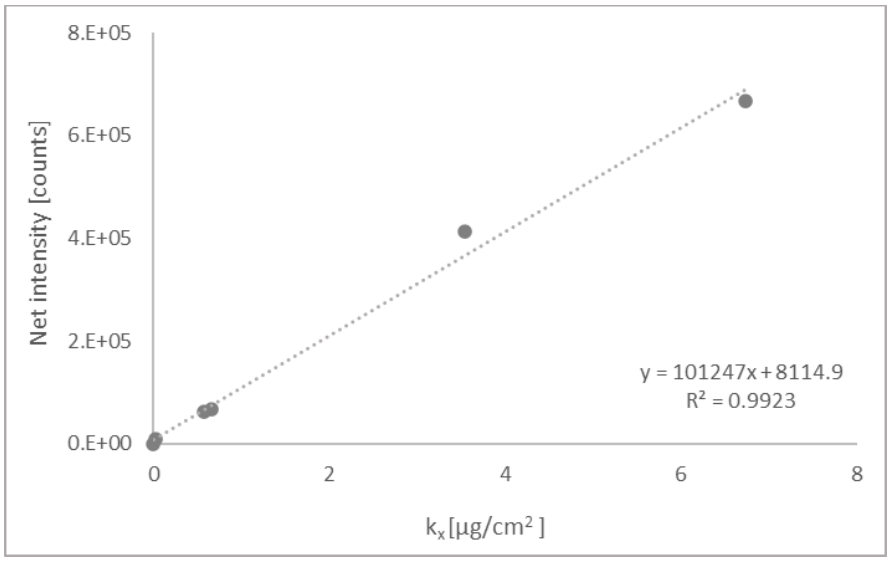

Figure 13 - Linear relationship between net Intensity of Pb Lα and Lβ and the term k_x related to the absorption phenomenon.

The presence of absorption phenomena for a certain mass deposition can be evaluated considering the factor ξ expressed in Equation (4):

$$\xi = \frac{k_x}{\rho d} = \frac{1-exp\,[-(\mu/\rho)_M \rho d]}{(\mu/\rho)_M \rho d} \qquad (4)$$

In real air filters lead loadings lower or close to the threshold value are expected, with a resulting ξ factor close to one. The custom-made instrument described in (Borgese et al. 2020) is not equipped with a goniometer, and the angular scan was run manually, so the glancing angle is supposedly in the range 0.08°- 0.24°. Therefore, ξ factor is calculated for all the reference samples, using Mo Kα and Rh Kα excitation energies and two α values (0.08° and 0.24°) and reported in Figure 14. As expected ξ factor moves away from 1 as the mass loading increases, meaning that absorption phenomena are mass dependent. For Rh ξ is closer to 1, fully consistent with the attenuation length in samples, which increases as the energy of the exciting radiation increases (Klockenkämper and Von Bohlen 2015). Indeed, for higher mass fraction (or area related elemental mass) a spectrometer equipped with a Rh tube presents a penetration depth advantage over a Mo tube, justifying the non-relevant absorption phenomena observed in (Borgese et al. 2020). These results confirm that the

assessment of the calibration range cannot be based simply on the ξ value. It was observed for instance that the sample Pb 078, while having ξ factor lower than 1 (0.84), cannot be excluded from the linear range with the selected statistical significance (99% for the Mandel test) considered in the empirical approach.

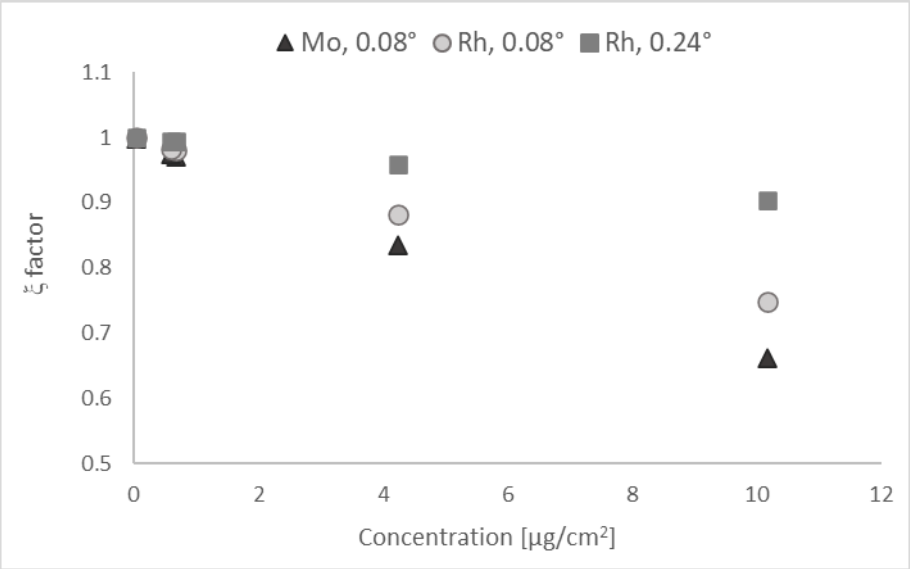

Figure 14 - Variation of the absorption factor calculated for the reference sample, both for Mo and Rh excitation source.

The linearity range identified with the empirical approach can be considered satisfying, as the upper limit (4.2 µg/cm^2) is ten times higher than the values that should not be overcome. The lead concentration in air corresponding to a filter having a mass loading equal to the upper limit of linearity would be 5.06 µg/m^3, that is significantly higher than the limits. The surface concentrations of Pb corresponding to the limit values and the standardized sampling conditions fall within the linear calibration range from 0.028 to 4.239 µg/cm^2.

Therefore, the method and the obtained linearity range can be considered satisfactory for environmental monitoring purposes. This represents the proof of concept of the method for direct analysis of air filters, as it demonstrates that it is possible to build a calibration curve for quantification purposes, using samples with known elemental mass loading, with commercial TXRF spectrometers.

4. DEVELOPMENT OF CALIBRATION SAMPLES

4.1. RMs: definition and history

Reference Materials (RMs) play a crucial role in ensuring the accuracy, reliability, and traceability of measurements and analyses in scientific and industrial fields. These materials, are carefully characterized to possess specific properties, making them invaluable benchmarks for quality assurance and precision in various laboratory processes. RMs serve as a cornerstone for analytical techniques, enabling researchers, scientists, and industries to calibrate instruments, validate methods, and verify the accuracy of their results.

RMs are defined as materials stable and homogeneous with respect to a specified property, which are suitable for their intended use in a measurement process (ISO 2015a). In addition, certified reference materials (CRMs) are also accompanied by a certificate that states the value of the specified property, together with the associated uncertainty, and a declaration of traceability.

The history of RMs has a close connection with the development of analytical chemistry (Stoeppler 2007). In 1901, the U.S. National Bureau of Standards (NBS), which is now the National Institute of Standards and Technology (NIST), was established in response to the growing need for a variety of standards in the quickly evolving engineering industries. The NBS reference material program helped the laboratories develop their measurement skills. Another important contribution in the history of RMs was given by the International Atomic Energy Agency (IAEA) in Vienna. The IAEA began an analytical quality control service aiming at assisting and improving the quality of analytical data in laboratories. Nowadays there are more than 300 RM producers worldwide and the most active of the organizations are reported in Jenks and Klich (2001).

In the 1970s, the Laboratoire National de Métrologie et d'Essais (LNE) in France proposed a Code d'Indexation des Matériaux de Référence (COMAR), a database that listed the available CRMs. The project grew over the years in terms of RMs listed and economies who joined the COMAR. In 2001 the Web-based version of the database was developed, and it was launched in March 2003 offering free access via internet (BAM 2023). COMAR provides the following information for each RM returned in a search: CRM name, address and contact details of the RM, CRM description and application description, packaging/storage of the CRM, fields of application, form of the material, matrix and list of

certified properties. COMAR contains information on some 10350 CRMs of 230 producers in 26 countries (Steiger and Pradel 2015).

4.2. ISO Guides for RMs

The selection of a reference material depends on the characteristics of the actual sample under analysis. The chosen reference material should closely resemble the experimental sample in terms of matrix composition, concentration level, physical state, and potential sources of interference (Quevauviller 2005). Most of the times, the lack of proper RMs necessitates laboratories to create their own materials exhibiting the desired properties for analysis.

RMs production process is regulated by ISO 17034:2016 *"General requirements for the competence of reference material producers"* (ISO 2016), which substitute the ISO Guide 34:2009, and specifies general requirements for the competence and consistent operation of reference material producers. It sets out the requirements in accordance with which reference materials are produced. It is intended to be used as part of the general quality assurance procedures of the reference material producer. It covers the production of all reference materials, including certified reference materials.

Important indications are given also in ISO Guide 35:2017 *"Reference materials – Guidance for characterization and assessment of homogeneity and stability"* (ISO 2017), which provides approaches to several aspects of the production of reference materials, such as assessing the homogeneity and the stability, characterizing and assigning value of properties of interest, and establishing the metrological traceability of certified property values. The guidance given supports the implementation of ISO 17034.

These two documents cover the whole production cycle of RMs, from the production planning up to the distribution phase, passing through the description of requirements for material handling and processing, measurement procedures, data evaluation, homogeneity and stability assessments, characterization, and labelling.

More specifically, ISO 17034 delineates the specifications governing the production of reference materials, serving as a framework for ensuring competence and consistency. This

international standard provided the technical and production requirements that must be met in the production of RM, that are the following:

- General requirements
- Production planning
- Production control
- Material handling and storage
- Material processing
- Measurement procedures
- Measuring equipment
- Data integrity and evaluation
- Metrological traceability of certified values
- Assessment of homogeneity
- Assessment and monitoring of stability
- Characterization
- Assignment of property values and their uncertainties
- RM documents and labels
- Distribution service
- Control of quality and technical records
- Management of non-conforming work
- Complaints

It is clear that the production of reference materials is fundamentally grounded on three key principles: (1) homogeneity, (2) stability, and (3) material characterization. These three points are well assessed in a comprehensive explanation in the ISO Guide 35, where a specific section is dedicated to each of these points.

Section 7 of the ISO Guide 35 is dedicated to the assessment of homogeneity. To make sure each RM is fit for its intended use, the RM producer must evaluate each candidate RM's homogeneity in its final packaged form. Homogeneity can refer to variation of a property between separate units of the material or to variation within each unit. *Between-unit homogeneity* is essential to ensure that each unit carries the same value for each property. On the other hand, the *within unit homogeneity* is important in those cases where the users analyse subsamples of the material. In most cases an experimental homogeneity study on the

candidate reference material is needed to assess the homogeneity. This must be determined for each property for which the material is stated to be sufficiently homogeneous for the intended use. The measurement procedure selected to perform measurement to assess the homogeneity should be chosen for its good precision during the measurement process. A statistical evaluation is used to compare the dispersion of observation in several units of the studied reference material, during a homogeneity study.

Section 8 of the ISO Guide 35 is dedicated to the assessment and monitoring of stability. Reference materials must exhibit adequate stability for their intended applications, ensuring that end-users can depend on the assigned values throughout the certificate's validity period. The value of each property can change over time, due to several motivations, in different degrees. Evaluation of stability should encompass various scenarios, including long-term storage, transport conditions, and, when applicable, storage conditions in the laboratory of the RM user. This assessment may also extend to post-opening stability considerations if reuse is permitted. Beyond the assessment of the long-term stability and the stability under proper transportation conditions, the producer should provide to the users some advice on storage and use of the material to maintain the stability.

Finally, section 9 of the ISO Guide 35 is dedicated to the description of the characterization of the material. Characterization is intended as the determination of the property values of the relevant properties of a RM, as part of the production process. The certified property values should not be just an average of a population, but it should be a reliable estimate of the true value. The characterization of a RM can be performed in several ways:

- Using a single reference measurement procedure in a single laboratory
- Using a network of competent laboratories
- Using a single measurement procedure in a single laboratory, by value transfer from a RM to a closely matched candidate RM
- Using mass or volume of ingredients used in the preparation of the RM.

In addition to the described indications, ISO developed other guides related to reference materials to ensure their quality, reliability, and traceability.

ISO Guide 30:2015 - *Reference materials - Selected terms and definitions* (ISO 2015a) provides definitions and descriptions of terms related to reference materials, offering a standardized terminology for better communication and understanding in the field, with a focus on terms utilised in product information sheets, certificates, and related certification reports,

ISO Guide 31:2015 - *Reference materials - Contents of certificates and labels* (ISO 2015b), which outlines the information that should be included in certificates and labels accompanying RMs. It lists and explains mandatory, recommended and other categories of information to be considered in the preparation of product information sheets and RM certificates. This information can be used by RM users and other stakeholders in confirming the suitability of an RM or CRM. It helps ensure that users have sufficient information to use the materials correctly.

For the users of RMs, the ISO community prepared a dedicated guide, the ISO Guide 33:2015 *"Reference materials – Good practice in using reference materials"* (ISO 2015c), which describes good practice in using RM, including the assessment of precision and trueness of measurement methods, quality control, assigning values to materials, calibration, and the establishment of conventional scales. The aim of this Guide is to provide general recommendations on the use of RMs, which are exemplified by real-world examples. The level of detail associated with RMs is considered useful for anyone with a responsibility for quality management in laboratories. The guide is addressed mainly to users dealing with measurement processes.

4.3. Calibration samples and RM of PM filters

4.3.1. Certified and non-certified RM

Reference materials for PM filters should have a composition that can be adjusted to suit the particular analytical context of use, in addition to the attributes mentioned in the guidelines. These contexts include workplace, environmental, and emissions scenarios, and all kinds of particulate matter are usually sampled in these scenarios.

In the case of PM filters, there are not several RMs available on the market. The only one is the NIST CRM 2783 "Air Particulate on Filter Media", a polycarbonate membrane with known deposited amount of urban air particulate matter (U.S. Department of Commerce 2011). To realize this sample some urban PM dust was collected with vacuum cleaners from the electrostatic filters of some air intake ducts, located in a mixed industrial urban area. The powder was milled to obtain a more homogeneous distribution of smaller particles and then it was suspended in pure water. The filter was mounted on the filtration apparatus, covered with pure water and then the suspension was pipetted on the top. The sample was finally dried under clean air flow.

Apart from the NIST CRM, the lack of RMs of PM filters in different substrates or different elemental composition leads laboratories to produce their own RMs and literature presents several examples of laboratory generated PM filters RMs, some of which are summarized in Table 5. Micromatter produces thin film standards for XRF analysis (Micromatter 2017), using only 99.9% or higher pure metals or compounds and are manufactured using ultra-high vacuum deposition techniques. Heat is transferred to the backing foils, or substrates, during evaporation processes, and these substrates must be made of thermally stable polymers. Mylar® polyester films or Nuclepore® polycarbonate membranes are preferred to Teflon® because of their superior heat tolerance and uniformity. Precision gravimetry is used to characterize Micromatter standards, by weighting each backing disc within the accuracy of 0.1 μg before and after the metal or compound is deposited. While NIST CRM 2783 is manufactured to closely mimic $PM_{2.5}$ on a membrane, the product concept of Micromatter is different because they do not try to create reference materials that exactly replicate the sample that will be examined. The XRF standards offered by Micromatter comprise individual elements or compounds and are designed for use in calibrating spectrometers, irrespective of matrix effects and sample composition.

In the study of (Heller-Zeisler et al. 1998) RM of PM filters were prepared milling and suspending in a liquid matrix PM material from an urban industrial area and filtering the solution on filter. Other laboratories started from incineration waste ashes, by pressing them on a filter until complete penetration into the fibres (Oster et al. 2015) or by resuspending them and collecting the aerosol onto a filter thanks to an air pump (Bescond et al. 2021) for the determination of emissions in the atmosphere.

The Air Quality group of the University of California prepared some mono and multi-element RMs by aerosol deposition, using a laboratory-built aerosol chamber (Yatkin et al. 2016, 2018) for air quality in the environment. Samples analysed in Borgese et al. (2020) and Cirelli et al. (2022) were realized by this research group, using lead acetate trihydrate salt. This salt was aerosolized and collected on the PTFE filter with loadings close to the EU limit values for Pb in atmospheric aerosols (EU 2008). The composition of the multi-element sample was selected to mimic the elemental profile of the atmospheric aerosol. Gravimetric analysis could not be used as a reference method for determining Pb loading on filters because the total PM on the lower range of RMs was near or below the uncertainty of the gravimetric analysis. The mass loading was determined by XRF and was proved to be equivalent to ICP-MS during the EPA Pb monitoring program. To verify the concentration values obtained with XRF, the measurements were compared to XRF analysis by three other laboratories.

Table 5 - Examples of RMs for PM filters found in the literature. Elements present in the samples, type of membrane, procedure of realization of the RMs and analytical technique used to characterize the sample are reported.

Authors	n° of elements	Substrate	Procedure	Analytical technique
U.S. Department of Commerce 2011	Certified: Al, As, Ba, Ca, Co, Cr, Cu, Fe, K, Mg, Mn, Na, Ni, Pb, Sb, Ti, V, Zn (18) Reference: Ce, Rb, S, Sc, Si, Sm, Th, U, W (9)	Polycarbonate filters	Air PM suspensions is pipetted on the filter	INAA, EDXRF, ICP-MS, PIXE, ID-ICP-MS
Micromatter 2017	On request, 70 elements available	Polycarbonate filters	Higher purity metals or compounds deposited by ultra-high vacuum deposition methods	Precision gravimetry
Heller-Zeisler et al. 1998	Al, As, Cu, Fe, La, Mg, Mn, Sb, Sc, Sm, Ti, V, W, Zn (14)	Polycarbonate filters	PM material from an urban industrial area milled and suspended in a liquid matrix and filtered on filter	INAA, EDXRF

Oster, et al. 2015	As, Cd, Ni, Pb (4)	Quartz filters	Incineration waste ashes pressed onto a filter	ICP-MS, IDMS
Bescond et al. 2021	V, Cr, Mn, Fe, Cu, Ni, Zn, As, Cd, Co, Pb (11)	Quartz filters	Powder from an incineration plat is resuspended and loaded onto a filter	ICP-MS
Yatkin et al. 2018	Na, Al, Si, S, K, Ti, V, Mn, Fe, Co, Ni, Se, As, Pb (14)	PTFE filters	Multi-element solution nebulised and collected onto a filter	EDXRF

4.3.2. Realization of calibration samples in the Chem4Tech Lab

To test and support the development of the method of filter analysis with XRF techniques, some calibration samples that can be candidate RMs of PM filters were prepared in the Chem4Tech lab of the University of Brescia. To realize the calibration samples a particle generator (model 7.811, Grimm Aerosol) was used. The instrument is equipped with two pumps inside, one for the flow through a nebulizer and a second pump which provides dry air for optional diluting and drying of the raw aerosol. For the preparation of the samples, a closed system was realised, to avoid aerosol losses. The instrumental setup consists in a mixing chamber, connected on one side to the ejector nozzle of the generator, and on the other side to an impactor, where a filter is placed. The impactor is then connected to an air pump (Leland Legacy Personal Sample Pump, SKC), that suck the air and facilitates the deposition of the aerosol on the membrane. A scheme of the instrumental setup is reported in Figure 15. By varying the concentration of the standard solution and the nebulization time, it was possible to obtain filters with different mass depositions. The filters used to collect the aerosol are politetrafluoroetilene (PTFE) membrane (Tecno-Lab) of 37mm diameter, 2 μm pore size and with a plastic supporting ring. PTFE filters were chosen for their chemical stability, high heat resistance, strong hydrophobicity, and ultra-high removal efficiency of particulates (Lu et al. 2022). The nebulized mass deposition of each filter was evaluated considering the weight of the nebulized solution, its concentration, and the area of the filter. Weighing was performed with a micro-balance (Sartorius), having a precision of 0.1 mg. All the filters were then subjected to the Smart Store® sample preparation procedure.

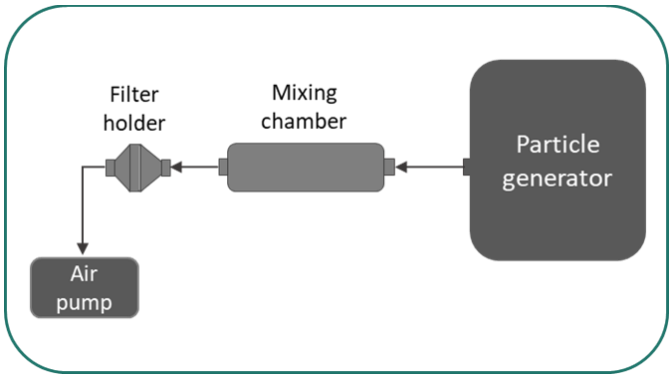

Figure 15 - Scheme of the instrumental setup employed to produce the calibration samples.

Three sets of samples were created:

- Set 1 – nebulization of the ICP multi-element standard solution IV Certipur® (Merck, Supelco), made of 23 elements diluted in nitric acid, in equal concentration of 1000 mg/l.
- Set 2 - nebulization of 10 mono-elemental reference solutions with a concentration of 1000 mg/L (ROMIL PrimAg Monocomponent). The elements are not in the same concentration in the final solution.
- Set 3 - nebulization of a multi-elemental standard solution (Bernd Kraft) made of 13 elements in equal concentration of 10 mg/l.

In addition, also the filter blank was created, consisting in a PTFE membrane with no aerosol deposition, subjected to the same preparation procedure of the other samples (described in section 4.3.3).

Table 6 reports all the details of the realized samples including the minimum and the maximum nebulized mass loading for each set of samples. A more detailed table with information about the nebulized elemental mass loading of each sample and the type of performed analysis is presented at the end of this chapter (Table 10). For a better understanding of the elemental composition of the three different set of samples, one spectrum for each set is reported at the end of this chapter (Figure 27).

Table 6 – Details for each of the three set of samples about type of nebulized solution, number of created samples, range of nebulized mass loading and elemental composition of the solutions.

Set	Nebulised solution	n°	Min nebulized mass loading [µg/cm^2]	Max nebulized mass loading [µg/cm^2]	Elements
1	ICP IV multielement solution	19	0.01	4.85	Ag, Al, B, Ba, Bi, Ca, Cd, Co, Cr, Cu, Fe, Ga, In, K, Li, Mg, Mn, Na, Ni, Pb, Sr, Tl, Zn. (23)
2	Mix of mono-elemental reference solutions	6	0.02	9.5	Ti, V, Mn, Ni, As, Cd, Pb, Fe, Cu, Zn. (10)
3	Multielement solution	7	0.05	0.82	As, Ca, Co, Cr, Cu, Fe, Mn, Ni, Se, Sr, Ti, V, Zn (13)

The planning phase of the calibration samples was dedicated to the definition of the desired concentration range of the samples to be employed for environment air quality monitoring purposes. In this regard, concentration limits for metals in air established by European Union for air quality monitoring were considered. In the two Air Quality Directives (2008/50/EC and 2004/107/EC)(EU 2004, 2008) the European Commission (EC) imposes some limits values for air pollutants concentration, in particular of As, Cd, Ni, Pb. Considering the sampling time, flow rate and filter diameter provided by the directives and the normative (UNI 2014), it is possible to convert the concentration limits in air [µg/m^3] in mass deposition onto filters [µg/cm^2]. The normative EN 12341, indeed, specifies that the exposed area through which the sampled air passes should be between 34 mm and 44 mm (i.e., filter diameter of 37 – 47 mm), and the sampling should be performed at a nominal flow rate of 2.3 m^3/h, over a nominal sampling period of 24 h. The limits imposed by the EC for the elements of interest were converted in values of mass deposition onto filters and included in the concentration range of the two sets of samples. Figure 16 show an example of the concentration range of the calibration samples for Pb. The concentration limit of lead provided by the EC directive (0.5 µg/m^3) is converted in value of mass loading onto filter considering a filter diameter of 37 and 47 mm. As represented in the graph, these limits are included in the range of concentrations of the samples.

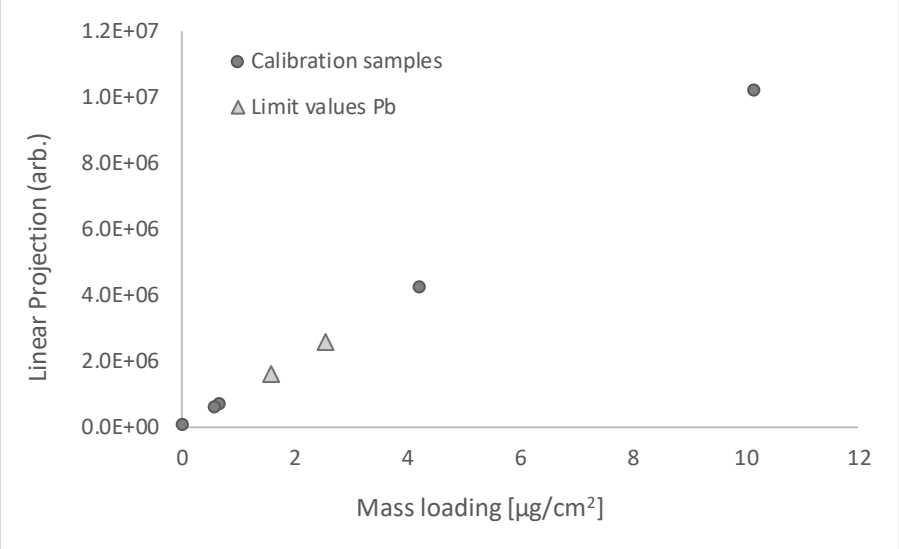

Figure 16 - Example of concentration range for Pb of the calibration samples (dots). The range includes the limit imposed by the directive (triangles) are included in the range.

4.3.3. Smart Store® handling procedure

The prepared filters underwent the same preparation procedure named Smart Store®, tested in Bilo et al. (2018) and Borgese et al. (2011, 2012, 2020). In those studies, the procedure was done manually. In 2021 the first engineered prototype was developed by the Smart Solution, a spinoff company of the University of Brescia (Smart Solutions 2022). The Smart Store® device allows for an automatic preparation of the sample: the filter is inserted, and the processing cycle is started. The device encloses the sample between two thin adhesive polymeric foils and cut the sample in a disc of 30 mm diameter (Figure 17). The obtained sample can be placed on the top of a quartz reflector, and it is ready to be analysed with X-ray based instrument. The polymeric layer does not affect the result of the analysis when the sample is measured with X-ray based instruments, because the used plastic is "transparent" to X-rays. The advantages of this preparation procedure are several: it is fast, non-destructive and allows to obtain a sample free of contaminations that can be preserved over time.

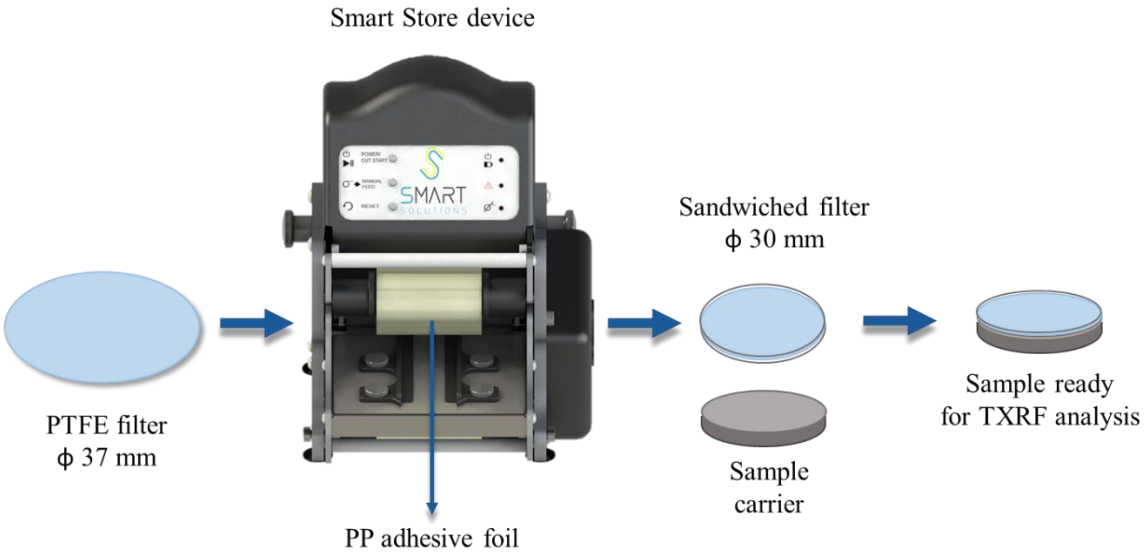

Figure 17 - Filter preparation with the Smart Store® device

The polymeric material has a crucial role in this sample preparation procedure. The sample provided by the University of California Davis and analysed in Borgese et al. (2020) and in chapter 3 were plasticized with a polyethylene (PE) film, having a thickness of 75 µm. To have a thinner sample a new film was searched and, after a careful selection, a polypropylene (PP) film 37 µm thick was chosen. The produced plasticized filter is thinner with the new film, and it adheres to the sample carrier with only a droplet of ethanol. This is an improvement over the previous film that, in comparison, produced a sample that was thicker and necessitated the use of glue to guarantee correct adherence on the carrier. This improvement extends to the quality of measurements as well. The use of the new film results in a flatter sample surface on the quartz, eliminating the potential for uneven distribution of glue that could cause less repeatable measurements. The choice of the new film was performed closely in order to select the best film that was thin and, most importantly, free of contamination, since it is meant to be used to prepare sample for elemental analysis. In Figure 18 it is possible to see the spectra of three different films; the selected one was the one with less contaminations (only traces of S and Fe).

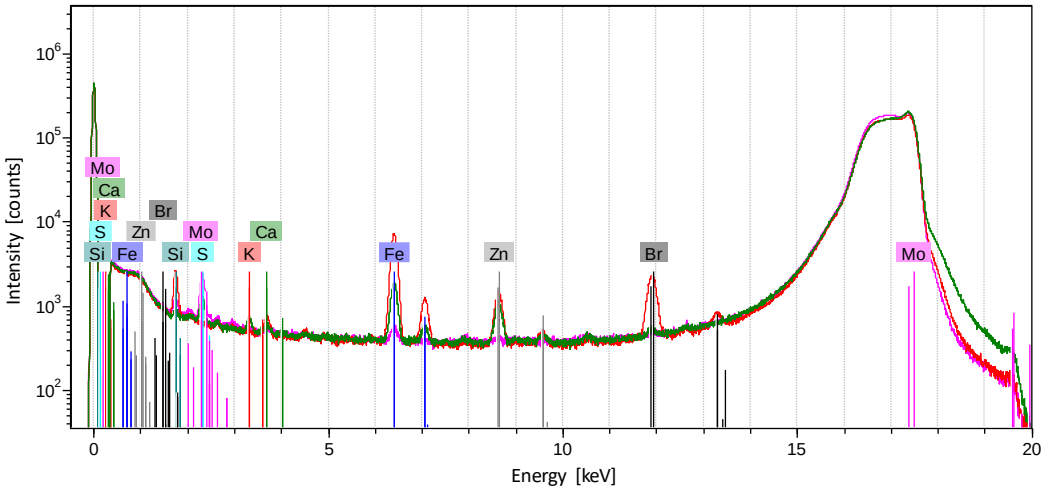

Figure 18 - Spectra of three different candidate polymeric film for the Smart Store® procedure. The film with the less contaminations was selected (pink spectrum).

This procedure can be defined green because it reflects the 10 principles of green sample preparation (GSP) described in (López-Lorente et al. 2022), which provides clear guidelines for the comprehensive and systematic improvement of the greenness of sample preparation methods. Firstly, the Smart Store® device is portable, favouring *in situ* sample preparation (principle 1). Then it is green because it avoids the use of chemical reagents such acids (principle 2), usually involved in digestion procedure, and consequently minimizes waste generation (principle 4). The amount of required sample is very small (principle 5) and the sample throughput is maximized because the sample preparation steps are fast and not time consuming (principle 6). The preparation process is automized (principle 7) and the energy consumption is minimized (principle 8), since no heating or high-pressure systems are needed, as in other preparation procedures. The obtained sample, without any further handling, can be analysed with a XRF spectrometers, and this represent a green choice (principle 9) because the analysis is fast, non-destructive and does not lead to the generation of waste. Lastly, Smart Store® preparation procedure complies also with the principle 10 of GSP: the procedure is safe for the operator because chemical hazards and exposure risks are equal to zero since no reagents are employed.

Besides air filters, this preparation procedure was tested with other types of samples, such as leaves (Bilo et al. 2017), cosmetics, oils, food, dust and soils, resulting very useful for screening and quality control purposes.

4.4. Study of the calibration samples

In agreement with the ISO Guide 35 and ISO 17034, calibration samples were deeply studied in order to assess the homogeneity and the stability, and to characterize them. A RM is defined in association with a specified property, which can be quantitative or qualitative. In the case of calibration samples under study, their characteristic property is both qualitative, because they have a known elemental composition, and quantitative, because they have a known nebulized mass loading (quantity expressed as mass per unit area $\mu g/cm^2$), calculated for each sample from the concentration and the weight loss of the nebulized solution, under the assumption of no material losses in the collection system. The homogeneity of the samples was assessed using micro-XRF technique, to check the homogeneous deposition of the aerosol on the surface of the filter. ICP-MS analysis was performed to check the repeatability of the production of the calibration samples.

4.4.1. Homogeneity

The property value that defines the calibration samples under study is the elemental mass loading on the surface of the filter. The lateral homogeneity of the nebulized elemental mass loading has to be assessed, because it represents an important requirement for RM, as indicated in the ISO Guide 35 (ISO 2017). Homogeneity can refer to variation of a property between separate units of the material, which consists in variation of the nebulized mass loading among samples with the same property value, or to variation within each unit (ISO 2017), which consists in variations on the nebulized mass loading on the surface of the same sample.

When samples are analysed with X-ray based instruments, the illuminated area of the sample goes from a spot of tens of a couple of nm up to almost the whole sample, depending on the employed instrument. Figure 19 shows the beam conditions used for the samples under study. The beam can have a circular shape with variable diameter according to the collimator employed: few mm or less for micro-XRF, bigger for the EDXRF spectrometers (9 mm with the JSX-1000S, 10 mm with the EDX 7200, 20 mm with the NEX CG II, and 28 mm with the S2 RANGER). When samples are analysed in XRF under grazing incidence condition, the beam shape is a strip of 7 mm width in case of S2 PICOFOX TXRF spectrometer and 80 μm in the case of SR-XRF. It is therefore important that the aerosol is distributed

homogeneously on the surface of the filter, thus requiring an investigation of the aerosol loading variation within the sample. In case of ICP-MS analysis, instead, the whole sample is digested, so the within sample homogeneity is less relevant.

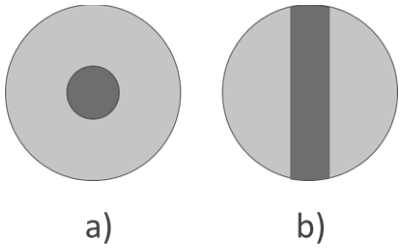

Figure 19 - Beam shape on the surface of the sample according to the employed instrument: (a) circular area with variable diameter dimension according to the collimator (from few mm up to 28 mm) with EDXRF spectrometer and micro-XRF spectrometer; (b) strip of different width when sample is analysed under grazing incidence conditions with TXRF or SR-XRF.

To investigate the homogeneity of the mass distribution 4 spectra were collected measuring sample 17 in 4 different positions under grazing incidence conditions with SR-XRF. There is a good overlap among the different spectra, highlighting the lateral homogeneity of the sample.

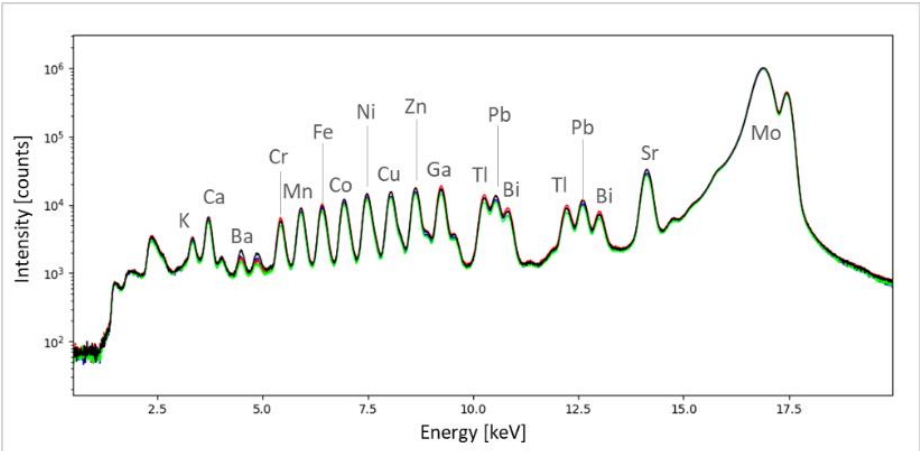

Figure 20 - Spectra collected with SR-XRF in 4 different positions of the same sample of set 1, having a nebulized mass loading of 0.72 µg/cm². The excitation energy is 17.4793 keV and the acquisition time is 300 s.

Some measurements were performed with the micro-XRF X-ray XDV-S to check the homogeneity of the nebulized mass loading of the sample. Sample 2 was analysed in 8 points equally spaced along the diagonal, with a 1 mm collimator, as schematized in Figure 21. Figure 22 shows the spectrum acquired from the measurement of the central point of the sample. Spectra acquired in each point were analysed and the detected elemental intensity was plotted for each point. As shown in Figure 23, there are no relevant differences in terms of elemental intensity in the different points for Cr, Mn, Fe, Co, Cu, Ni, Zn, Ga. Data of the elements with a high characteristic energy (such as Pb, Tl, Bi) are not presented because spectra have a higher background in that region due to the high excitation energy used (W). There is a slight edge effect that may be caused by the reduction in mass loading due to the rarefaction of the filter deposition surface, which depends on the geometry of the impactor. The average elemental intensities were calculated over the eight points and reported in Table 7 together with the standard deviations and the RSD (%). The obtained RSDs are lower than 15% for all the elements. If the points closer to the edges are neglected (points 1 and 8), the RSDs are lower than 8%, thus confirming the presence of an edge effect.

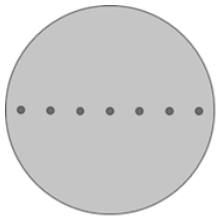

Figure 21 - Schematic representation of the analysis performed with the micro-XRF on a calibration sample.

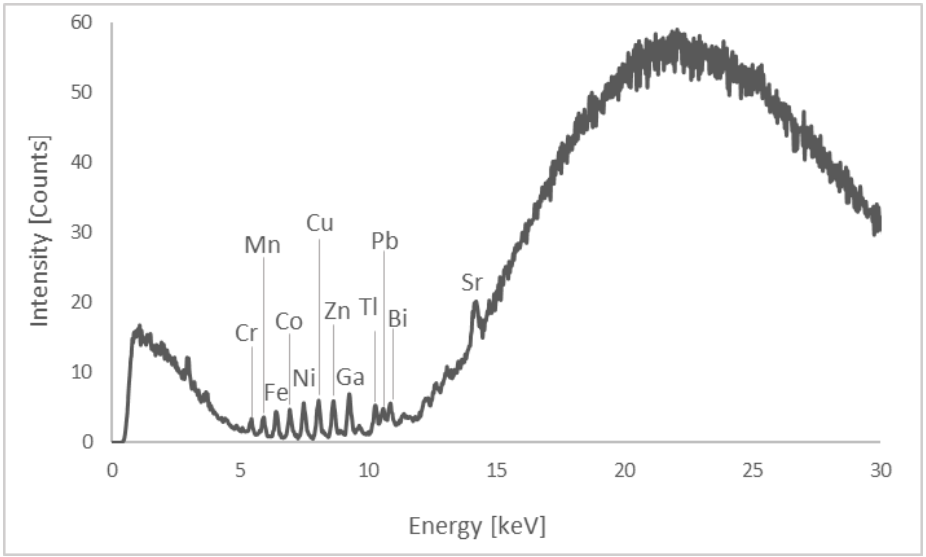

Figure 22 - Spectrum of point 4 of the line scan performed with the Miro-XRF spectrometer.

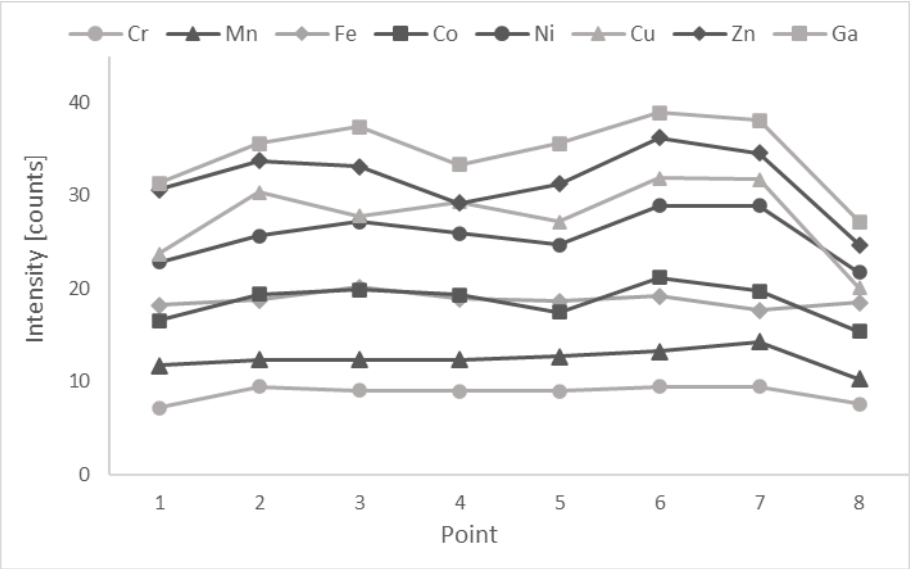

Figure 23 - Trend of the elemental intensity in 8 points along the diagonal of sample 2.

Table 7 - Average elemental intensity, standard deviation and RSD evaluated considering the intensities obtained in 8 points along the diagonal of sample 2.

	Average intensity [counts]	Standard Deviation [counts]	RSD (%)
Cr	8.8	0.9	10
Mn	12.4	1.1	9
Fe	18.8	0.7	4
Co	18.6	1.9	10
Ni	25.8	2.6	10
Cu	27.8	4.1	15
Zn	31.7	3.6	11
Ga	34.7	3.9	11

With the same spectrometer also 2D map was acquired (Figure 24) analysing a grid of 15x15 points covering the whole sample. Each point was measured for 30 s with a 3 mm collimator. Evaluation of the resulting EDXRF spectra and quantification by fundamental parameters were made using WinFTM software, version 6.19. Theoretical basis and practical applications of this software package are found in Roessiger and Nensel (Beckhoff et al. 2006). Sample under study was the sample of set 1 characterized by a nebulized mass loading of 4.85 μg/cm^2 and this value is in the same order of magnitude of the concentration values

estimated by the software. Also in these maps an edge effect is visible. For some elements there are areas with a higher concentration, but the distribution of these areas is not the same among the different elements, meaning that there are not accumulations of aerosol deposition.

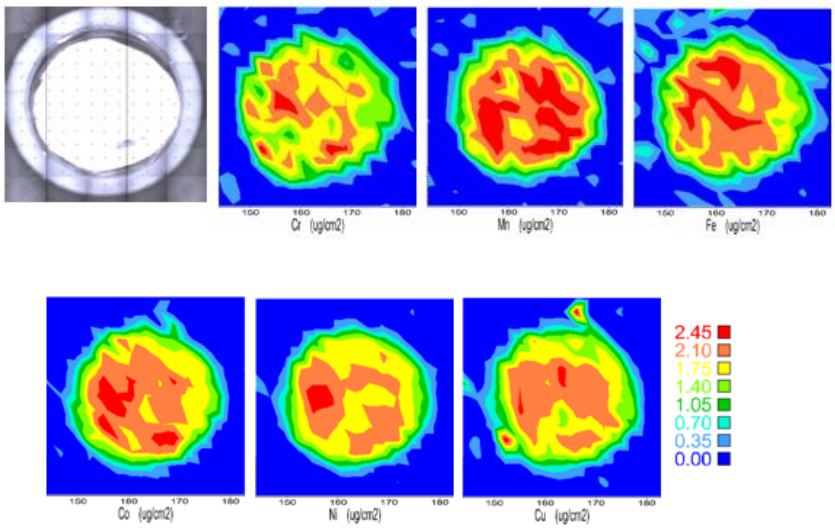

Figure 24 - 2D maps of a sample obtained with the micro-XRF spectrometer. Results are presented for Cr, Mn, Fe, Co, Ni and Cu. Data are in µg/cm².

The Horiba micro-XRF XGT-500 was used to obtain a map of the sample. As it can be observed in Figure 25, the elemental distribution over the surface of the sample seems homogeneous. However, the concentration of the sample is low and there is not a clear distinction between the sample and the background.

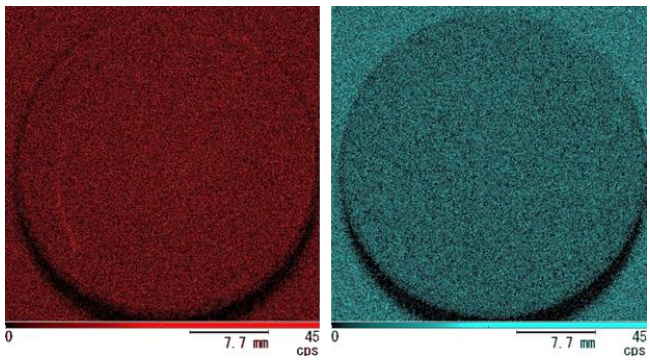

Figure 25 – Elemental distribution of Mn (left) and Ni (right) in sample Mix 5, obtained after analysis with Horiba Micro-XRF XGT-500

Also the M4 TORNADO micro-XRF was employed to obtain information about and element distribution of the calibration sample. One sample of set 3 was analysed but, due to its low nebulized mass loading (0.8 μg/cm^2), the obtained elemental maps are not sufficient to assess the homogeneity. The nebulization seems homogeneously distributed on the surface of the sample in the maps reported in Figure 26 for Ti and Ni. Also the map of Ga is reported, which was an element not present in the nebulized solution. In all the three maps an edge effect is visible, due to some reflections on the edge of the sample.

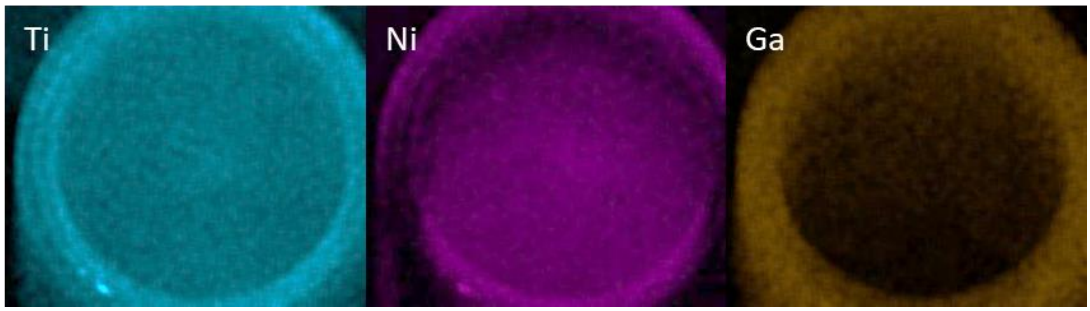

Figure 26 - Elemental distribution of Ti, Ni and Ga in sample 23, obtained after analysis with M4 TORNADO micro-XRF. Ti and Ga are elements present in the samples, while Ga was absent in the nebulized solution.

4.4.2. Time stability

An important issue for a RM is the stability of the property of interest, which, in this case, is the nebulized mass loading of the samples. The stability of the calibration samples is ensured by the preparation procedure: by plasticizing the filter with the Smart Store® device material losses, sample contaminations or damages are avoided, ensuring a constant elemental surface concentration over time. Samples were stored individually in small plastic bags, to avoid damages from external factors. Under the adopted storage conditions, the samples remained unchanged, also during transportation. Consequently, a long shelf life in ensured, as the sample remains isolated thanks to the polymeric coating. This study is thus a demonstration the Smart Store® procedure enable the proper conservation of filter samples increasing their stability over time. Samples of set 1 were analysed in several laboratories across the world (Italy, Spain, Germany, France, and Japan) in the time frame of one year, and no changes in the sample occurred, as it can be seen from the obtained calibration [chapter 6]. Samples of set 2 are more recent and were analysed within a period of 6 months. Therefore, under proper

storage condition samples are stable and can be easily transported without any particular problem. Considering the available data, the stability of the prepared samples is at least 1-year, additional tests should be performed to evaluate their stability in a longer period.

4.4.3. Repeatability

The repeatability of the mass deposition was tested preparing 6 samples in the same conditions: same nebulization time and same nebulized solution (Set 1). The nebulized mass loading was not the same as little variations in the nebulization flow, being manually regulated, may occur with a calculated variability about 13.9% over the 6 samples (37, 38, 39, 47, 48, 49). Three were prepared according to the Smart Store® procedure and three were left as realized to assess potential variability in the results due to sample handling treatment. All the 6 samples were digested and analysed with ICP-MS.

In the digestion step some residues of the PTFE filter were still present in each vessel, meaning that there was not a complete digestion of the sample, even though strong digestion conditions were employed. Indeed, this is an issue that can occur when PTFE filters are digested (Karthikeyan et al. 2006), which may affect the accuracy of determination. Table 8 reports the mass deposition (%) of each element in each sample calculated as the ratio between the value measured by ICP and the nebulized mass loading. The average deposition ratio (about 30%) is lower than what could be expected from literature about 70% (Heller-Zeisler et al. 1998). Only sample 48 shows a higher deposition percentage, but the higher values are coherent for all the elements in the sample. However, a possible source of underestimation could be due to the PTFE filter substrates, which are not fully digested. The not complete digestion of the sample represents a source of possible errors and thus, some standard operating procedures for analysing properly PTFE filters with ICP-MS should be assessed. To calibrate ICP-MS it would be better to use materials of reference with a matrix consisting of digested blank filters, this will be improved in future studies. As all the elements present in the nebulized solutions were in identical concentration the average mass deposition ratio over all the elements was calculated and resulted about 34%, 34%, 32%, 25%, 42% and 25% for samples 37, 38, 39, 47, 48, 49 respectively, with RSD% spanning in the range from 10 to 23%. It is worth notice that the Smart Store® procedure does not

significantly affect the recovery values, highlighting that the plasticizing procedure is compatible also with ICP-MS analysis. The two polymeric layers enclosing the filter, indeed, were completely dissolved during the digestion procedure.

Table 8 - Deposition percentage (%) between mass loading values evaluated with ICP-MS and nebulized values.

	Filters prepared with Smart Store®			Filters not prepared with Smart Store®		
	37	**38**	**39**	**47**	**48**	**49**
Cr	29.7	31.5	30.0	25.8	45.5	40.4
Mn	32.6	33.4	31.7	25.7	41.6	24.9
Co	30.5	30.5	30.5	25.0	41.0	24.2
Ni	35.9	36.1	31.9	25.3	41.1	22.6
Cu	32.3	33.9	32.2	25.9	43.7	25.6
Zn	53.1	50.7	42.6	26.2	50.0	25.6
Ga	28.0	30.5	27.9	22.1	37.1	20.2
Sr	30.2	31.0	28.7	23.3	38.1	21.1
Cd	33.1	31.9	28.6	21.9	36.2	20.0
Tl	32.0	32.0	32.3	26.2	42.1	25.4
Pb	36.0	30.3	31.7	27.3	44.4	24.6

As a further assessment of the repeatability of nebulized solution collection, the three samples prepared by Smart Store® (37, 38, 39) were analysed with the S2 Ranger EDXRF spectrometer. The acquired spectra were analysed with the open-source software PyMca and the obtained elemental intensities were normalised considering the nebulized mass loading of each sample for comparison. The variability of the normalized XRF elemental intensity was calculated and reported in Table 9, excluding the elements present in the blank. The analysis of a blank, indeed, revealed the presence of several peaks due to the metallic sample holder. The average variability of the normalised elemental fluorescence intensity is of 10% which is slightly higher than that obtained from ICP-MS analysis of the same samples, about 4%. This discrepancy could be due to the smaller measured area of the sample but also to the spectra fitting procedure by the software.

Table 9 - Variability (%) of the normalised elemental intensity obtained from XRF analysis (left) and of the recovery values from ICP-MS analysis, of the three samples 37, 38, 39.

Element	Variability (%) norm. XRF intensity	Variability (%) recovery ICP-MS
Cr	9.3	3.2
Mn	12.9	2.6
Co	11.1	0.09
Ni	8.0	6.9
Ga	10.9	5.2
Average	10.4	3.6

4.4.4. Assessment of the realization process

The production and the study of the calibration samples were conducted in compliance with ISO guide 35 and ISO 17034. The planning phase of the calibration samples was carefully conducted considering several factors such as material selection, setup for the preparation of the samples, elements of interest and elemental concentration for the intended sample use (i.e. air quality monitoring).

The homogeneity of the nebulized mass loading was tested using micro-XRF and SR-XRF. The results appear to confirm the homogenous distribution of the aerosol on the filter. However, as the results were not clearly noticeable in the fluorescence maps that were obtained, further research should be implemented on samples characterized by a higher nebulized mass loading. A careful study should be made on the edge of the sample to check that the distribution of aerosol is not different from the central part.

The stability of the calibration samples was confirmed, as they were analysed in a long-time interval. The storage and the transport of the calibration samples pose no significant challenges thanks to the Smart Store® plasticization procedure, which guarantees that proper sample handling does not lead to any damage. Each sample, stored in individual small plastic bags, can be easily transported and preserved over an extended period without compromising their integrity.

The repeatability of the sample production was tested and confirmed. While minor variations may arise from the manual flow regulation in the nebulizer, these can be effectively

addressed through procedures such as accurate weighing of the vessel containing the solution both before and after nebulization, coupled with a precise verification of the nebulization time. These measures ensure a consistent and reliable sample production, minimizing the impact of manual adjustments on the overall precision of the process.

Sample characterization remains to be assessed. Some problems arose in the digestion affecting the accuracy of the consequent ICP-MS analysis of the filters. The digestion of the filters, indeed, was not complete because some residue remained in the digestion vesseles, thus the values obtained from ICP-MS analysis may reflect this problem. Considering the difficult nature of PFTE membrane in being digested, already documented in literature, some guidelines for the complete digestion of the filters should be determined. A change in the type, amount or concentration of the employed acids could lead to a complete sample digestion. This is of significant importance for the determination of the real elemental loading of the calibration samples and is the missing piece for their characterization as reference materials. The correct value of mass loading should be associated to each sample, together with the related uncertainty. By addressing the mentioned issues, these calibration samples could represent promising candidate RMs.

Table 10 – Details of the elemental nebulized mass loading of each sample and of the instrument employed to analyse the sample.

		Nebulized mass loading [μg/cm²]															
set n°	id sample	Ag, Al, B, Ba, Bi, Ga, In, K, Li, Mg, Na, Tl	As	Ca	Cd	Co	Cr	Cu	Fe	Mn	Ni	Pb	Se	Sr	Ti	V	Zn	Analysis
1	5	0.010	-	0.010	0.010	0.010	0.010	0.010	0.010	0.010	0.010	0.010	-	0.010	-	-	0.010	TXRF
1	6	0.012	-	0.012	0.012	0.012	0.012	0.012	0.012	0.012	0.012	0.012	-	0.012	-	-	0.012	TXRF
1	12	0.053	-	0.053	0.053	0.053	0.053	0.053	0.053	0.053	0.053	0.053	-	0.053	-	-	0.053	TXRF
1	11	0.072	-	0.072	0.072	0.072	0.072	0.072	0.072	0.072	0.072	0.072	-	0.072	-	-	0.072	TXRF, EDXRF
1	14	0.115	-	0.115	0.115	0.115	0.115	0.115	0.115	0.115	0.115	0.115	-	0.115	-	-	0.115	TXRF, EDXRF
1	10	0.166	-	0.166	0.166	0.166	0.166	0.166	0.166	0.166	0.166	0.166	-	0.166	-	-	0.166	TXRF, EDXRF
1	13	0.196	-	0.196	0.196	0.196	0.196	0.196	0.196	0.196	0.196	0.196	-	0.196	-	-	0.196	TXRF, EDXRF
1	15	0.33	-	0.33	0.33	0.33	0.33	0.33	0.33	0.33	0.33	0.33	-	0.33	-	-	0.33	TXRF, EDXRF
1	16	0.542	-	0.542	0.542	0.542	0.542	0.542	0.542	0.542	0.542	0.542	-	0.542	-	-	0.542	TXRF, EDXRF
1	17	0.722	-	0.722	0.722	0.722	0.722	0.722	0.722	0.722	0.722	0.722	-	0.722	-	-	0.722	TXRF, EDXRF, SR-XRF
1	1	0.830	-	0.830	0.830	0.830	0.830	0.830	0.830	0.830	0.830	0.830	-	0.830	-	-	0.830	TXRF, EDXRF
1	18	3.15	-	3.15	3.15	3.15	3.15	3.15	3.15	3.15	3.15	3.15	-	3.15	-	-	3.15	TXRF, EDXRF
1	2	4.85	-	4.85	4.85	4.85	4.85	4.85	4.85	4.85	4.85	4.85	-	4.85	-	-	4.85	TXRF, EDXRF, Micro-XRF
1	37	0.18	-	0.18	0.18	0.18	0.18	0.18	0.18	0.18	0.18	0.18	-	0.18	-	-	0.18	EDXRF, ICP-MS
1	38	0.154	-	0.154	0.154	0.154	0.154	0.154	0.154	0.154	0.154	0.154	-	0.154	-	-	0.154	EDXRF, ICP-MS
1	39	0.156	-	0.156	0.156	0.156	0.156	0.156	0.156	0.156	0.156	0.156	-	0.156	-	-	0.156	EDXRF, ICP-MS
1	47	0.158	-	0.158	0.158	0.158	0.158	0.158	0.158	0.158	0.158	0.158	-	0.158	-	-	0.158	ICP-MS
1	48	0.137	-	0.137	0.137	0.137	0.137	0.137	0.137	0.137	0.137	0.137	-	0.137	-	-	0.137	ICP-MS
1	49	0.118	-	0.118	0.118	0.118	0.118	0.118	0.118	0.118	0.118	0.118	-	0.118	-	-	0.118	ICP-MS

2	mix 1	-	0.025	-	0.077	-	-	0.253	0.078	0.024	0.202	0.203	-	-	0.025	0.076	0.128	TXRF, EDXRF
2	mix 2	-	0.066	-	0.179	-	-	0.067	0.115	0.066	0.068	0.022	-	-	0.066	0.18	0.224	TXRF, EDXRF
2	mix 3	-	0.19	-	0.024	-	-	0.117	0.244	0.192	0.024	0.071	-	-	0.186	0.023	0.071	TXRF, EDXRF
2	mix 4	-	3.7	-	8.41	-	-	1.61	9.52	1.83	3.73	1.82	-	-	3.64	8.39	3.73	TXRF, EDXRF
2	mix 5	-	8.26	-	3.64	-	-	3.63	1.66	8.22	1.8	3.62	-	-	1.76	3.63	9.14	TXRF, EDXRF, Micro-XRF
2	mix 6	-	1.67	-	1.68	-	-	8.38	3.45	3.38	7.6	7.58	-	-	7.41	1.68	1.49	TXRF, EDXRF
3	19	-	0.355	0.355	-	0.355	0.355	0.355	0.355	0.355	0.355	-	0.355	0.355	0.355	0.355	0.355	TXRF, EDXRF
3	20	-	0.532	0.532	-	0.532	0.532	0.532	0.532	0.532	0.532	-	0.532	0.532	0.532	0.532	0.532	TXRF, EDXRF
3	21	-	0.222	0.222	-	0.222	0.222	0.222	0.222	0.222	0.222	-	0.222	0.222	0.222	0.222	0.222	TXRF, EDXRF
3	22	-	0.068	0.068	-	0.068	0.068	0.068	0.068	0.068	0.068	-	0.068	0.068	0.068	0.068	0.068	TXRF, EDXRF
3	23	-	0.819	0.819	-	0.819	0.819	0.819	0.819	0.819	0.819	-	0.819	0.819	0.819	0.819	0.819	TXRF, EDXRF
3	25	-	0.165	0.165	-	0.165	0.165	0.165	0.165	0.165	0.165	-	0.165	0.165	0.165	0.165	0.165	TXRF, EDXRF
3	26	-	0.051	0.051	-	0.051	0.051	0.051	0.051	0.051	0.051	-	0.051	0.051	0.051	0.051	0.051	TXRF, EDXRF
-	Blank	-	-	-	-	-	-	-	-	-	-	-	-	-	-	-	-	TXRF, EDXRF

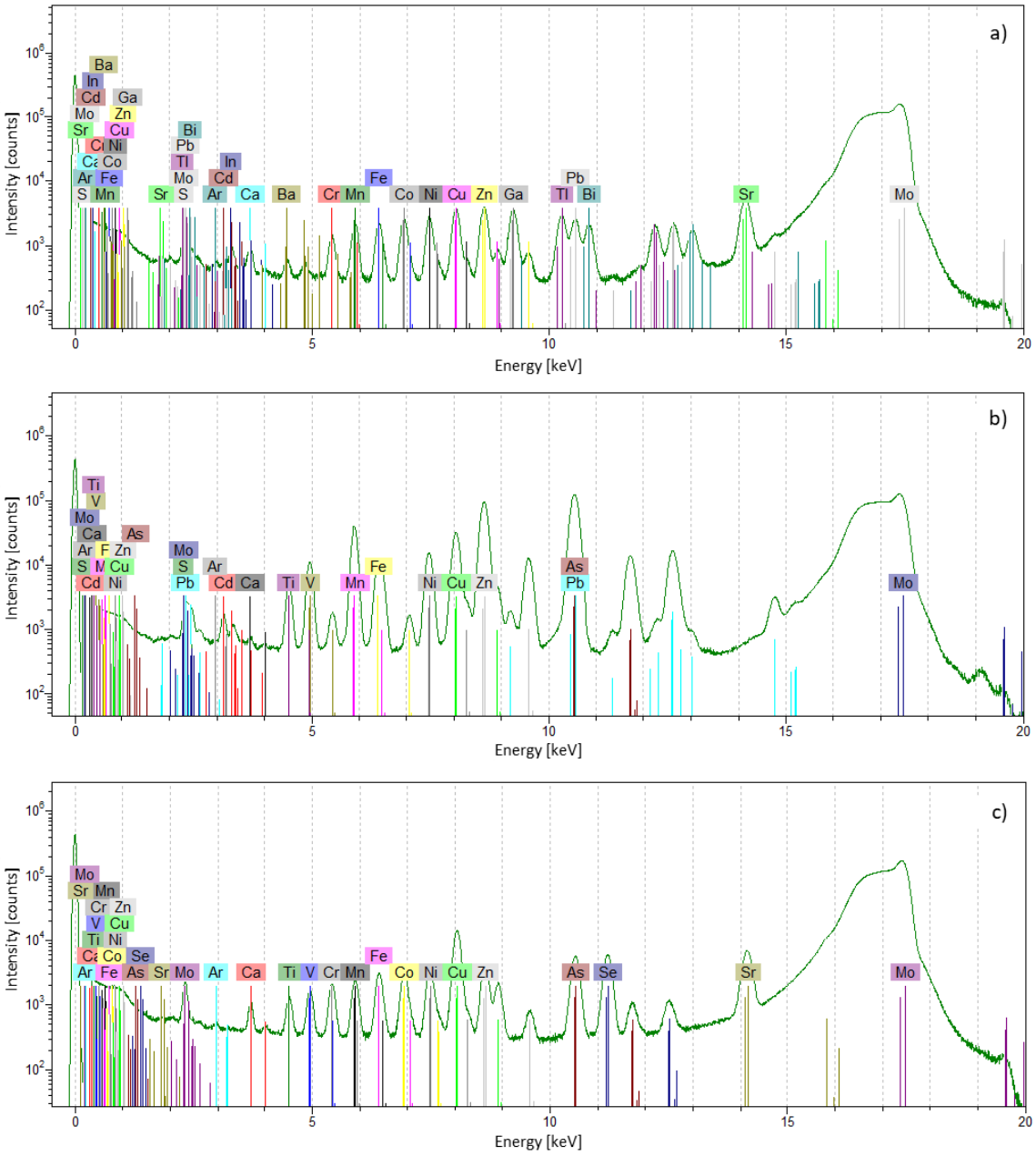

Figure 27 – Spectra with elements identification of one sample of set 1 (a), set 2 (b) and set 3 (c).

5. XRF MEASUREMENT UNDER GRAZING INCIDENCE

5.1. Optimization of measuring conditions

As already mentioned, calibration samples under study represent unconventional samples for TXRF analysis. In TXRF analysis samples usually consist of a dried residue on the surface of a quartz carrier. The layered structure of the calibration samples consisting in a filter enclosed between two polymeric layers (≈ 37 μm thickness), schematized in Figure 28, represents a challenging sample. When sample is analysed under grazing incidence condition with a TXRF spectrometer the elemental fluorescence intensity changes if the incoming X-ray beam hits the sample on the top layer, on the bottom layer or on the filter surface. As a consequence, the sample positioning was deeply investigated in order to assess the best measuring conditions. In this regard, calibration sample were studied with SR-XRF at ESRF, with the GNR diffractometer and with the custom-made TXRF Wobicompact.

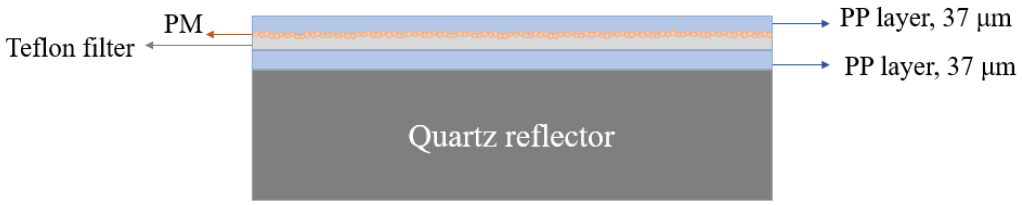

Figure 28 - Schematic representation of the structure of a calibration sample, placed on a quartz reflector.

5.2. Diffractometer

Sample 10 (set 1) was studied with the GNR Explorer diffractometer, to evaluate how the position of the sample with respect to the X-ray beam affects the transmitted intensity.

First of all, the sample, consisting in a quartz reflector with a calibration sample on the top, had to be placed parallel to the beam direction. The beam must be half intercepted by the sample when incidence angle is equal to zero. A scan is performed rotating the sample on its axis of 0.01° and collecting the transmitted intensity (Figure 29) with the XRR detector. At the beginning the intensity is equal to zero because the direct beam is covered by the sample. As the sample is rotated, the X-ray beam becomes more visible until it reaches the maximum

when the surface of the sample is parallel to the beam. Then the transmitted intensity starts decreasing, as long as the beam is completely stopped by the back of the quartz reflector. The position corresponding to the maximum intensity is selected and a vertical scan of the sample was performed.

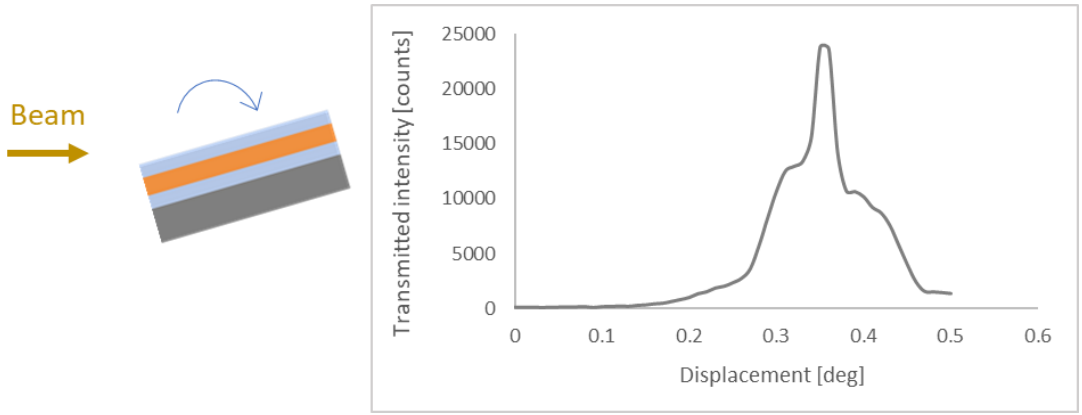

Figure 29 – Profile of the transmitted intensity collected rotating the sample. The maximum transmitted intensity is obtained when the sample is parallel to the direct beam and this position is selected to perform successive measurements.

A second scan was performed by translating the sample vertically of 0.01 mm. From the profile of the vertical scan reported in Figure 30 it is possible to describe how the position of the sample with respect to the incoming beam affects the transmitted intensity. At the beginning the whole beam passes because its path is not disturbed by anything. As the sample is lifted and intercept the path of the beam, the transmitted intensity starts decreasing *(1)*. There is a slight increase in the recorded intensity *(2)* probably due to the accomplishment of the total reflection condition and then the transmitted intensity decreases steeper as the sample is lifted *(3)*, obstructing the passage of the incoming beam. The beam illuminates the central part of the sample, corresponding to the filter *(4)* and finally the beam is completely blocked by the quartz support and the transmitted intensity is equal to zero *(5)*. Since the particles of PM are on the surface of the filter, a good position to measure the sample is between position (2) and position (3).

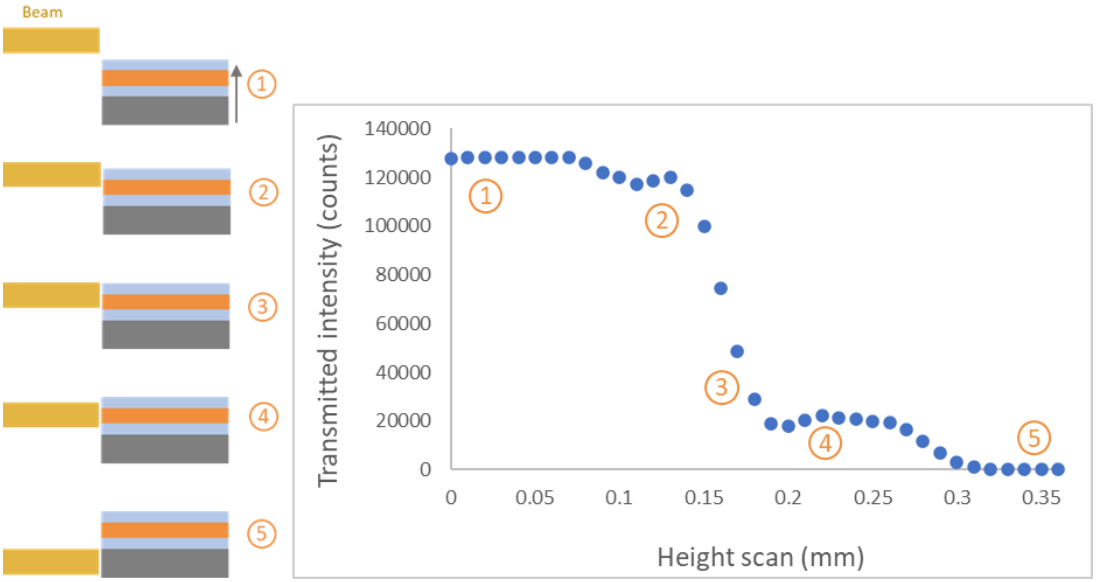

Figure 30 – Profile of the transmitted intensity recorded as the sample is lifted and intercept the path of the X-ray beam. On the left it is presented a schematic representation of the position of the sample (consisting in a sandwiched filter on the top of a quartz reflector) with respect to the X-ray beam.

5.3. SR-XRF

The alignment procedure performed at ESRF was the same for all the calibration samples. Figure 31 shows the adopted reference system; the direct beam is in the x direction. The first step of the alignment procedure was performed on the direct beam. A vertical scan on the sample is run and the variation of the transmitted intensity as the sample is lifted is shown in Figure 32. At the beginning the intensity is maximum because all the direct beam passed. Then, as the sample is lifted (increasing z), the intensity starts decreasing, because the beam is covered by the sample. The reduction of the intensity become less steep when the direct beam reaches the filter. Finally, the intensity goes to zero because the sample cover completely the X-ray beam. The selected position is at half of the curve, corresponding to a condition of filter illuminated by the X-ray beam. The obtained profile is in agreement with the one obtained with the GNR Explorer diffractometer.

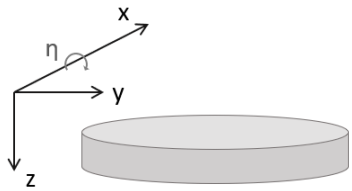

Figure 31 – Reference system of the sample stage.

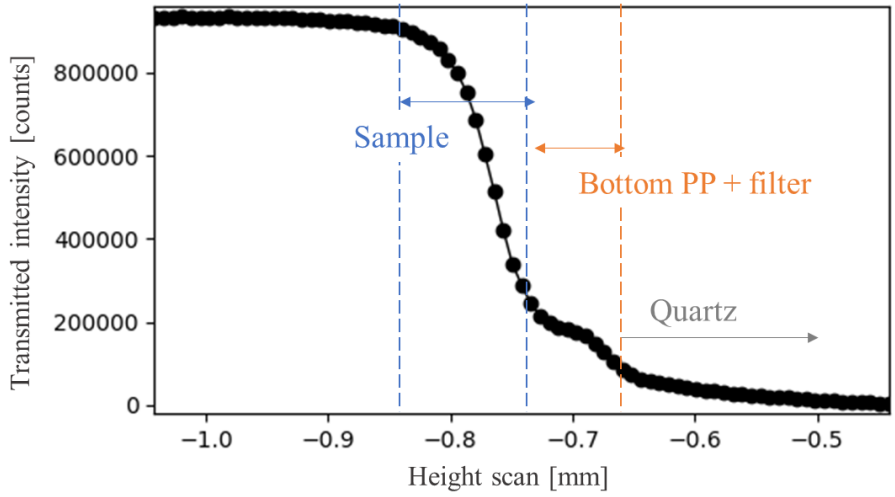

Figure 32 - z-scan of one of the calibration samples placed on the quartz reflector. The variation of the transmitted intensity as the direct beam passes through all the layers of the sample is shown.

A second scan is performed at fixed z, rotating the sample on its axis (η scan) to align the sample parallel to the direct beam. A bell-shaped profile is obtained (Figure 33-a) and the η position corresponding to the maximum intensity is selected.

Then, the XRR detector is moved so that it is aligned with the reflected beam. In this position another η scan is performed (Figure 33-b) and the maximum is selected. Another z scan is performed and overlapped to the z scan previously obtained on the direct beam (Figure 33-c). The bell-shaped profile obtained in this second z scan has a maximum in correspondence of the same position where the filter was identified on the first scan. The positioning of the sample at the maximum of the curve ensures that it is parallel to the direct beam.

The last step of the alignment procedure is performed considering the fluorescence signal collected by the SDD detector on the top of the sample. Again, a z scan is performed collecting the fluorescence intensity of five different regions of interest (ROIs) corresponding to the Kα peak of Si, Ti, Ni, Cr and Ga. In (Figure 33-d) the profiles of the intensity of Si and Ga ROIs are reported. The profile of the Si fluorescence intensity is slightly shifted with respect to the one of Ga, and this is because the Ga comes from the filter, while the Si is from the quartz support, below the filter. The position corresponding to the maximum intensity in the z scan is selected, and the fluorescence intensity of the selected ROIs is then collected in 4 different points along the y-axis of the sample (Figure 33-e), to check the homogeneity of the mass loading. In these 4 points spectra of the sample are

collected, for a measuring time of 300 s. This procedure was repeated for all the calibration samples.

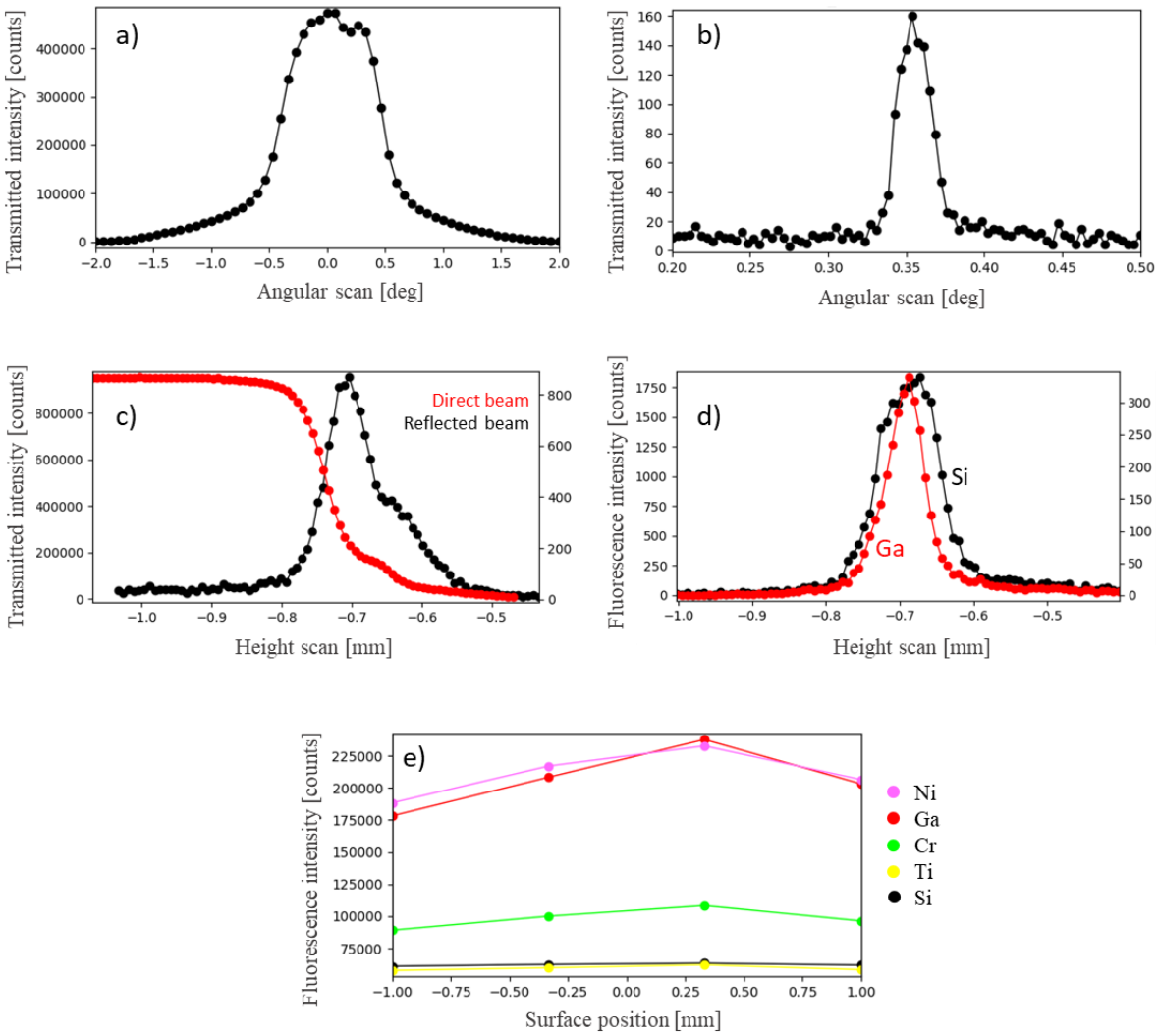

Figure 33 – Alignment procedure of a calibration samples (sample 15). A η scan is performed on the direct beam (a). Then on the reflected beam another η scan is run (b) and a z- scan is performed and compared to the one obtained on the direct beam (c). With the fluorescence detector the intensities of Ga and Si are collected in a z-scan (d) and the elemental intensities of Ni, Ga, Cr, Ti and Si are collected in 4 different point along the surface of the sample.

5.4. Custom-made TXRF: Wobicompact

As explained in the experimental section, the Wobicompact spectrometer was built by the Atominstitut (ATI). Due to a change of the X-ray generator and the detector, the instrumental set-up needed to be re-aligned before analysing the calibration samples. Thanks to a virtual mentoring activity with ATI, it was possible to bring back in use the system. In Figure 34 it is reported the instrumental setup, once the spectrometer was mounted and aligned.

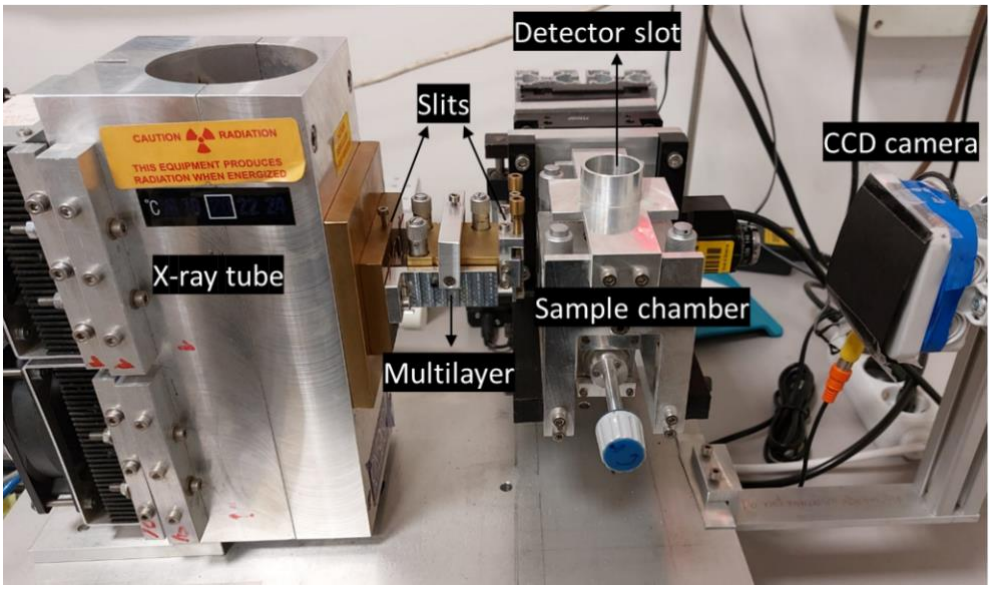

Figure 34 - Instrumental setup of the Wobicompact spectrometer.

To align the system, first of all a slit was placed in front of the X-ray tube, in order to shape the beam like a strip of paper.

Then the multilayer, which is responsible for monochromatizing the primary beam, had to be mounted. The multilayer is used as Bragg reflector, with a definite energy band selected at a particular angle of reflection. When a parallel monochromatic beam of wavelength λ impinges on the multilayer under a glancing angle ϑ, the photons will be scattered by the atoms in the material. Only in certain directions, in which the path difference between two rays is equal to an integral number of wavelengths ($n\lambda$), constructive interference between the scattered rays occurs.

The angles ϑ for which this diffraction phenomenon occurs for a given wavelength λ and crystal spacing d are given by Bragg's law (Adams 2017):

$$n\lambda = 2d \sin\theta$$

Multilayers can be produced as flat or curved optics and they consist of about 150 up 500 individual bilayers, which are a combination of heavy and light element. Several bilayers of a heavy element and B_4C as second layer are commercially available. They are used to select a strong K or L peak of the anode material of an X-ray tube (Klockenkämper and Von Bohlen 2015). In the case of the Wobicompact, the multilayer is made of a combination of Pd/ B_4C to select the Rh-Kα.

The multilayer of the Wobicompact is provided with three screws: two for vertical displacement (n° 2 and 3 in Figure 35) and one for rotation (screw n° 1). First the surface of the mirror was placed parallel to the incoming beam, then the multilayer was inclined to define the Bragg angle. Thanks to the CCD camera placed in front of the direct beam it was possible to check the position of the beam. The direct beam was clearly visible on the screen (Figure 36-a), then, by moving the multilayer, the beam split and both the direct and the reflected beam were visible (Figure 36-b). Adjusting the inclination of the multilayer the reflected beam became more intense until the primary beam was no more present (Figure 36-c). Finally, tilting further the multilayer the Bragg angle was found (Figure 36-d), which correspond to a monochromatized beam.

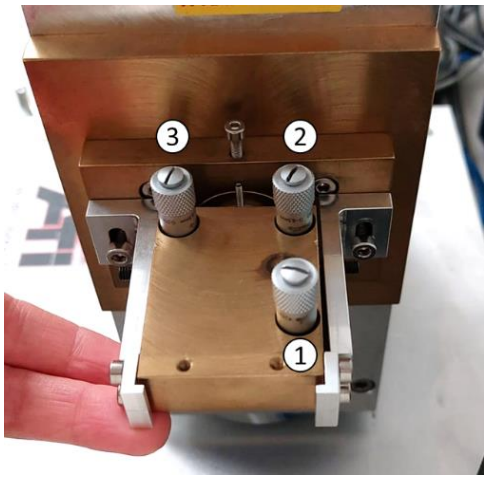

Figure 35 – Multilayer with three positioning screws: (1) for rotation, (2) and (3) for vertical displacement.

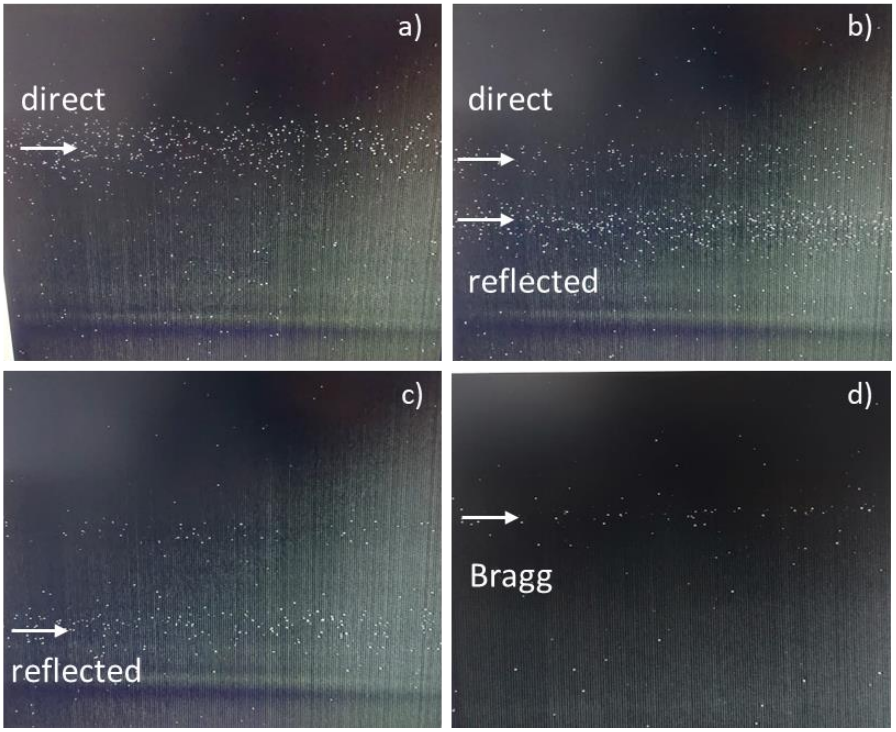

Figure 36 – Alignment procedure seen from the CCD camera. First only the direct beam is visible (a). Then, the direct beam splits and also the reflected beam is visible (b), becoming more and more intense (c). By further tilting the multilayer the Bragg angle is found (d).

The second slit was positioned after the multilayer. By adjusting the two screws, the height at which the beam can pass through the slit was determined. Finally, the chamber with the sample holder was mounted.

After the mounting of the detector on the top of the sample chamber, a sample was placed in the chamber and the sample alignment was performed. The sample employed for the alignment consisted in a quartz with 10 µl Ga residue in a concentration of 10 mg/l. Alignment was performed manually, by moving the internal micrometer for high-precision measurement of the height of the chamber and the graduated screw for regulating its inclination with respect to the incoming X-ray beam. First the height of the chamber was adjusted, performing a z-scan and recording the fluorescence intensities of Ga and Si. The intensity profiles of the two were plotted, resulting in a graph similar to the one obtained at the synchrotron (Figure 37). After selecting the z position corresponding to the maximum Ga intensity, the optimal chamber inclination was determined by exploring the angular

positions that achieved the total reflection condition. This critical condition was assessed by inspecting the X-ray beam with the assistance of the CCD camera.

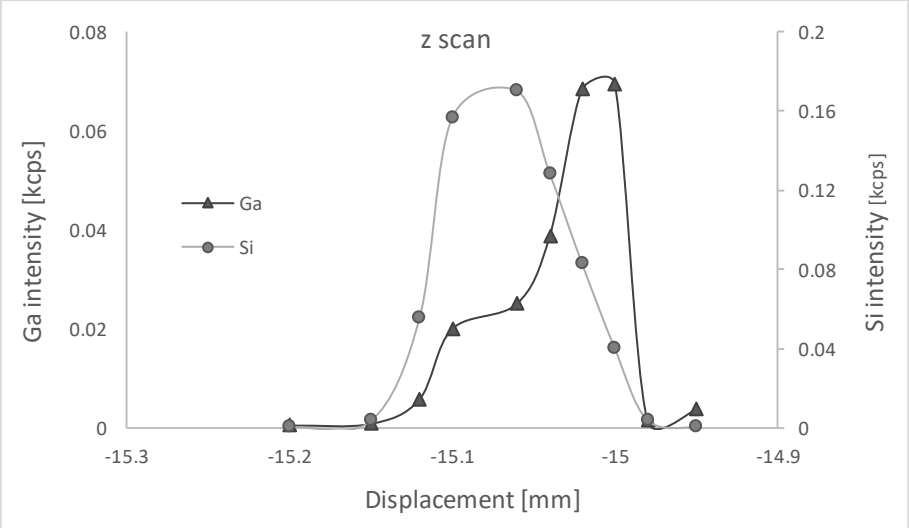

Figure 37 – intensity profiles of Ga and Si obtained after a z-scan of the reflector.

6. CALIBRATION CURVES

6.1. Building calibration curves

The main goal of realizing these samples is to use them for calibration purposes. These samples, indeed, were created with a nebulized elemental loading close to the limit imposed by EU in air, for health protection. If the linearity of the mass deposition is verified, these samples could be employed for monitoring purposes and the mass deposition could be modulated according to the intended use. It means that sample could be created also for monitoring workplace emissions, where the emission limits are higher. The linearity range should be investigated as well, because for high nebulized mass loading matrix effect could lead to absorption phenomena, resulting in a bending of the calibration line. In Borgese et al. (2012) a calibration line was built using a set of reference samples prepared in laboratory by means of atomic layer deposition (ALD), depositing Ti on PTFE filters. The thin film thickness, which is directly proportional to the mass, is directly related to the number of ALD cycles. It was noted that at higher cycle numbers there was a deviation from the linearity, because the critical mass for that system was reached. Absorption phenomena were also noticed in the analysis of the samples provided by the University of California Davis and described in chapter 3, where a theoretical approach was employed to take into account matrix effects.

For sake of brevity, calibration curves in this chapter are reported only for Ni, Cr or Mn, according to the elemental loading of the sample, because they are element of environmental interest. Similar results were obtained also for the other elements in the samples. Pb, which is an element of elemental interest as well, was not chosen because its characteristic line is at a higher excitation energy than the other elements and with some spectrometers the background in that part of the spectrum is higher.

6.2. EDXRF spectrometers

To check the actual linearity of the mass deposition, the Set 1 of samples was measured with two EDXRF spectrometers, the Bruker S2 Ranger and the Jeol JSX-1000S. Spectra of the same samples obtained with the two EDXRF spectrometers are presented in Figure 38. As it can be seen from the two spectra, the excitation source is different: Pd (21.176 keV) for the

S2 Ranger and Rh (20.214 keV) for the JSX-1000S. In the low energy region, the high peak in the JSX-1000S spectrum is due to argon, since measurements were performed in air, while this peak is absent in the other spectrum because the S2 Ranger worked in helium. The lower background in the central energy region of the spectrum acquired with the S2 Ranger is due to the use of an Al filter.

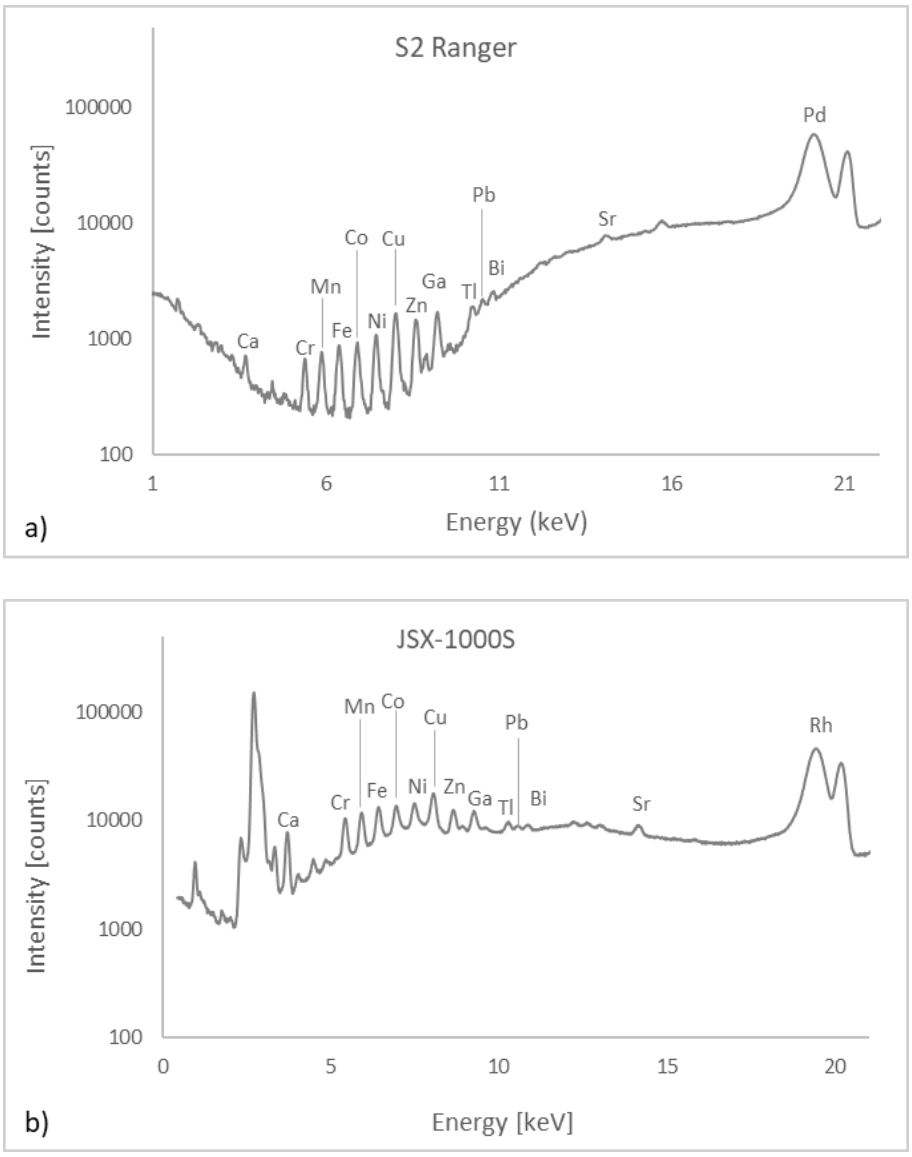

Figure 38 - Spectra of sample 2 acquired with (a) S2 Ranger, measuring the sample in He with an Al filter 500 µm thick, with an excitation energy of 21.176 keV and (b) Jeol JSX, measuring the sample in air, with an excitation energy of 20.214 keV.

The spectra acquired by Bruker S2 Ranger were analysed by the instrument software. The software gives both the intensity values and the XRF concentration, evaluated considering variable absorption corrections factors. Calibration curves, presented for Ni and Cr (Figure 39), were obtained plotting both the net intensity calculated by the instrument software in correspondence of the nebulized mass loading of each sample, to check the linearity. Each sample was measured one time, including the blank sample. An outlier (sample1), circled in the graphs, was identified and excluded by all the data elaboration performed with other instruments. For that sample, indeed, the net intensity was much higher than the trend line for all the elements in the sample. The same was noticed analysing the sample also with other spectrometers, this confirming that some mistake was made in the preparation of that sample.

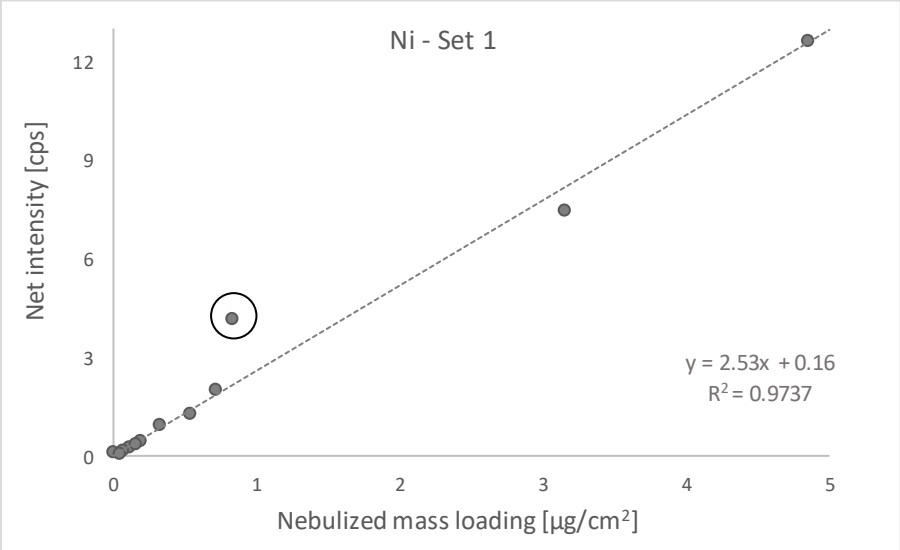

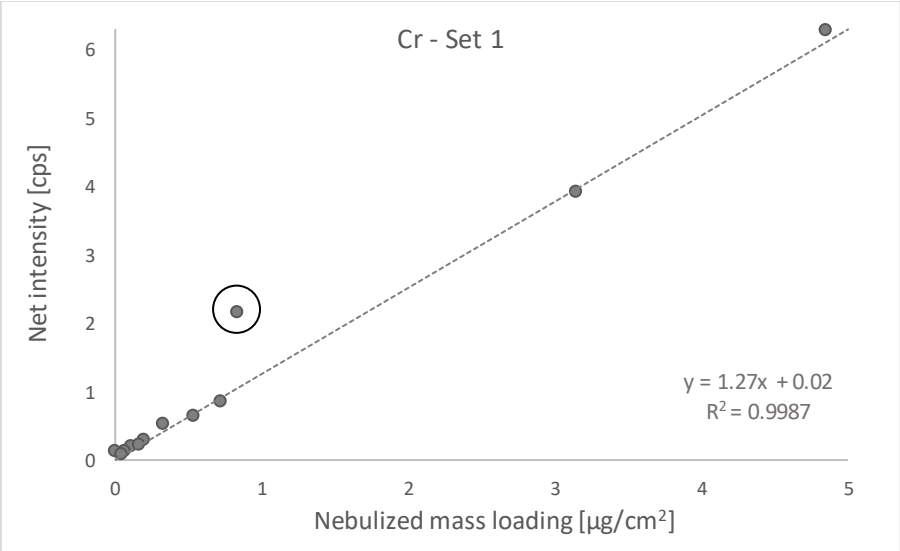

Figure 39 - Calibration curve obtained with Bruker S2 Ranger EDXRF spectrometer for Ni and Cr, after analysis of Set 1 of samples. An outlier samples is identified (circled) and excluded from the other measurements.

The same samples were analysed also with the Jeol JSX-1000S EDXRF spectrometer. The acquired spectra were analysed with PyMca software to obtain the elemental net area, which was plotted in correspondence of each sample nebulized mass loading. Results are presented for Ni and Cr (Figure 40). With both the spectrometers a good data correlation with the mass loading is observed, and this is stressed by a coefficient of correlation R^2 very close to 1.

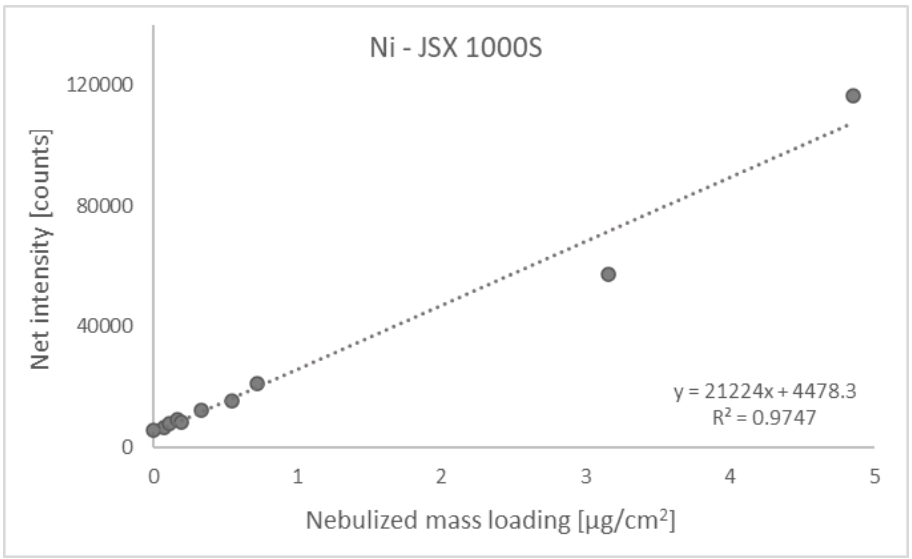

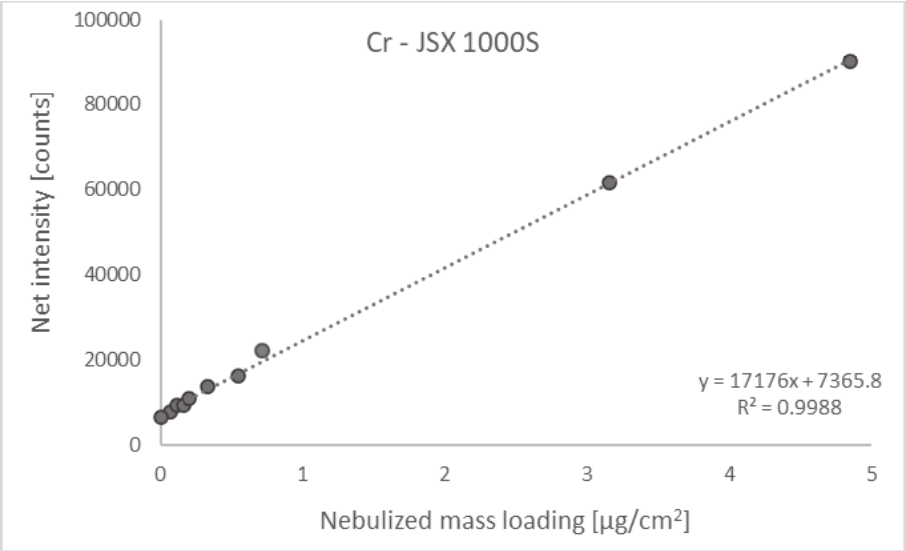

Figure 40 - Calibration obtained with the Jeol JSX EDXRF spectrometer for Ni and Cr, after analysis of Set 1 of samples.

Set 3 of samples was measured with the Bruker S2 Ranger and the net intensity values were calculated by the instrumental software are plotted in Figure 41 for Ni and Mn. The obtained results are not as good as the ones obtained with set 1, also for the other elements not displayed in the graphs. Even limiting the concentration range of set 1 up to 1 µg/cm^2, to be more consistent with concentration range of set 3, the latter shows slightly worse results. This may be due to the solution used to create the set of samples, which is not certified unlike the other two sets. For this reason, analysis with other spectrometers was focused on set 1 and set 2.

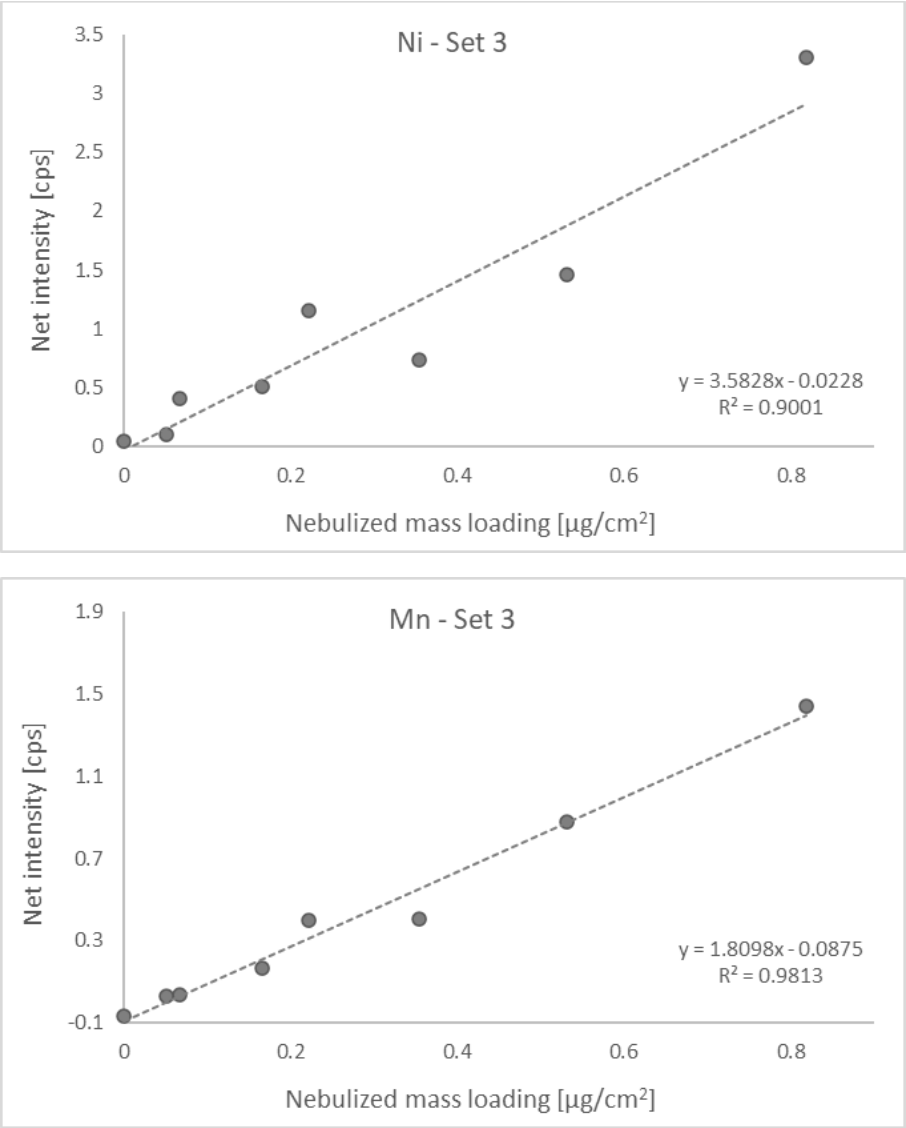

Figure 41 - Calibration curves obtained with Bruker S2 Ranger EDXRF spectrometer for Ni and Mn, after analysis of Set 3 of samples.

Set 2 and blank sample were measured at the Osaka Metropolitan University with three EDXRF spectrometers: Jeol JSX-1000S, Shimadzu EDX-7200, Rigaku NEX CG II. Spectra obtained with the JSX-1000S and EDX-7200 spectrometers were analysed with PyMca software, while spectra form NEX CG II were analysed by the respective instrumental software. Results are shown for Ni and Mn in Figure 42, results of blank sample analysis were included in the graph and not subtracted. With all the three spectrometers the obtained calibration curves confirm the linearity of the mass deposition for increasing nebulization times.

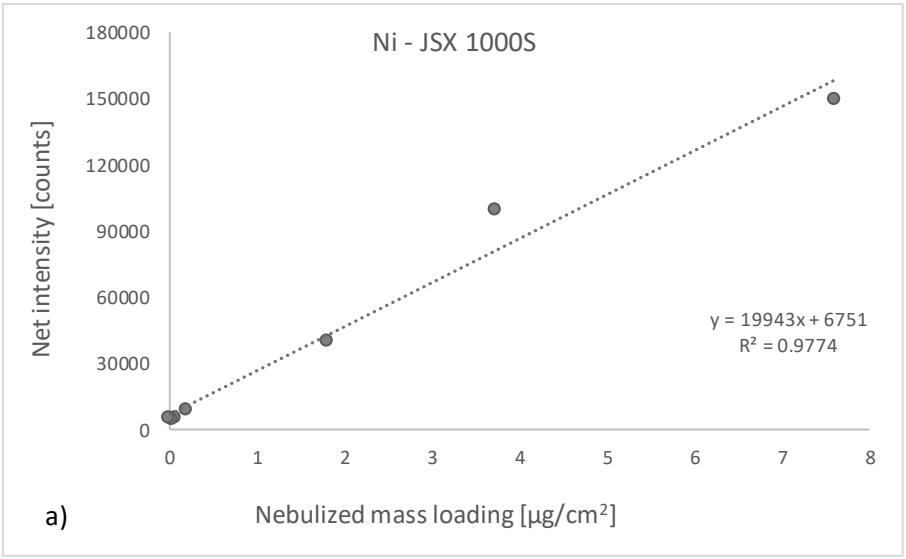
Ni - JSX 1000S
Net intensity [counts]
180000
150000
120000
90000
60000
30000
0
0
1
2
3
4
5
6
7
8
y = 19943x + 6751
R² = 0.9774
a)
Nebulized mass loading [µg/cm²]

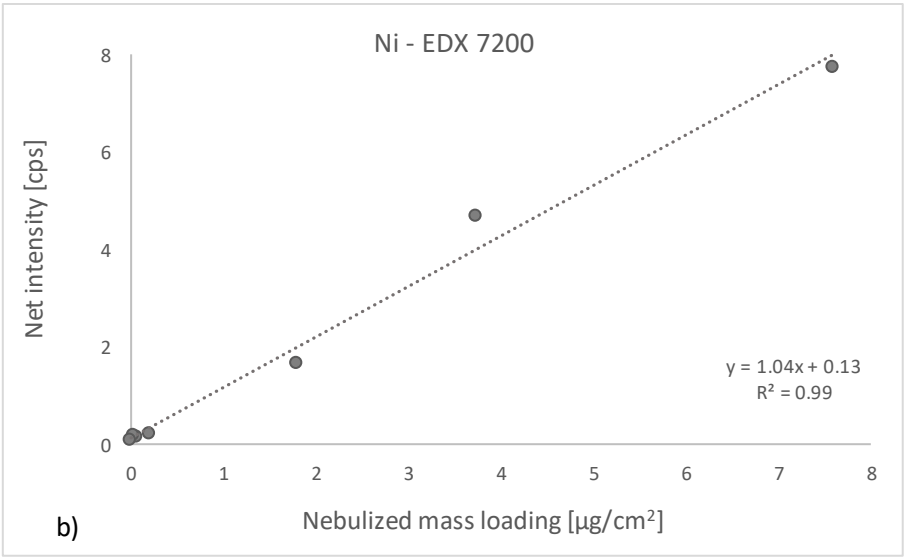
Ni - EDX 7200
Net intensity [cps]
8
6
4
2
0
0
1
2
3
4
5
6
7
8
y = 1.04x + 0.13
R² = 0.99
b)
Nebulized mass loading [µg/cm²]

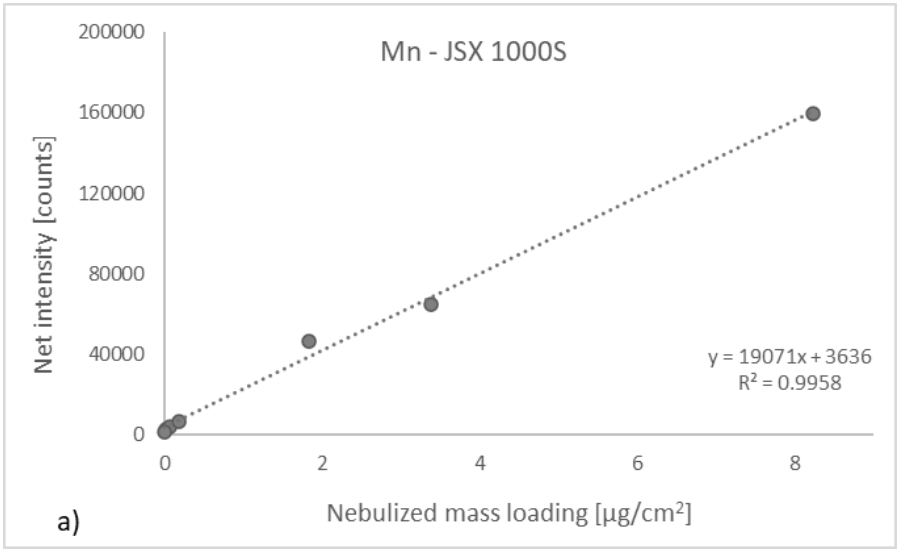
Mn - JSX 1000S
Net intensity [counts]
200000
160000
120000
80000
40000
0
0
2
4
6
8
y = 19071x + 3636
R² = 0.9958
a)
Nebulized mass loading [µg/cm²]

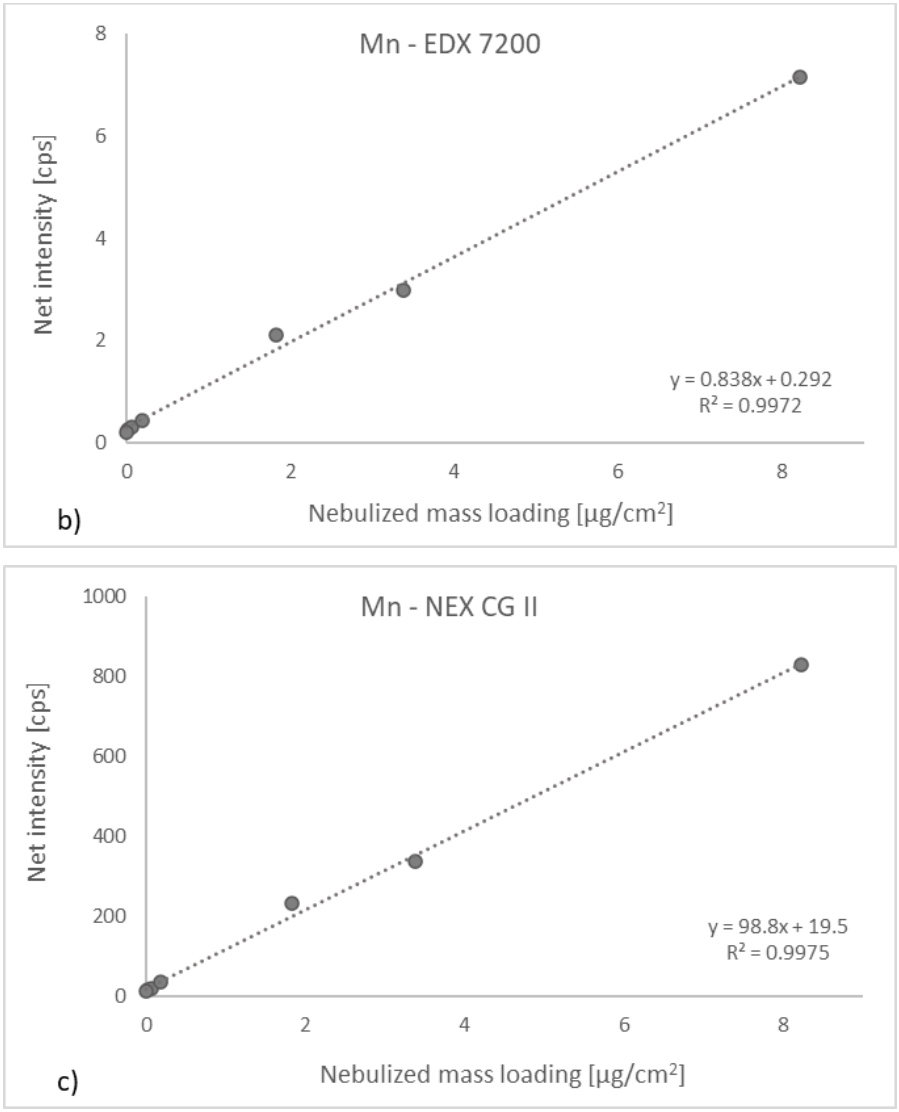

Figure 42 – Calibrations for Ni and Mn obtained analysing set 2 of samples with three different EDXRF spectrometers: (a) Jeol JSX, (b) Shimadzu EDX 7200, (c) Rigaku NEX CG II.

One sample (mix 4) was measured 3 times after a rotation of approximately 120°, to test the repeatability. The relative standard deviation (RSD %) of the elemental intensity was calculated and reported in Table 11. Values below 5% were obtained for almost all the elements, with the exception of Pb, because it is the only element identified by a L (α + β) characteristic line instead of K (α + β) as the other elements. Higer value of RSD for Pb may also be due to the overlapping of Pb Lα line (10.551 keV) and As Kα line (10.543 keV).

Table 11 - Relative standard deviation (RSD %) of the elemental fluorescence intensity calculated over three replicate measurements of the same sample after a rotation of approximately 120°, with the JSX-1000S EDXRF spectrometer.

Element	**RSD (%)**
Ti	3.0
V	2.9
Mn	2.4
Fe	3.4
Ni	1.9
Cu	2.7
Zn	2.3
As	2.2
Pb	13.6

The reproducibility of the sample realization setup was confirmed by the data acquired more recently measuring with the Jeol spectrometer set 1 and set 2, prepared 8 months apart and using different nebulization solutions. Results are reported in Figure 43 for Mn and Ni. For the elements identified by K characteristic line (such as Mn and Ni) there is a good agreement between the calibration lines built with the two sets, while there is a criticality with those elements identified by L characteristic line (such as Pb).

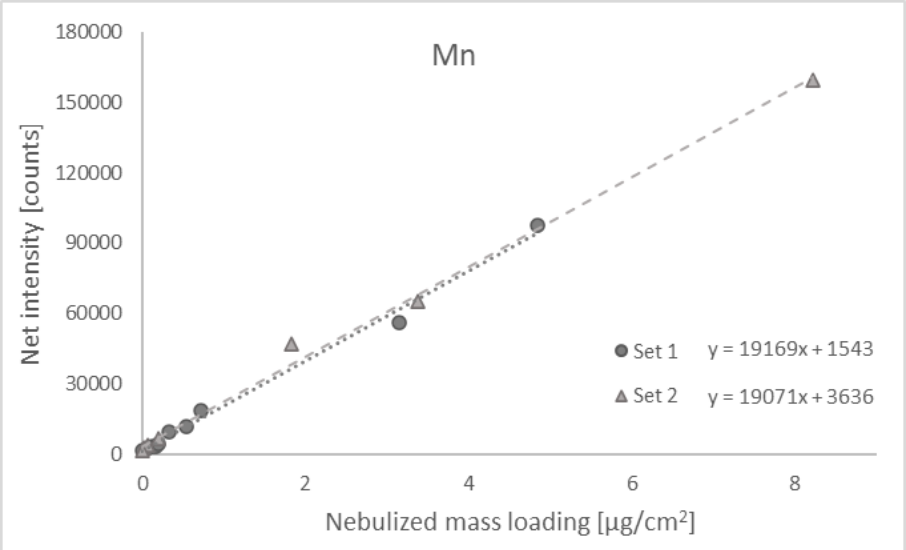

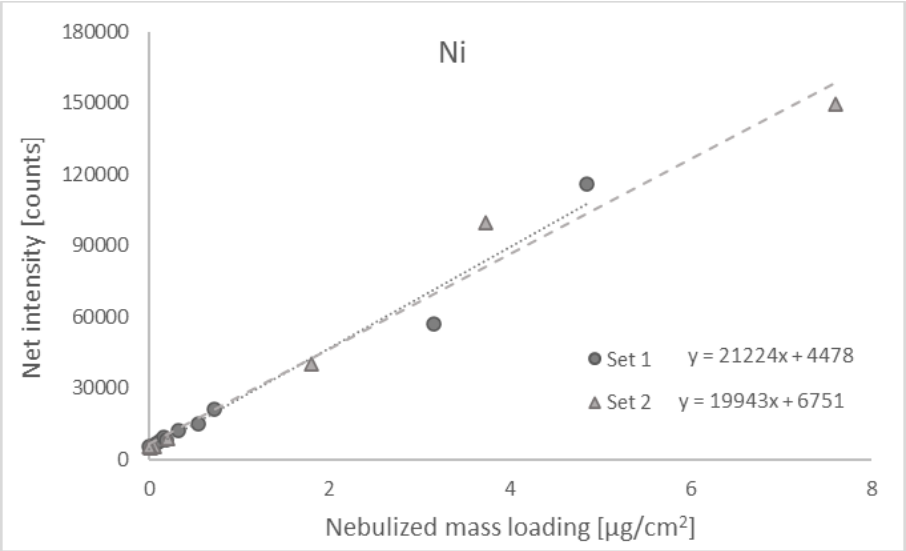

Figure 43 - Comparison of calibration lines obtained after analysis of set 1 (circles) and set 2 (triangles) with the Jeol JSX-1000S EDXRF spectrometer. Results are presented for Mn and Ni.

Considering for example a Mn detected fluorescence intensity of 80000 counts from an unknown sample, the obtained Mn nebulized mass loading is equal to 4.09 ± 0.17 µg/cm^2 with the calibration line obtained from Set 1, and equal to 4.00±0.25 µg/cm^2 considering the calibration from Set 2. If the same detected fluorescence intensity of 80000 counts is considered for Ni, the obtained Ni nebulized mass loading is equal to 3.56 ± 0.30 µg/cm^2 with the calibration line obtained from Set 1, and equal to 3.67 ± 0.65 µg/cm^2 with Set 2. Gradient, intercept and respective uncertainties of the two lines are presented in Table 12 (Hughes, Ifan G., Hase 2010). Further assessment is needed for other elements where the fitting procedure may strongly impact the results. This confirm that the production of samples is stable: the two sets were produced in different moments and with different starting solutions and the calibration lines obtained after analysis with the same instrument agree.

Table 12 - Parameters of the trend line (y = mx + c) of Mn and Ni for the two sets of samples. α is the uncertainty of the slope (m) and of the intercept (c). in the example, mass loading values are calculated from linear regression, considering a detected fluorescence intensity of 80000 counts for both Mn and Ni

	Mn		**Ni**	
	Set 1	**Set 2**	**Set 1**	**Set 2**
m	19169	19071	21224	19943
c	1543	3636	4478	6751
α (c)	1008	2171	2243	5885
α (m)	543	633	1208	1798
	Example: $\bar{y}$=80000 [counts]			
$\bar{x}$ [µg/cm^2]	4.09	4.00	3.56	3.67
α ($\bar{x}$)	0.17	0.25	0.30	0.65

6.3. TXRF spectrometers

The S2 Picofox TXRF spectrometer was utilized to measure the three sets of samples, aiming to assess whether the different geometry of the instrumental setup has an impact on the analysis outcomes. The instrument is configured with a non-focused beam, providing a notable advantage over the focused beams commonly employed in TXRF spectrometers. This advantage arises from the larger irradiated area, leading to a more comprehensive analysis of the sample and a better consideration of its morphology. Figure 44 presents the spectrum of a filter sample (set 1) obtained with this TXRF spectrometer.

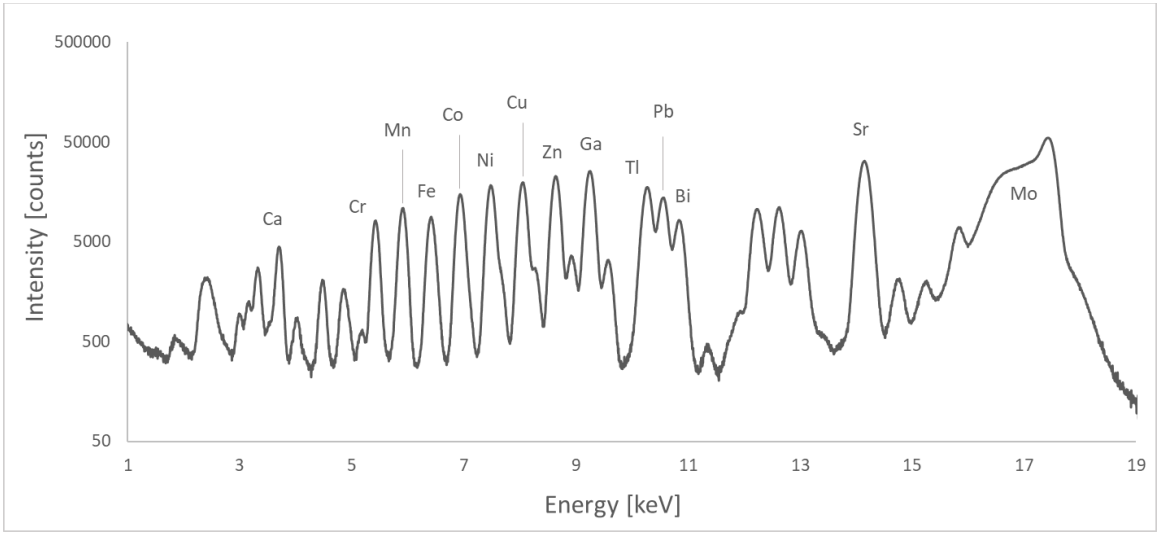

Figure 44 – Spectrum of sample 16 (set 1) obtained with the S2 Picofox spectrometer.

Each sample was measured 3 times, after a rotation of approximately 120°. Acquired spectra were analysed with the software implemented by the manufacturer and the average elemental fluorescence intensity over the three replicate measurements was calculated for each sample. The relative standard deviation (RSD %) of the elemental intensity over the three replicates was calculated and the results are reported in Table 13 for set 1, set 2 and set 3. The obtained values are on average equal to 25% for both set 1 and set 2, while around 30 % for set 3. For some samples, such as sample 18 and sample 2, the RSD values are higher. This may be due to some issues in the sample repositioning of the instrument: even small variation in beam glancing angle or sample to detector distance can lead to changes in the illuminated area and thus in the detected fluorescence intensity. A similar issue in replicate measurements was observed also in the measures of Pb loaded samples with the same TXRF spectrometer described in chapter 3. The higher RSD (%) values of set 3 with respect to set 1 and 2 was expected, because samples of this set were problematic, as already notice from EDXRF measurements, probably due to a minor purity of the starting solution.

Table 13 - Relative standard deviation (RSD) of the elemental fluorescence intensity calculated over the three measurements for each sample of set 1, 2 and 3.

	Set 1 - RSD (%)												
Element	5	6	12	11	14	10	13	15	16	1	18	2	**Average (%)**
Ca	22	10	29	17	27	9.5	7.4	14	11	41	45	41	23
Cr	49	9.1	34	20	12	14	13	34	6.6	37	46	41	26
Mn	26	8.9	33	18	8.9	11	9.4	15	12	40	45	41	22
Fe	11	8.0	25	18	29	15	12	31	6.6	37	48	58	25
Co	13	19	37	20	11	12	9.2	22	10	38	45	39	23
Ni	27	13	34	21	16	11	11	27	8.7	38	45	38	24
Cu	23	5.4	37	18	10	11	8.6	20	10	39	45	40	22
Zn	25	5.1	24	13	11	12	8.0	20	10	39	45	39	21
Ga	24	22	42	18	10	13	11	32	5.9	36	45	37	25
Sr	38	22	69	20	10	13	11	26	8.1	37	47	38	28
Tl	23	14	50	18	9.1	14	8.0	18	11	38	45	38	24
Pb	23	4.5	36	17	9.0	11	9.4	22	9.1	39	46	41	22
Bi	47	130	39	19	10	14	11	27	7.8	39	45	62	38

	Set 2 - RSD (%)						
Element	Mix 1	Mix 2	Mix 3	Mix 4	Mix 5	Mix 6	**Average (%)**
Ti	21	13	11	37	8	54	24
V	3	16	10	37	8	54	21
Mn	1	12	13	46	12	44	21
Fe	15	10	5	37	9	54	22
Ni	11	16	10	42	13	44	23
Cu	10	15	12	45	10	48	23
Zn	8	16	11	46	10	43	22
As	10	16	5	35	8	53	21
Pb	12	30	11	38	9	52	25

	Set 3 - RSD (%)							
Element	26	22	25	21	19	20	23	**Average (%)**
Ca	11	40	71	38	52	18	4	33
Ti	10	25	73	37	51	25	14	34
V	16	22	83	36	52	26	14	36
Cr	8	24	82	33	51	25	14	34
Mn	11	6	62	32	53	14	1	26
Fe	12	20	74	32	51	22	14	32
Co	11	8	62	32	54	12	3	26
Ni	15	11	66	32	53	14	4	28
Cu	18	6	59	31	53	13	5	26
Zn	20	4	55	31	54	11	4	26
As	12	22	78	33	51	25	14	34
Se	14	23	81	34	51	25	14	35
Sr	16	22	79	34	52	21	8	33

The elemental net area was plotted in correspondence of the nebulized mass loading for each sample, and Figure 45 reports the results obtained for Ni and Mn, for all the set of samples. Error bars represent the standard deviation of the average elemental intensity over the set of measurements. With both set 1 and set 2 of samples a good correlation between the nebulized mass loading and the average elemental intensity was obtained, confirming the linearity of the mass deposition also with TXRF spectrometer. The advantage of this instrument is the higher sensitivity, due to the almost parallel X-ray beam that allows to obtain spectra with a very low background.

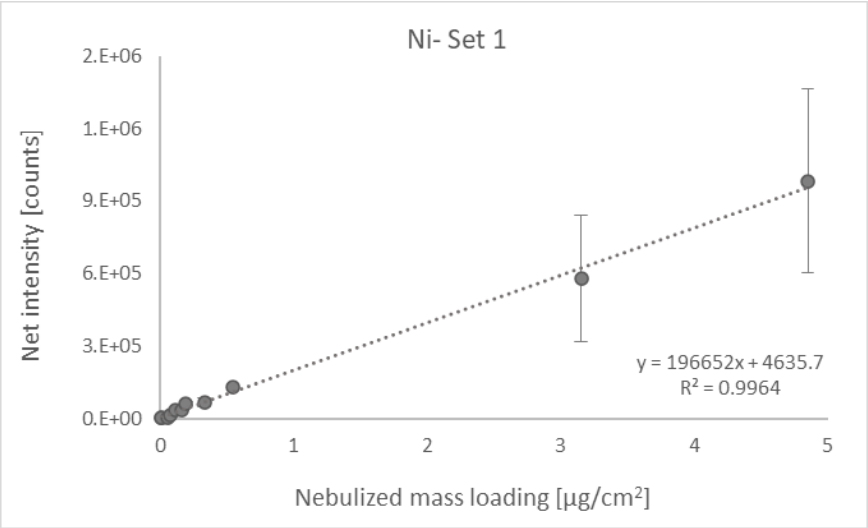
Ni- Set 1
Net intensity [counts]
2.E+06
1.E+06
9.E+05
6.E+05
3.E+05
0.E+00
0
1
2
3
4
5
y = 196652x + 4635.7
R² = 0.9964
Nebulized mass loading [µg/cm²]

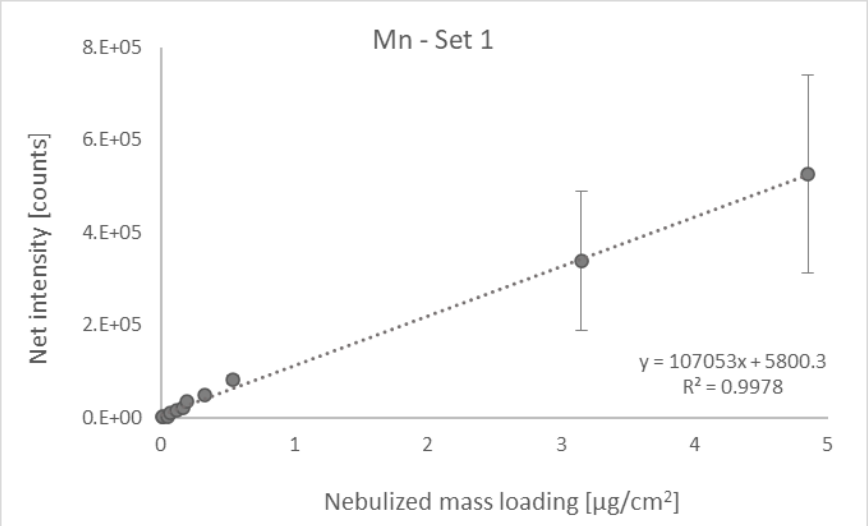
Mn - Set 1
Net intensity [counts]
8.E+05
6.E+05
4.E+05
2.E+05
0.E+00
0
1
2
3
4
5
y = 107053x + 5800.3
R² = 0.9978
Nebulized mass loading [µg/cm²]

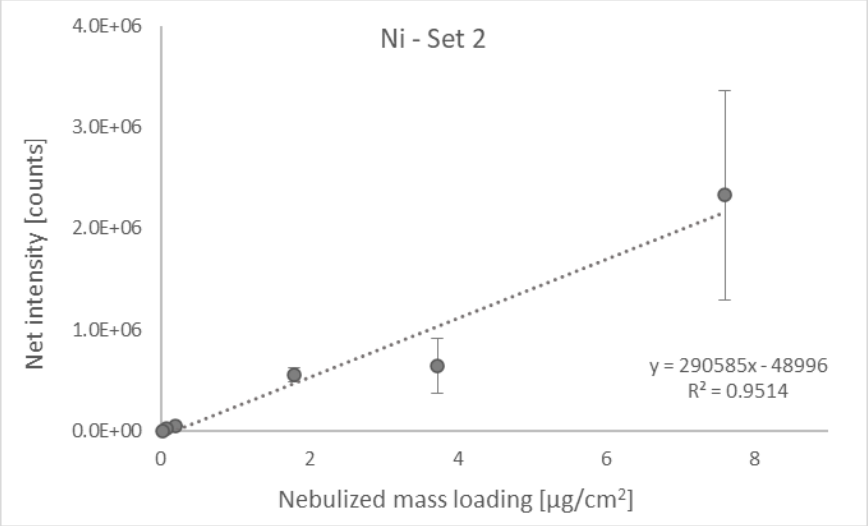
Ni - Set 2
Net intensity [counts]
4.0E+06
3.0E+06
2.0E+06
1.0E+06
0.0E+00
0
2
4
6
8
y = 290585x - 48996
R² = 0.9514
Nebulized mass loading [µg/cm²]

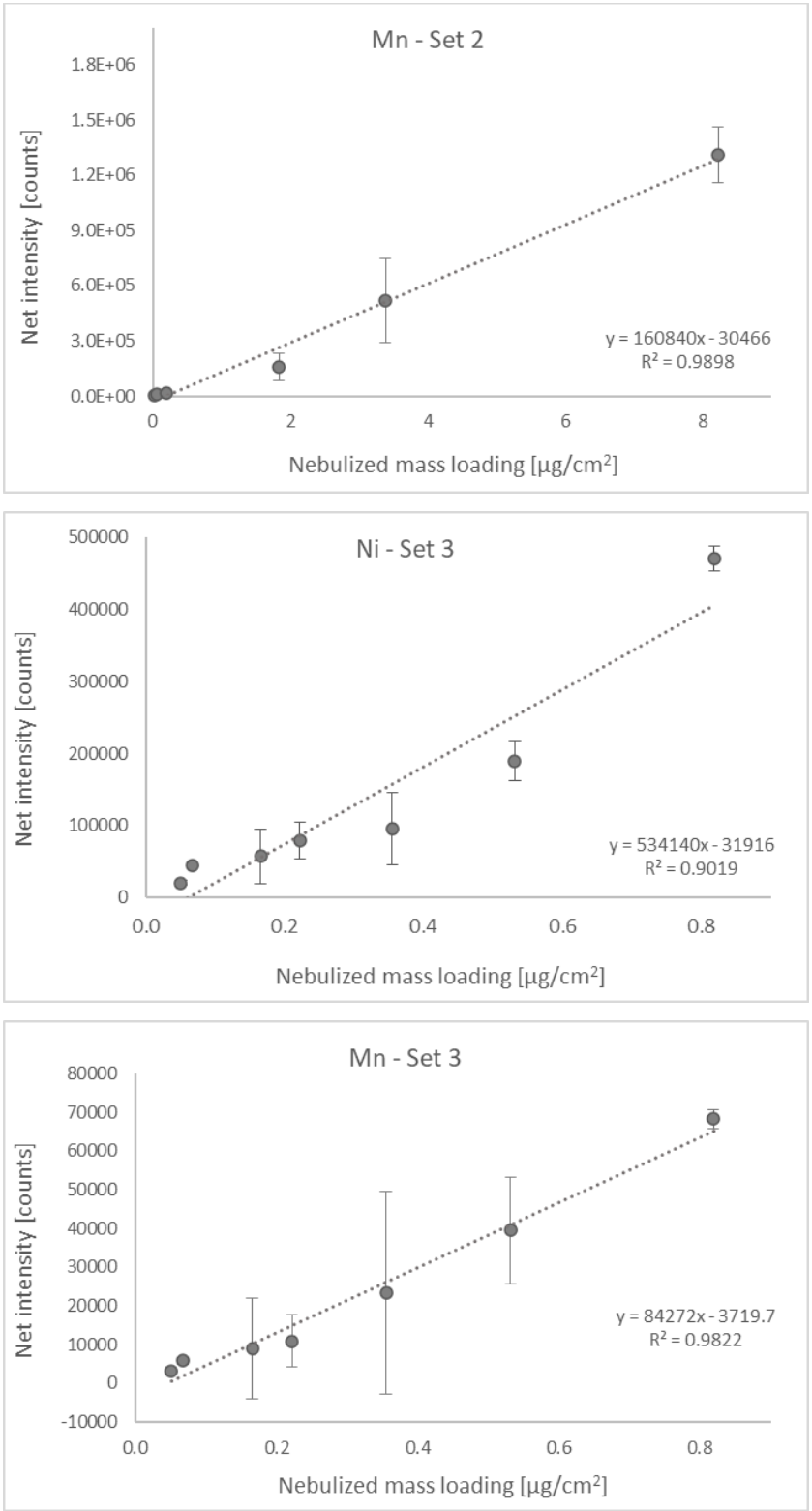

Figure 45 - Calibrations obtained for Ni and Mn with the TXRF spectrometer S2 Picofox after analysis of Set 1, set 2 and set 3. Error bars represent the standard deviation of the average elemental intensity over the replicate measurements of each sample.

Some samples of set 1 were measured also with the Bruker S4 T-STAR® TXRF spectrometer. This instrument is equipped with both Mo and W X-ray tube. According to the investigated element the excitation source should be carefully selected. With this instrument it was possible to detect also potentially toxic element such as Cd (Figure 46). With this instrument only few samples were analysed, and data were not sufficient to build a calibration line.

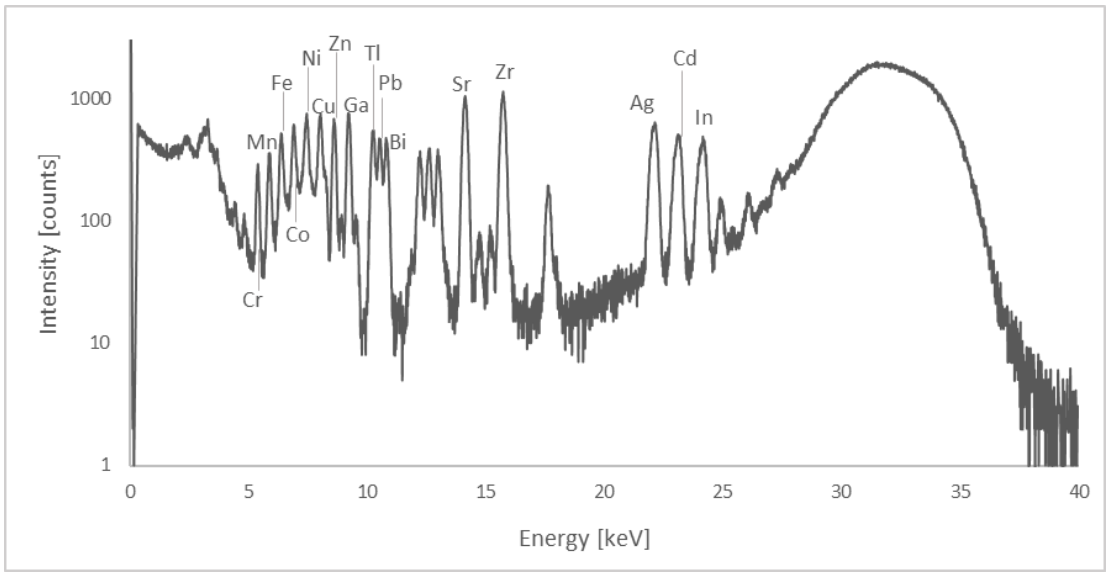

Figure 46 - Spectrum of a sample of set 1 acquired with the Bruker S4 T-Star TXRF spectrometer.

The calibration samples from Set 1 and 2 underwent additional measurements using the Nanohunter II TXRF spectrometer. Differently from the other TXRF instruments, the Nanohunter II allows for angular scan of the sample, which permits the evaluation of the dependence of the fluorescence intensity from the glancing angle. To explore this angle-dependent relationship, an angular scan was specifically conducted on Sample 15. The objective was to determine the optimal position for conducting measurements on all the other samples at a fixed angle. The angular scan was done setting the glancing angle at 0.05°, with a step width of 0.01°. The trend of the elemental intensity is presented in Figure 47.

Two positions were selected to perform the measurements of all the samples (represented by a dotted line in the graph).

1) glancing angle equal to 0.05° and the converging angle equal to 0.05°,
2) glancing angle equal to 0.15° and the converging angle equal to 0.1°

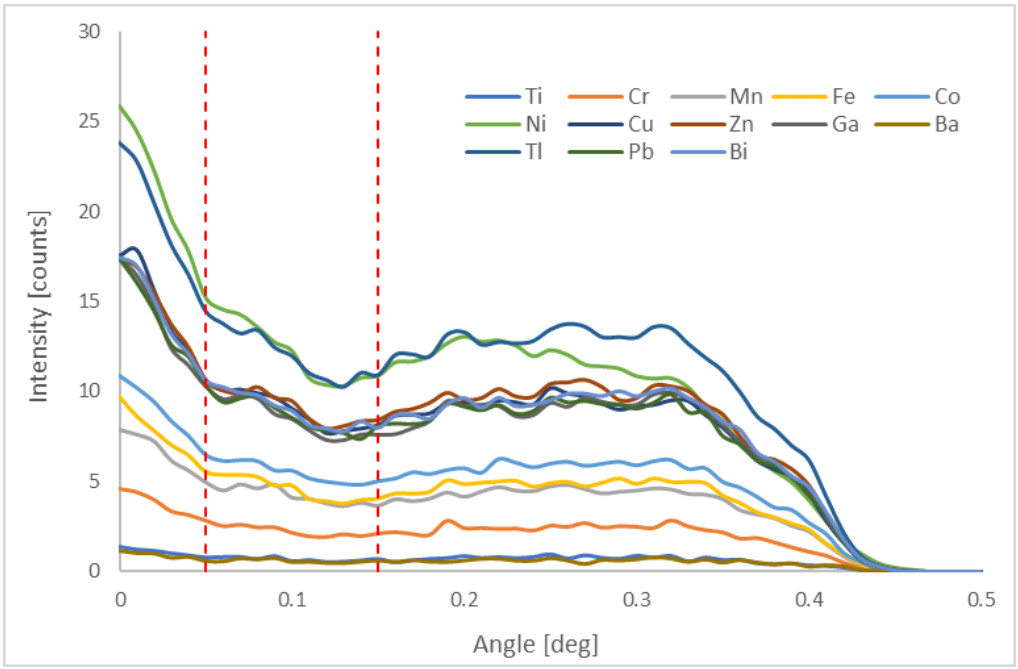

Figure 47 - Angular scan of a sample of set 1 (Sample 15) performed with the Nanohunter II spectrometer. Dotted lines represent the angular position selected to perform the measurements of all the other samples.

Two spectra of the same sample measured in the two conditions are shown in Figure 48. In condition (1) the background is lower, as expected, because the glancing angle is lower. On the other hand, the fluorescence intensity is higher in condition (2), and this could be explained considering that a higher converging angle results in a bigger illuminated area.

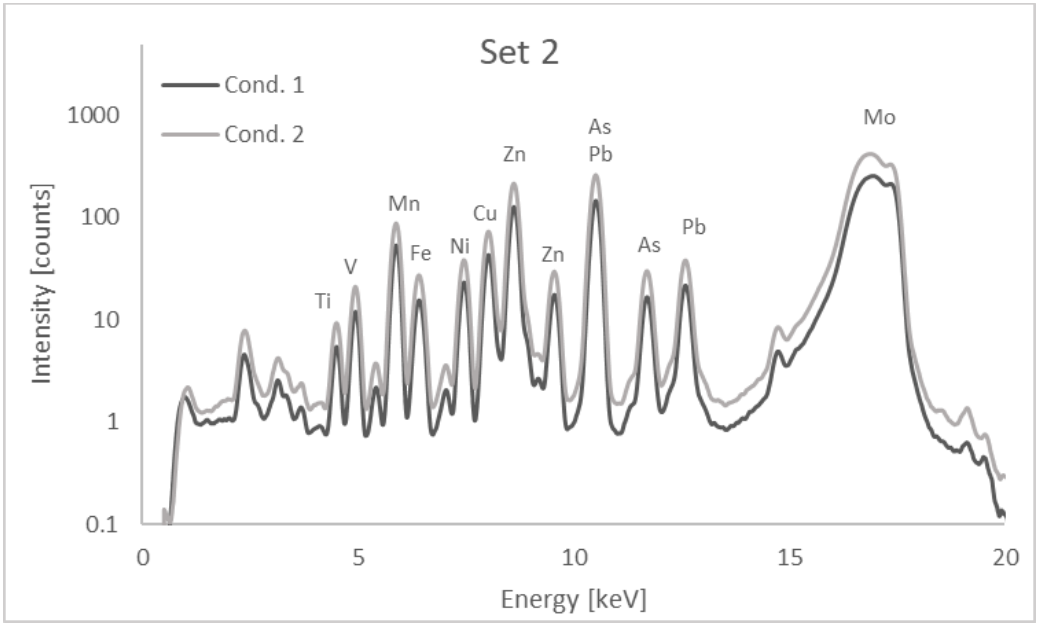

Figure 48 – Spectra of the same sample (Mix 5) obtained with the Nanohunter II spectrometer in the two selected measuring conditions: glancing angle equal to 0.05° and the converging angle equal to 0.05° (1), glancing angle equal to 0.15° and the converging angle equal to 0.1° (2).

All the samples were measured one time in the two selected conditions. After spectral analysis with PyMca software, the elemental intensity was plotted in correspondence of the nebulized mass loading of the samples. Results are shown in Figure 49 for Ni and Mn. Better results were obtained in condition (2), suggesting that when samples are analysed in XRF under grazing incidence conditions, a bigger illuminated area provides betters results.

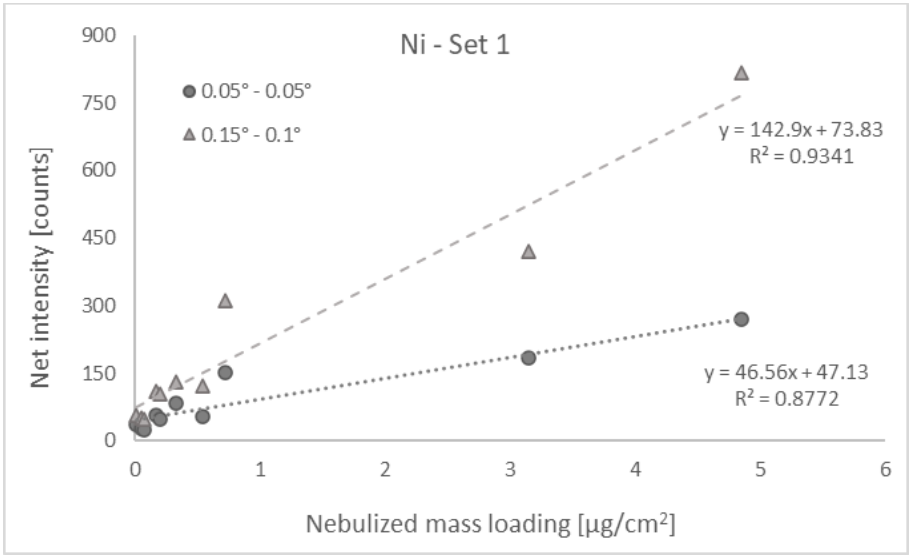
Ni - Set 1
0.05° - 0.05°
0.15° - 0.1°
y = 142.9x + 73.83
R² = 0.9341
y = 46.56x + 47.13
R² = 0.8772
Net intensity [counts]
Nebulized mass loading [µg/cm²]
900
750
600
450
300
150
0
0
1
2
3
4
5
6

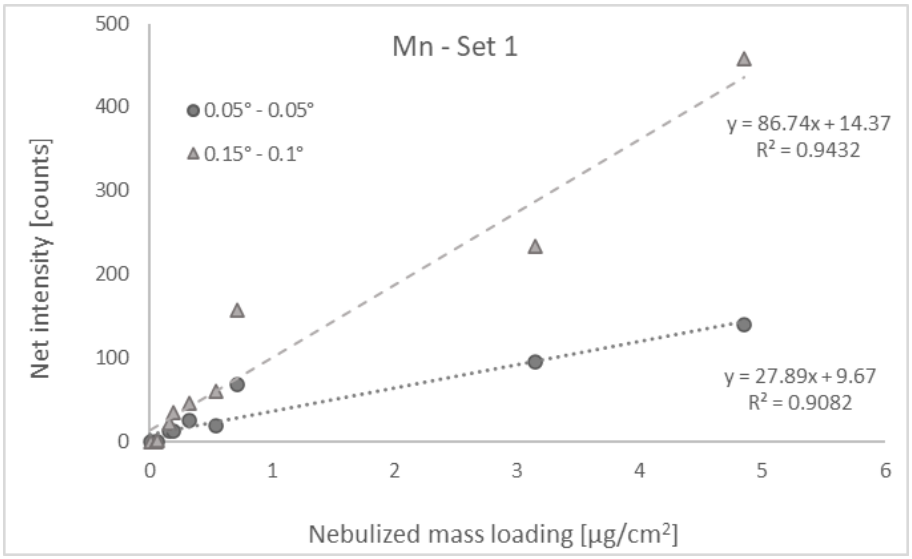
Mn - Set 1
0.05° - 0.05°
0.15° - 0.1°
y = 86.74x + 14.37
R² = 0.9432
y = 27.89x + 9.67
R² = 0.9082
Net intensity [counts]
Nebulized mass loading [µg/cm²]
500
400
300
200
100
0
0
1
2
3
4
5
6

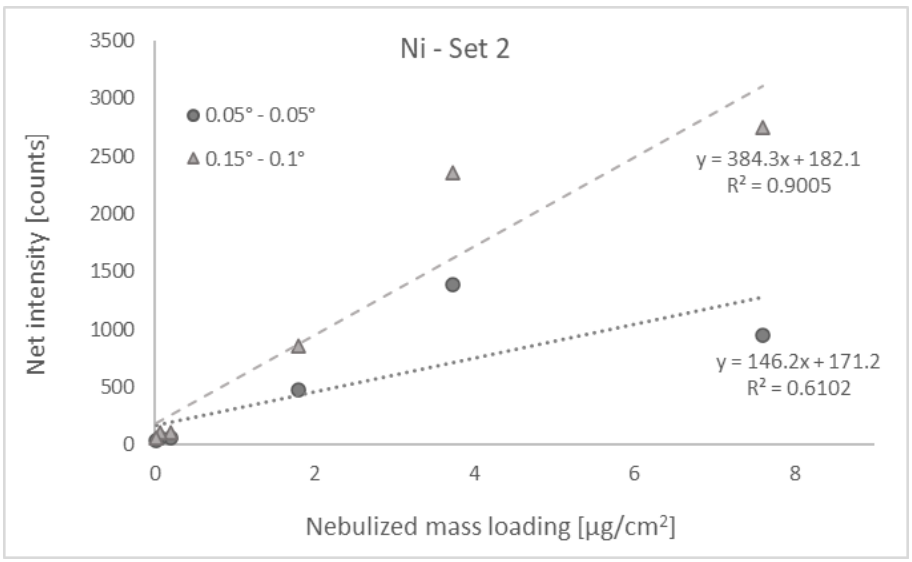
Ni - Set 2
0.05° - 0.05°
0.15° - 0.1°
y = 384.3x + 182.1
R² = 0.9005
y = 146.2x + 171.2
R² = 0.6102
Net intensity [counts]
Nebulized mass loading [µg/cm²]
3500
3000
2500
2000
1500
1000
500
0
0
2
4
6
8

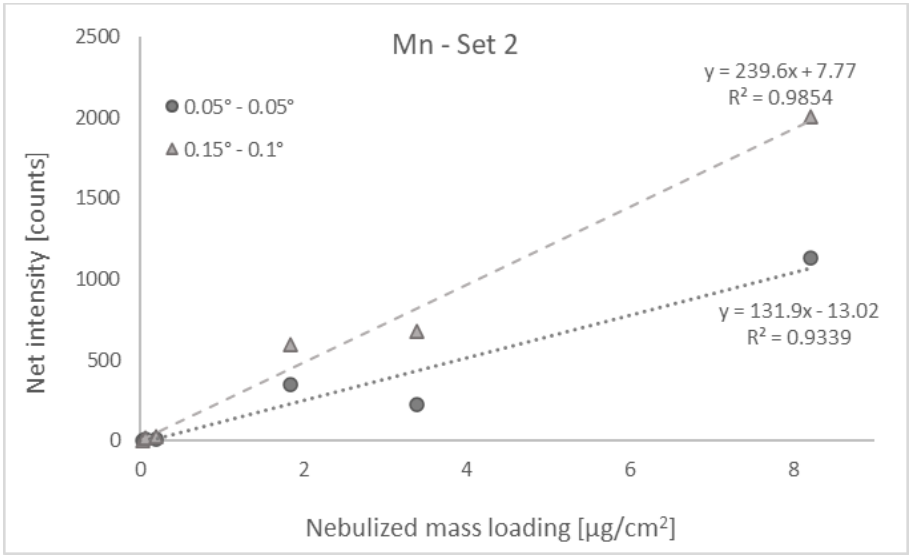

Figure 49 - Calibrations obtained for Ni and Mn with the Nanohunter II TXRF spectrometer after analysis of Set 1 and Set 2.

Calibration samples were measured also with the custom made Wobicompact spectrometer, after the alignment procedure described in section 5.4. This specific instrument allows manual adjustments of both the sample height and the angle of incidence of the beam with respect to the sample. The alignment process took place on a quartz reflector, ensuring the accomplishment of total reflection condition, thanks to the CCD camera. Subsequently, all calibration samples were measured in this position, undergoing three measurements each lasting 600 seconds. Due to the manual positioning of the sample, small variations in the height positioning of the samples occurred, this leading to variations in the illuminated area of the sample and consequently in the detected elemental intensity. To mitigate these effects, the elemental intensities derived from spectral analysis using PyMca were normalized based on the total counts recorded for each acquisition. This normalization procedure aims to account for the inherent variations arising from manual sample positioning, ensuring a more accurate and consistent assessment of elemental intensities during the subsequent analyses.

The average normalized elemental intensities were calculated over the three replicate measurements and then plotted in correspondence of the nebulized mass loading. Results are reported in Figure 50 for Ni and Mn for both set 1 and set 2 of calibration samples. Error bars represent the standard deviation of the average normalized intensity, calculated over the three replicate measurements. As it is possible to notice, the obtained curves are quite

different from the calibration lines obtained with the other spectrometers. This might be the consequence of the manual positioning of the sample in the Wobicompact spectrometer. The automatic positioning in the commercial instrument ensured that the sample height with respect to the incoming beam is always the same and this may be lacking in the case of the custom-made spectrometer.

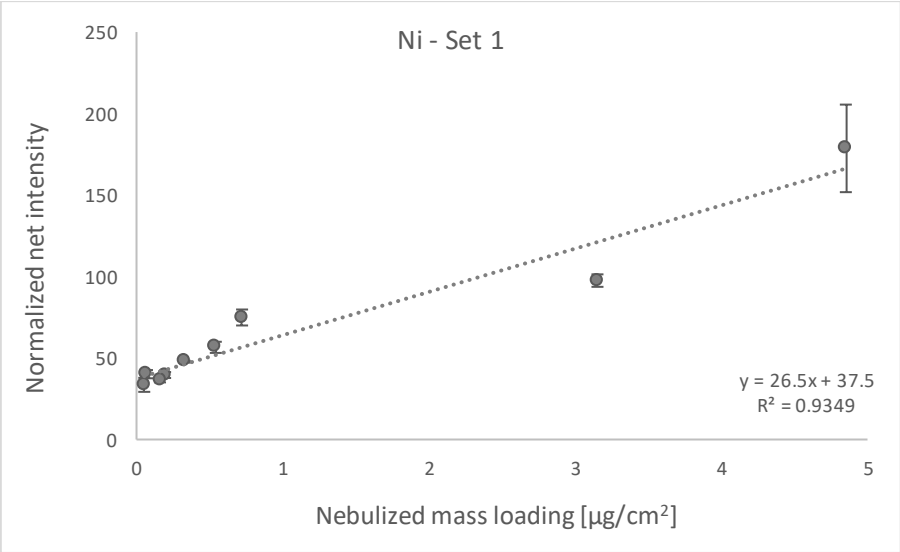

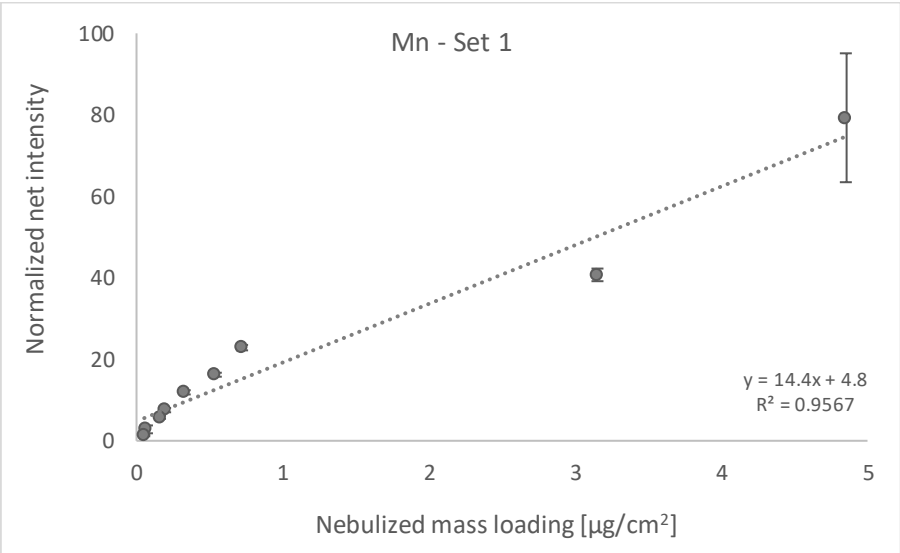

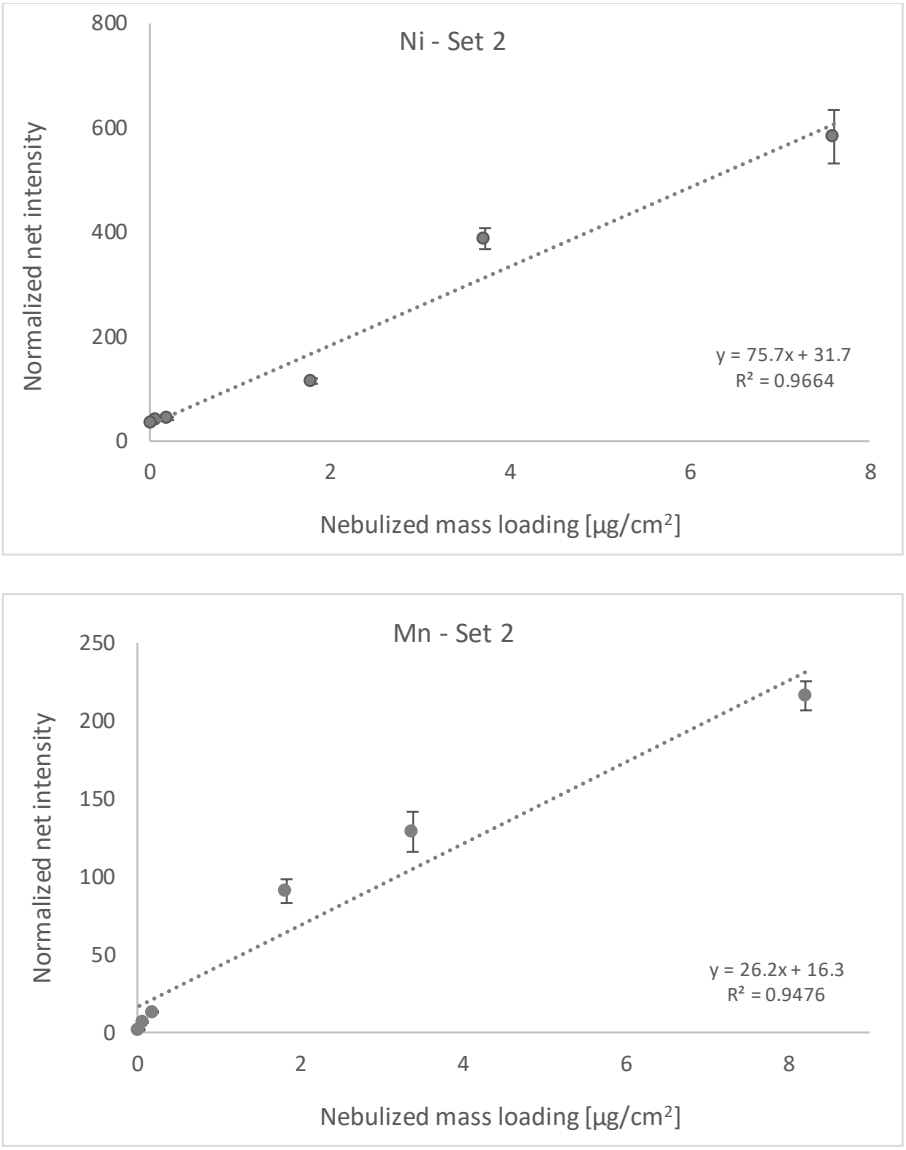

Figure 50 - Calibrations obtained for Ni and Mn with the Wobicompact spectrometer after analysis of set 1 and set 2. Error bars represent the standard deviation of the average normalized elemental intensity over the three replicate measurements of each sample.

Some samples of set 1 were measured ESRF, after a deep study of the sample positioning described in section 5.3. The described alignment process was repeated for each calibration sample, after which samples were measured in 4 different points for a measuring time of 300 s. The acquired spectra underwent deconvolution utilizing the PyMca software and the average elemental intensity was calculated. This calculated average intensity was plotted in correspondence of the nebulized mass loading and obtained results are reported in Figure 51. To visualize the variability related to the 4 measurements performed for each sample, the

error bars accompanying the plotted data symbolize the standard deviation of the average elemental intensity.

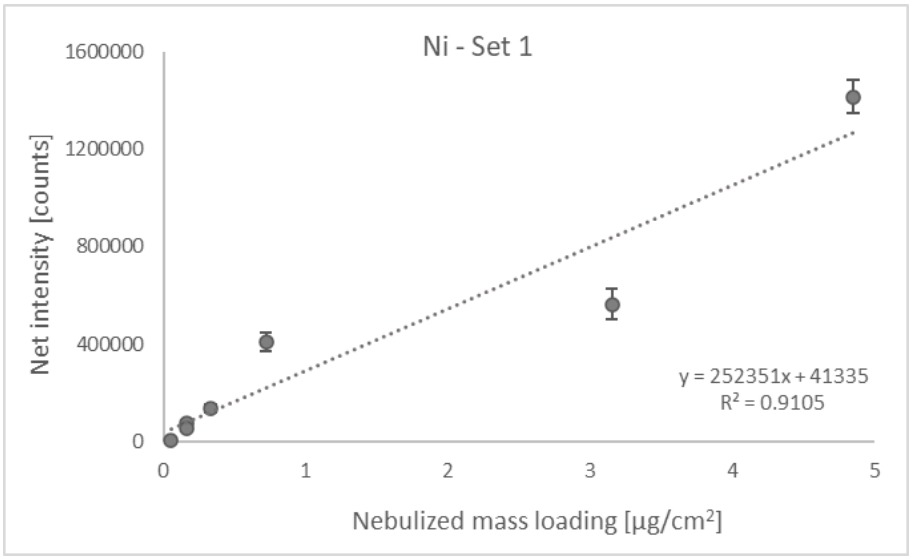

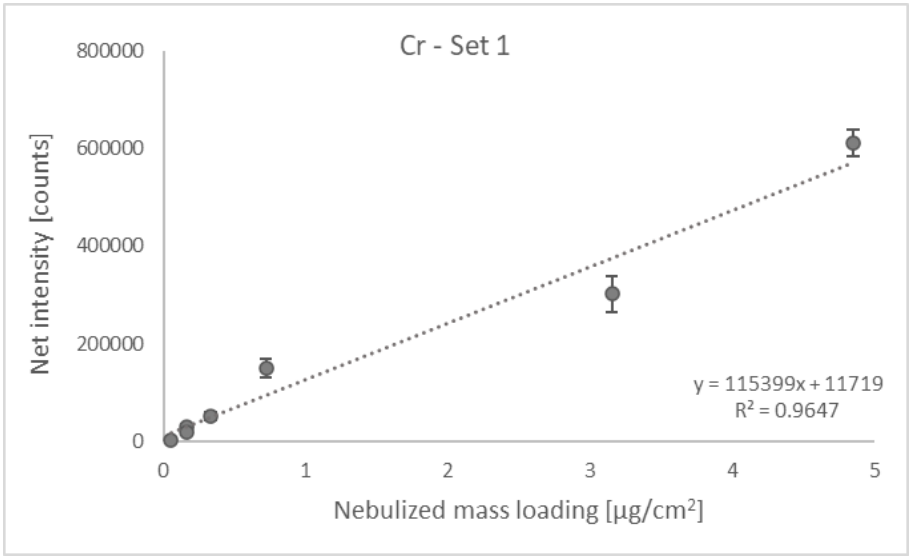

Figure 51 - Calibrations obtained for Ni and Cr after the analysis of set 1 with SR-XRF. Error bars represent the standard deviation of the average normalized elemental intensity over the four replicate measurements of each sample.

6.4. Discussion

Promising outcomes were achieved with all the typology of instruments: commercial EDXRF and TXRF spectrometers, custom made TXRF and SR-XRF. The correlation between the elemental fluorescence intensity and the nebulized mass loading was close to 1 for the majority of the sample's elements, irrespective of the specific spectrometer employed. The EDXRF spectrometers exhibited superior repeatability in measurements, as reported in the analysis presented in Table 11. This was expected because with the EDXRF spectrometers the irradiated area is bigger and the maximization of the illuminated area by the incoming X-ray beam improves measurement repeatability for this type of samples. This is confirmed also by the measurements performed with the Nanohunter II TXRF spectrometer, which provided better results when samples were measured under conditions corresponding to a broader sample illumination.

The advantage of using TXRF spectrometer, however, is the higher sensitivity that can be achieved. Thanks to their instrumental configuration, with the incoming X-ray beam almost parallel and the detector at a few millimetres distance from the sample the background is significantly reduced. Figure 52 reports the spectra acquired with a TXRF spectrometer (the S2 Picofox) and with EDXRF spectrometers (JSX-1000S and EDX 7200) of the same sample characterized by a very low mass deposition (sample Mix-1). As it is possible to note, the elemental peaks are more visible in the case of the spectrum acquired with the TXRF spectrometer, and the background is low.

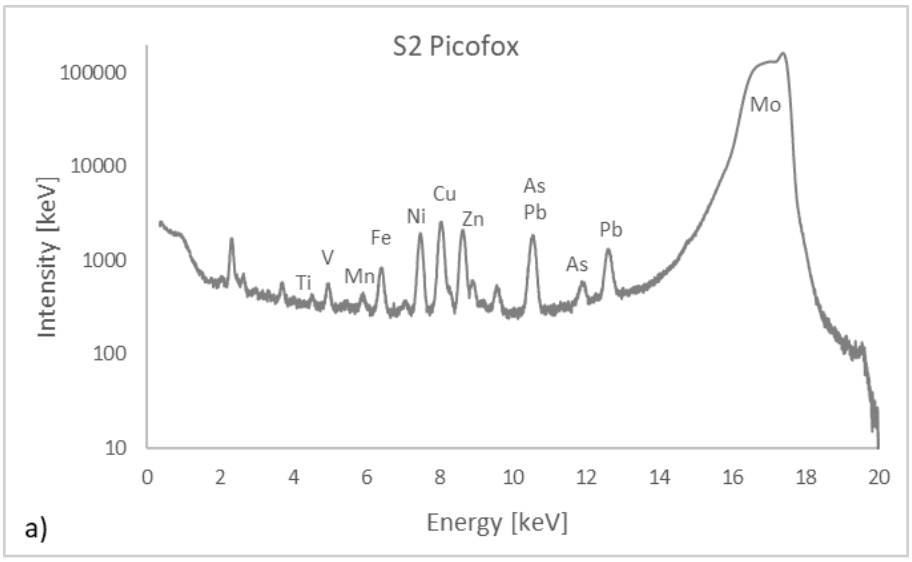

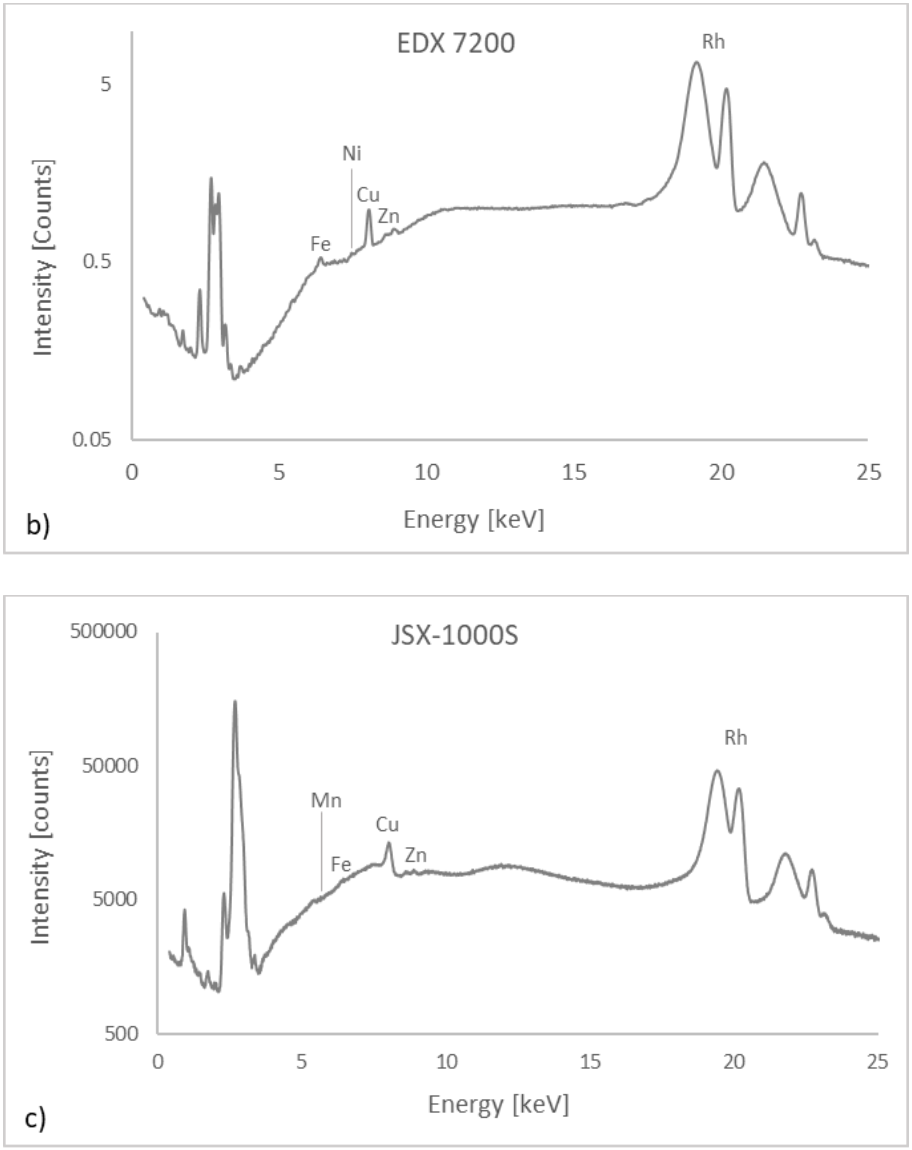

Figure 52 – Spectra of the same sample (Mix 1) characterized by a low concentration, acquired with the TXRF spectrometer S2 PCIOFOX (a) and with two EDXRF spectrometers, the EDX 7200 (b) and the JSX-1000S (c).

With all the employed spectrometers the obtained calibration curves confirm the linearity of the mass deposition for increasing nebulization times. This significant consistency is maintained despite variations in instrumental geometry, excitation sources and measuring conditions, including measuring time, collimator dimensions and sample-to-detector distance. It is essential to highlight that calibration lines were not uniformly constructed across all instruments. As already specified in the text, for some instruments the spectral deconvolution was performed with the instrumental software, while others utilized the

PyMca software for this purpose. Despite the differences in the data treatment, the mass loading obtained from linear regression is consistent with the nebulized one, for all the spectrometers.

The observed linearity in this context confirms that the actual concentration of the calibration samples maintains a proportional relationship with the nebulized mass loading, though with the inclusion of a correction factor. It is important to stress that the actual concentration of the samples is supposed to be less than the nebulized mass loading, with the latter representing the ideal value calculated under the assumption of no losses during the sample preparation phase. Future investigations will be dedicated to the precise determination of this correction factor, which is designed to consider aerosol losses related to the sample preparation process. This search aims to understand the true concentration of the samples and improve the accuracy of the proposed method for direct filter analysis with X-ray based instruments.

The calibration samples were created with a nebulized mass loading within the range of the limits imposed by EC in air, for the protection of human health. This implies that the concentration of potentially hazardous elements in PM can be measured using X-ray based devices calibrated using these samples. The methodology presented for environmental monitoring not only finds utility in its intended purpose but also holds potential applications in diverse contexts, such as workplaces monitoring. By varying the concentration of the nebulized solution and the nebulization time, indeed, it is possible to create samples with higher concentration. This flexibility is particularly advantageous when addressing air monitoring in workplace environments where permissible concentration limits are higher. The ability to tailor the method to different concentration levels enhances its versatility, making it a valuable tool for monitoring and ensuring compliance with regulatory standards in various settings, including occupational environments.

This procedure for filter preparation presents several advantages. First of all, it is adjustable to the need of the user: the elemental composition can be chosen, it is possible to create both multi- and mono-element samples. The concentration range is tunable as well and can be personalized according to the intended use. The produced samples can be employed for calibration purposes but also for method comparison, to evaluate correspondence between XRF and ICP techniques. Due to the marketable application of these calibration samples,

these further investigations will be carried out in the context of the COST Innovator Grant (CIG) 18130 "AIR particulate reference material for elemental quantification and CALibration procedures" (Air-Cal). The primary goal of this CIG is to provide RMs of PM filters with their associated guidelines, and specific standard operating procedures for their use with XRF based techniques but also ICP based techniques. The activities of Air-Cal are aimed at improving production processes of the calibration samples, to bring them into compliance with technical requirements for RMs provided for in ISO 17034, to adapt the quantification range to meet the needs of the EU directives for the various application fields, and to ensure traceability with regard to preexisting CRM. The expected outcome of this CIG is to validate this innovative way to prepare RMs from the technological, normative, and business point of view. The ultimate goal of Air-Cal is making available on the market these RMs of PM filters, with the possibility to personalize elemental composition and concentration range according to the user's willingness.

In addition to the determination of the correction factor relating the nebulized mass loading and the actual elemental concentration of the samples, other steps should be taken in the future. First, the accuracy of the results obtained with the samples under study should be determined. Further investigations on sample homogeneity are also needed. Then, it would be interesting to create some calibration samples adding latex particles of variable dimension and/or microplastics to the nebulization solution, to mimic the presence of dust and organic compounds in real PM. This would be useful to evaluate matrix effects that can arise when real air filters are measured. To deepen the evaluation of the stability of calibration samples, future measurements using the spectrometers utilized in this research should be conducted on the sets discussed here. This will enable to determine if the resulting calibration lines are affected over time. Additionally, it is important to evaluate the elemental limits of detection that can be obtained with different spectrometers, to compare the performance between EDXRF and TXRF techniques.

CONCLUSION

This doctoral research was aimed at proving the applicability of X-ray based instrument for the direct analysis of air filters, for obtaining quantitative information about the elemental content of PM.

The method for filter analysis underwent initial testing with commercially available TXRF spectrometers, using mono-elemental samples supplied by an external research centre. To further assess the applicability of the method for other elements of environmental interest, three sets of PTFE filters, each varying in elemental composition and concentration of the deposition, were created within the laboratory setting. The nebulized mass loading was selected for environmental monitoring purposes, considering the limits imposed by EC in the two Air Quality Directives. Samples underwent to the Smart Store® preparation procedure, which consists in enclosing the filtering membrane between two polymeric thin layer and enables the direct analysis of the filters. This easy and fast procedure is essential to preserve the sample over time, free of contamination. Sample production and characterization was carried out following the indications provided by the ISO Guides for RMs.

Since the obtained samples are unconventional in XRF analysis, sample alignment was deeply assessed both at synchrotron facility and with benchtop instruments, to define the best measuring conditions. The calibration samples were analysed with several spectrometers, differing in geometry, excitation source and instrumental setup, and with all of them a satisfactory linearity between nebulized mass loading and elemental fluorescence intensity was obtained. The main advantage of these samples is the fact that they are customizable, allowing for the production of samples containing specific elements at adjustable concentrations tailored to meet specific needs or purposes. Due to some issues in samples digestion, the actual mass loading of the calibration samples will be further investigated. Considering the proved linearity between nebulized mass loading and elemental intensity, the actual mass loading is supposed to be directly proportional to the nebulized one, and a correction factor must be determined.

Additional studies will be carried on for the qualification of these calibration samples as RMs for PM filters. This development is part of the objectives outlined in the COST IG 18130 "AIR particulate reference material for elemental quantification and CALibration

procedures". The primary objective of this initiative is to create RMs for PM filters, facilitating traceability and enabling comparisons across diverse elemental analysis techniques.

These findings will be included in ISO AWI 23971, which seeks to standardize a method for the direct analysis of PM filters using X-ray-based instruments. With respect to conventional methods for filter analysis, the X-ray fluorescence under grazing incidence this method is faster, greener and non-destructive. The adoption of the methodology proposed in the standard facilitates the acquisition of quantitative information regarding PM composition, thereby simplifying and encouraging air quality monitoring processes.

ACKNOWLEDGMENT

I would like to express my deepest gratitude to Professor Laura Borgese, my supervisor, for her guidance and mentorship during my doctoral studies. She guided me carefully, always leaving me independent and believing in my capabilities. She constantly encouraged me to strive for excellence. I am sincerely thankful for the many opportunities she offered me and for all the diverse activities I did during these three years. She always supported me and my academic growth and represented an important reference point. I would also like to thank Prof. Depero, tireless leader of the Chem4Tech lab, and all my colleagues for the time spent together.

These three years represented a memorable journey, both metaphorically and literally. It was an enriching journey of personal growth, during which I had the chance to face new challenges, each contributing to my personal development. This PhD was also a real trip: I travelled in 8 countries in 3 different continents for research activities and conferences. I would like to deeply thank all the amazing people that I met during these travels, for their help, their teaching, and their hospitality. In particular, I would like to thank Prof. Eva Marguí and Dr. Ignasi Queralt from the University of Girona, Prof. Kouichi Tsuji and Dr. Tsugufumi Matsuyama from the Osaka Metropolitan University, Dr. Hikari Takahara from Rigaku, Dr. Giacomo Siviero from GNR srl, Dr. Diane Eichert from Elettra-Sincrotrone, Prof. Tom Hase from Warwik University, Dr. Armin Gross and Dr. Hagen Stosnach from Bruker Nano GmbH. I acknowledge CA 18130 ENFORCE TXRF and CIG 18130 Air-Cal for supporting and funding these research activities.

For the emotional support I thank my parents and my sister, always standing by me, offering encouragement even in moments of self-doubt. Their understanding and constant belief in my abilities have been the cornerstone of my academic journey. I am deeply grateful for the love, patience, and support they demonstrated. They have always served as role models of hard work, dedication, and commitment.

Last but not least, thanks to the *Pomele*, my beloved friends, my steadfast anchor, who have remained a constant presence throughout the highs and lows of my journey. The carefree moments we spent together were essential in lighten my minds. It would have been much harder for me to go through these three years without all of you girls. I hope our friendship can remain solid even in the challenges that the future holds for us.

BIBLIOGRAPHY

Abelsohn, Alan, and Dave M Stieb. 2011. "Health Effects of Outdoor Air Pollution: Approach to Counseling Patients Using the Air Quality Health Index." *Canadian family physician Medecin de famille canadien* 57(8): 881–87, e280-7. http://www.ncbi.nlm.nih.gov/pubmed/21841106%0Ahttp://www.pubmedcentral.nih.gov/articlerender.fcgi?artid=PMC3155438.

Adams, Freddy C. 2017. "X-Ray Absorption and Diffraction—Overview." In *Reference Module in Chemistry, Molecular Sciences and Chemical Engineering*, Elsevier, 391–403. https://linkinghub.elsevier.com/retrieve/pii/B9780124095472142635.

Adams, Kate et al. 2015. "Particulate Matter Components, Sources, and Health: Systematic Approaches to Testing Effects." *Journal of the Air and Waste Management Association* 65(5): 544–58. http://dx.doi.org/10.1080/10962247.2014.1001884.

Allegretta, I. et al. 2019. "Rapid Multi- Element Characterization of Microgreens via Total-Reflection X-Ray Fluorescence (TXRF) Spectrometry." *Food Chemistry* 296: 86–93.

Andrade, J. M., and M. P. Gómez-Carracedo. 2013. "Notes on the Use of Mandel's Test to Check for Nonlinearity in Laboratory Calibrations." *Analytical Methods* 5(5): 1145–49.

Bacon, Jeffrey R et al. 2019. "Atomic Spectrometry Update – a Review of Advances in Environmental Analysis." *J. Anal. At. Spectrom.* 34(1): 9–58.

BAM. 2023. "COMAR." https://www.comar.org/index.htm (January 27, 2024).

Beckhoff, B et al. 2006. "Analysis of Layers." In *Handbook of Practical X-Ray Fluorescence Analysis*, Berlin: Springer-Verlag, 554–600.

Berger, M.J. et al. 2010. "XCOM: Photon Cross Sections Database." *NIST, PML, Radiation Physics Division*. https://physics.nist.gov/PhysRefData/Xcom/html/xcom1.html (February 16, 2021).

Bescond, Alexandre et al. 2021. "Method for Preparation of a Candidate Reference Material of Pm10 and Pm2.5 Airborne Particulate Filters Loaded with Incineration Ash-Inter Comparison Results for Metal Concentrations." *Atmosphere* 12(1): 1–19.

Bilo, F. et al. 2017. "Elemental Analysis of Tree Leaves by Total Reflection X-Ray Fluorescence: New Approaches for Air Quality Monitoring." *Chemosphere* 178: 504–12.

Bilo, F. et al., 2018. “Comparison of Multiple X-Ray Fluorescence Techniques for Elemental Analysis of Particulate Matter Collected on Air Filters.” *Journal of Aerosol Science* 122(May): 1–10. https://doi.org/10.1016/j.jaerosci.2018.05.003.

Boman, Johan, Annemarie Wagner, and Michael J. Gatari. 2010. “Trace Elements in PM2.5 in Gothenburg, Sweden.” *Spectrochimica Acta - Part B Atomic Spectroscopy* 65(6): 478–82. http://dx.doi.org/10.1016/j.sab.2010.03.014.

Borges, Daniel L.G., and James A. Holcombe. 2017. “Graphite Furnace Atomic Absorption Spectrometry.” *Encyclopedia of Analytical Chemistry*: 1–20.

Borgese, L. et al. 2012. “Airborne Particulate Matter (PM) Filter Analysis and Modeling by Total Reflection X-Ray Fluorescence (TXRF) and X-Ray Standing Wave (XSW).” *Talanta* 89: 99–104. http://dx.doi.org/10.1016/j.talanta.2011.11.073.

Borgese, L. et al. 2011. “A New Non-Destructive Method for Chemical Analysis of Particulate Matter Filters: The Case of Manganese Air Pollution in Vallecamonica (Italy).” *Talanta* 84(1): 192–98.

Borgese, L. et al. 2018. “Comprehensive Approach to the Validation of the Standard Method for Total Reflection X-Ray Fluorescence Analysis of Water.” *Talanta* 181(October 2017): 165–71.

Borgese, L. et al. 2020. “The Assessment of a Method for Measurements and Lead Quantification in Air Particulate Matter Using Total Reflection X-Ray Fluorescence Spectrometers.” *Spectrochimica Acta - Part B Atomic Spectroscopy* 167(March): 105840. https://doi.org/10.1016/j.sab.2020.105840.

Brown, Richard J.C. et al. 2010. “Comparison of ED-XRF and LA-ICP-MS with the European Reference Method of Acid Digestion-ICP-MS for the Measurement of Metals in Ambient Particulate Matter.” *Accreditation and Quality Assurance* 15(9): 493–502.

Calzolai, Giulia et al. 2008. “PIXE and XRF Analysis of Particulate Matter Samples: An Inter-Laboratory Comparison.” *Nuclear Instruments and Methods in Physics Research, Section B: Beam Interactions with Materials and Atoms* 266(10): 2401–4.

Celo, Valbona, Ewa Dabek-Zlotorzynska, David Mathieu, and Irinna Okonskaia. 2011. “Validation of a Simple Microwave-Assisted Acid Digestion Method Using Microvessels for Analysis of Trace Elements in Atmospheric PM2.5 in Monitoring and Fingerprinting Studies.” *The Open Chemical and Biomedical Methods Journal* 3(1): 143–52.

Cirelli, P. et al. 2022. “Assessment of Calibration Methods for Pb-Loaded Aerosol Filters Analysed with X-Ray Fluorescence under Grazing Incidence.” *Spectrochimica Acta - Part B Atomic Spectroscopy* 192(March): 106414. https://doi.org/10.1016/j.sab.2022.106414.

COST. 2019. “CA 18130 ‘ENFORCE TXRF’ - EUROPEAN NETWORK FOR CHEMICAL ELEMENTAL ANALYSIS BY TOTAL REFLECTION X-RAY FLUORESCENCE.” https://enforcetxrf.eu/.

Dalipi R., Marguí E., Borgese L., and Depero L. E. 2017. “Multi-Element Analysis of Vegetal Foodstuff by Means of Low Power Total Reflection X-Ray Fluorescence (TXRF) Spectrometry.” *Food Chemistry* 218: 348–55. http://dx.doi.org/10.1016/j.foodchem.2016.09.022.

EEA. 2019. EEA Report No 10/2019 *Air Pollution by Ozone Across Europe: Handbook of Environmental Chemistry*. https://www.eea.europa.eu/publications/air-quality-in-europe-2019.

EEA. 2023. EEA Technical report *European Union Emission Inventory Report 1990–2014 under the UNECE Convention on Long-Range Transboundary Air Pollution (LRTAP)*.

Elias, Md Suhaimi et al. 2023. “Assessment and Sources Identification of Air Quality Pollution in Klang Valley, Kuala Lumpur, Malaysia.” *IOP Conference Series: Materials Science and Engineering* 1285(1): 012017.

Elsayed, Yehya, Sofian Kanan, and Ahmad Farhat. 2021. “Meteorological Patterns, Technical Validation, and Chemical Comparison of Atmospheric Dust Depositions and Bulk Sand in the Arabian Gulf Region.” *Environmental Pollution* 269.

EU. 2004. “Directive 2004/26/EC of the European Parliament and of the Council of 21 April 2004 Amending Directive 97/68/EC on the Approximation of the Laws of the Member States Relating to Measures against the Emission of Gaseous and Particle Pollutants from Interna.” *Official Journal of the European Union* L 225/3.

EU. 2008. “Directive 2008/50/EC of the European Parliament and of the Council of 21/05/2008 on Ambient Air Quality and Cleaner Air for Europe.” *Official Journal of the European Union* L 152/1.

European Commission. 2022. “Zero Pollution Action Plan.” https://environment.ec.europa.eu/strategy/zero-pollution-action-plan_en (January 27, 2024).

European Environment Agency (EEA). 2022. “Health Impacts of Air Pollution in Europe, 2022.” https://www.eea.europa.eu/publications/air-quality-in-europe-2022/health-impacts-of-air-pollution (January 27, 2024).

Fernández-Ruiz, Ramón. 2019. “TXRF Workgroup: An Alternative Environment for Scientific Collaboration.” *Spectroscopy Europe* 31(1): 18–21. https://orcid.org/0000-0003-4769-3484,http://www.uam.es/sidi.

Garcia, Amanda et al. 2023. “Toxicological Effects of Fine Particulate Matter (PM2.5): Health Risks and Associated Systemic Injuries—Systematic Review.” *Water, Air, and Soil Pollution* 234(6): 1–23. https://doi.org/10.1007/s11270-023-06278-9.

Gemeiner, Hendryk et al. 2017. “Elemental and Isotopic Determination of Lead (Pb) in Particulate Matter in the Brazilian City of Goiânia (GO) Using ICP-MS Technique.” *Environmental Science and Pollution Research* 24(25): 20616–25.

Harvey, David. 2009. “Developing a Standard Method.” In *Analytical Chemistry 2.0*, , 945–94.

Heller-Zeisler, Susan F. et al. 1998. “Examination of a Procedure for the Production of a Simulated Filter-Based Air Particulate Matter Reference Material.” *Fresenius' Journal of Analytical Chemistry* 360(3–4): 435–38.

Hughes, Ifan G., Hase, Thomas P.A. 2010. *Uncertainties in Single-Variable*. Oxford.

ISO. 2015a. 2015 *ISO Guide 30:2015. Reference Materials - Selected Terms and Definitions*.

ISO. 2015b. *ISO Guide 31:2015. Reference Materials - Contents of Certificates and Labels*. https://www.iso.org/standard/52468.html.

ISO. 2015c. *ISO Guide 33: Reference Materials - Good Practice in Using Reference Materials*. https://www.iso.org/standard/46212.html.

ISO. 2016. *ISO 17034 - General Requirements for the Competence of Reference Material Producers*. https://www.iso.org/standard/29357.html.

ISO. 2017. *ISO Guide 35:2017. Reference Materials - Guidance for Characterization and Assessment of Homogeneity and Stability*. https://www.iso.org/standard/60281.html.

IUPAC. 1997. *Compendium of Chemical Terminology*. 2nd ed. (t. eds. A. D. McNaught and A. Wilkinson. Blackwell Scientific Publications.

Jenks, Peter J., and Harry Klich. 2001. “Availability and Sources of Information.” In *Reference Materials for Chemical Analysis. Certification, Availability, and Proper*

Usage, eds. Markus Stoeppler, Wayne R. Wolf, and Peter J. Jenks. Wiley, 256–78.

Karthikeyan, Sathrugnan, Umid Man, and Rajasekhar Balasubramanian. 2006. "Microwave Assisted Sample Preparation for Determining Water-Soluble Fraction of Trace Elements in Urban Airborne Particulate Matter : Evaluation of Bioavailability ଝ." 576: 23–30.

Klockenkämper, R., and A. von bohlen. 1989. "Determination of the Critical Thickness and the Sensitivity for Thin-Film Analysis by Total Reflection X-Ray Fluorescence Spectrometry." *Spectrochimica Acta Part B: Atomic Spectroscopy* 44(5): 461–69.

Klockenkämper, R., and A. Von Bohlen. 2015. *Total Reflection X-Ray Fluorescence Analysis and Related Methods*. 2nd ed. Wiley.

Kregsamer, Peter. 2009. "QXAS - Quantitative X-Ray Analysis System (User ' s Manual and Guide to X-Ray Fluorescence Technique)."

Krittanawong, Chayakrit et al. 2023. "International Journal of Cardiology Cardiovascular Risk and Prevention PM 2 . 5 and Cardiovascular Diseases : State-of-the-Art Review." 19(October).

Lee, Byeong Jae, Bumseok Kim, and Kyuhong Lee. 2014. "Air Pollution Exposure and Cardiovascular Disease." *Toxicological Research* 30(2): 71–75.

López-Lorente, Ángela I. et al. 2022. "The Ten Principles of Green Sample Preparation." *TrAC - Trends in Analytical Chemistry* 148.

Lu, Xin et al. 2022. "Amphiphobic Polytetrafluoroethylene Membrane with a Ring-on-String-like Micro/Nano Structure for Air Purification." *Journal of Membrane Science* 652(18): 120476. https://doi.org/10.1016/j.memsci.2022.120476.

Marguí, E. et al. 2010. "Applicability of Direct Total Reflection X-Ray Fluorescence Analysis for Selenium Determination in Solutions Related to Environmental and Geochemical Studies." *Spectrochimica Acta Part B: Atomic Spectroscopy* 65(12): 1002–7.

Menzel, N., P. Schramel, and K. Wittmaack. 2002. "Elemental Composition of Aerosol Particulate Matter Collected on Membrane Filters: A Comparison of Results by PIXE and ICP-AES." *Nuclear Instruments and Methods in Physics Research, Section B: Beam Interactions with Materials and Atoms* 189(1–4): 94–99.

Micromatter. 2017. "XRF Calibration Standards." https://www.micromatter.com/XRFCalibrationStandards.aspx (January 27, 2024).

Mukherjee, Arideep, and Madhoolika Agrawal. 2017. “World Air Particulate Matter: Sources, Distribution and Health Effects.” *Environmental Chemistry Letters* 15(2): 283–309.

Niu, Jianjun et al. 2010. “Evaluation of Airborne Particulate Matter and Metals Data in Personal, Indoor and Outdoor Environments Using ED-XRF and ICP-MS and Co-Located Duplicate Samples.” *Atmospheric Environment* 44(2): 235–45.

Oster, Caroline, Guillaume Labarraque, and Paola Fisicaro. 2015. “Certification of a Reference Material of Metal Content in Atmospheric Particles Deposited on Filters.” *Analytical and Bioanalytical Chemistry* 407(11): 3035–43.

Öztürk, Fatma, Abdullah Zararsiz, Ridvan Kirmaz, and Gürdal Tuncel. 2011. “An Approach to Measure Trace Elements in Particles Collected on Fiber Filters Using EDXRF.” *Talanta* 83(3): 823–31.

Pfeiffer, R.L. 2015. “Sampling For PM10 and PM2.5 Particulates.” : 227–45.

Quevauviller, P. 2005. “Production of Reference Materials.” In *Encyclopedia of Analytical Science*, , 458–62.

Ruiz, Ramón Fernández. 2014. “TXRF Spectrometry as a Powerful Tool for the Study of Metallic Traces in Biological Systems.” *Development in Analytical Chemistry* 1(July). www.seipub.org/dac.

Samek, L. et al. 2006. “Speciation of Selected Metals in Aerosol Samples by TXRF after Sequential Leaching.” *X-Ray Spectrometry* 35: 226–31.

Schmeling, M. 2001. “Total-Reflection X-Ray Fluorescence - A Tool to Obtain Information about Different Air Masses and Air Pollution.” *Spectrochimica Acta - Part B Atomic Spectroscopy* 56(11): 2127–36.

Schmeling, Martina. 2019. 10 Encyclopedia of Analytical Science *X-Ray Fluorescence and Emission | Total Reflection X-Ray Fluorescence*. Third Edit. Elsevier. http://dx.doi.org/10.1016/B978-0-12-409547-2.00582-5.

Shaltout, Abdallah A. et al. 2020. “Elemental Composition and Source Apportionment of Atmospheric Aerosols Collected from Urban and Residential Areas of Jordan Using Multi-Secondary Targets Energy Dispersive X-Ray Fluorescence.” *Spectrochimica Acta - Part B Atomic Spectroscopy* 170(March): 105900. https://doi.org/10.1016/j.sab.2020.105900.

Smart Solutions. 2022. “Smart Store System.” https://www.smartstore.systems/ (September 23, 2023).

Smichowski, Patricia, Julieta Marrero, and Darío Gómez. 2005. “Inductively Coupled Plasma Optical Emission Spectrometric Determination of Trace Element in PM10 Airborne Particulate Matter Collected in an Industrial Area of Argentina.” *Microchemical Journal* 80(1): 9–17.

Solé, V. A. et al. 2007. “A Multiplatform Code for the Analysis of Energy-Dispersive X-Ray Fluorescence Spectra.” *Spectrochimica Acta - Part B Atomic Spectroscopy* 62(1): 63–68.

Steiger, Thomas, and Rita Pradel. 2015. “COMAR: The International Database for Certified Reference Materials—an Overview.” *Accreditation and Quality Assurance* 20(1): 47–52.

Stoeppler, Markus. 2007. “From Planning to Production.” *References Materials for Chemical Analysis* (2069): 20–48.

U.S. Department of Commerce. 2011. “NIST SRM 2783; Air Particulate on Filter Media.” chrome-extension://efaidnbmnnnibpcajpcglclefindmkaj/https://tsapps.nist.gov/srmext/certificates/2783.pdf.

U.S. Environmental Protection Agency. 1999. “SAMPLING OF AMBIENT AIR FOR TOTAL SUSPENDED PARTICULATE MATTER (SPM) AND PM10 USING HIGH VOLUME (HV) SAMPLER - Compendium Method IO-2.1.” (June).

U.S. EPA. 1999a. “Compendium Method IO-3.1: Selection, Preparation and Extraction of Filter Material.” *Center for Environmental Research Information Office of Research and Development US Environmental Protection Agency* (June): 1–30. https://www.epa.gov/sites/default/files/2015-07/documents/epa-io-3.1.pdf.

U.S. EPA. 1999b. “Compendium of Methods for the Determination of Inorganic Compounds in Ambient Air. Determination of Metals in Ambient Particulate Matter Using X-Ray Fluorescence (XRF) Spectroscopy.” (June): 20–56. http://www3.epa.gov/ttnamti1/files/ambient/inorganic/mthd-3-3.pdf.

U.S. EPA. 2016. “Definition and Procedure for the Determination of the Method Detection Limit—Revision 1.11.” *Epa 821-R-16-006* (December): 1–8. https://www.law.cornell.edu/cfr/text/40/part-136/appendix-B%5Cnhttp://www.epa.gov/region9/qa/pdfs/40cfr136_03.pdf.

UNI. 2005. *UNI EN 14902:2005; Ambient Air Quality - Standard Method for the Measurement of Pb, Cd, As and Ni in the PM10 Fraction of Suspended Particulate Matter*. https://standards.iteh.ai/catalog/standards/cen/374ad39c-7a3c-4eb4-9421-

5ff2bec3f12e/en-14902-2005 (accessed September4, 2021).

UNI. 2014. *UNI EN 12341:2014; Ambient Air - Standard Gravimetric Measurement Method for the Determination of the PM10 or PM2,5 Mass Concentration of Suspended Particulate Matter*. http://store.uni.com/catalogo/uni-en-12341-2014?___store=en&___from_store=it.

VAMAS. 2023. "Vamas, TWA 2." http://www.vamas.org/twa2/ (January 26, 2024).

Vernekohl, Don, Stratis Tzoumas, Wei Zhao, and Lei Xing. 2018. "Polarized X-Ray Excitation for Scatter Reduction in x-Ray Fluorescence Computed Tomography." *Medical Physics* 45(8): 3741–48.

Wadinga Fomba, Khanneh et al. 2020. "Application of TXRF in Monitoring Trace Metals in Particulate Matter and Cloud Water." *Atmospheric Measurement Techniques* 13(9): 4773–90.

Wagner, Annemarie, and Margarete Mages. 2010. "Total-Reflection X-Ray Fluorescence Analysis of Elements in Size-Fractionated Particulate Matter Sampled on Polycarbonate Filters - Composition and Sources of Aerosol Particles in Göteborg, Sweden." *Spectrochimica Acta - Part B Atomic Spectroscopy* 65(6): 471–77. http://dx.doi.org/10.1016/j.sab.2010.02.007.

Wang, Chu Fang, Jenq Yann Yang, and Cheng Hsiung Ke. 1996. "Multi-Element Analysis of Airborne Particulate Matter by Various Spectrometric Methods after Microwave Digestion." *Analytica Chimica Acta* 320(2–3): 207–16.

Wilschefski, Scott C., and Matthew R. Baxter. 2019. "Inductively Coupled Plasma Mass Spectrometry: Introduction to Analytical Aspects." *Clinical Biochemist Reviews* 40(3): 115–33.

Wobrauschek, P. 2007. "Total Reflection X-Ray Fluorescence Analysis—a Review." *X-Ray Spectrometry* 36: 289–300.

Yang, Xiao Jin, Pingyu Wan, and Roy Foley. 2012. "Effect of Sample Digestion, Air Filter Contamination, and Post-Adsorption on the Analysis of Trace Elements in Air Particulate Matter." *Clean - Soil, Air, Water* 40(11): 1217–21.

Yatkin, S., M. Gerboles, and A. Borowiak. 2011. "Evaluation of EDXRF for the Determination of Elements in PM10 Filters." *JRC Scientific and Technical Reports*. https://linkinghub.elsevier.com/retrieve/pii/S135223101200177X.

Yatkin, Sinan, Hardik S. Amin, Krystyna Trzepla, and Ann M. Dillner. 2016. "Preparation of Lead (Pb) X-Ray Fluorescence Reference Materials for the EPA Pb Monitoring

Program and the IMPROVE Network Using an Aerosol Deposition Method." *Aerosol Science and Technology* 50(4): 309–20. http://dx.doi.org/10.1080/02786826.2016.1150956.

Yatkin, Sinan, Krystyna Trzepla, Warren H White, and Nicole Pauly Hyslop. 2018. "Generation of Multi-Element Reference Materials on PTFE Filters Mimicking Ambient Aerosol Characteristics." *Atmospheric Environment* 189: 41–49. https://linkinghub.elsevier.com/retrieve/pii/S1352231018304254.